Wave-Structure Interactions on Point Absorbers - an experimental study

Jakobsen, Morten Møller

DOI (link to publication from Publisher):
10.5278/vbn.phd.engsci.00030

Publication date:
2015

Document Version
Publisher's PDF, also known as Version of record

WAVE-STRUCTURE INTERACTIONS ON POINT ABSORBERS – AN EXPERIMENTAL STUDY

BY
MORTEN MØLLER JAKOBSEN

DISSERTATION SUBMITTED 2015

AALBORG UNIVERSITY
DENMARK

Wave-Structure Interactions on Point Absorbers - an experimental study

Ph.D. Dissertation

Morten Møller Jakobsen

Dissertation submitted month 07, 2015

Thesis submitted: August 2015

PhD supervisor: Assoc. Prof. Morten Mejlhede Kramer
Aalborg University

PhD committee: Associate Professor Thomas Lykke Andersen (chair)
Department of Civil Engineering
Aalborg University

Professor Deborah M. Graves
School of Marine Science and Engineering
University of Plymouth

Dr. David Irving Moffat Forehand
School of Engineering
The University of Edinburgh

PhD Series: Faculty of Engineering and Science, Aalborg University

ISSN (online): 2246-1248
ISBN (online): 978-87-7112-331-9

Published by:
Aalborg University Press
Skjernvej 4A, 2nd floor
DK – 9220 Aalborg Ø
Phone: +45 99407140
aauf@forlag.aau.dk
forlag.aau.dk

Printed in Denmark by Rosendahls, 2015

Curriculum Vitae

Morten Møller Jakobsen

DATE OF BIRTH:
29th January 1984

WORK ADDRESS:
Department of Civil Engineering
Sofiendalsvej 11
Room: 11.218
9200 Aalborg SV, DK

AFFILIATION:

May 2013 to May 2014	Event Coordinator, International Network on Offshore Renewable Energy, INORE

PRESENT POSITION:

July 2012 to present	Ph.d. Student, Wave Energy Research Group, Aalborg University

CAREER:

August 2011 to June 2012	Research Assistant, Wave Energy Research Group, Aalborg University
August 2009 to June 2011	M.Sc. Student, Structural Engineering, Aalborg University
August 2006 to June 2009	B.Sc. Student, Civil Engineering, Aalborg University

EXPERIENCE:
Morten Jakobsen is a Ph.D. student within the Department of Civil Engineering (DCE) at Aalborg University. He is writing his Ph.D. thesis in renewable energy based on his work with physical and numerical modelling. The work

includes extreme loads, load distribution and Power Take-Off control. During his Ph.D. he made an successful application to Marine Renewables Infrastructure Network (MARINET) to do four weeks of large scale experiments (1:5). In collaboration with Coastal Ocean and Sediment Transport Laboratories (COaST) at Plymouth University the wave energy device was tested in the COaST ocean wave basin. Before that he was an event coordinator for INORE (1400+ members). He arranged the INORE workshop (100+ attendees) and dinner at EWTEC 2013 conference. He assisted in arranging the seven day international symposium (80 attendees) in La Vega, Spain. Before his Ph.D. he was working as research assistant with 3D wave generation and analysis and created software (with graphical user interface) to do advanced generation and analysis of both 2D and 3D waves.

Summary

We are facing a significant challenge when it comes to securing the energy needed to sustain our standard of living in the future. With the increasing global temperature and the climbing levels of carbon dioxide in our atmosphere we need to reduce the consumption of fossil fuels. The renewable technologies will play a key role in achieving this. The renewable energy sector consists of a wide range of technologies yet the source with the highest energy density is still untapped. The extraction of energy from the ocean has shown to be costly and difficult.
This thesis deals with the development of a wave energy device by determining the loads on the device. The loads plays a key part in optimizing the power extraction, reducing the structural cost, and increasing the survivability. Experiments are carried out in small and large scale and compared to simulations and empirical functions. The WEC used in the case studies is a pitching point absorber (Wavestar).
The central part of the thesis deals with the challenges, choices, and experiences gained during the Ph.D. The more in-depth technical details and results are presented in peer-reviewed publications and technical reports. The challenges addressed in this thesis can be summarized as:

1 **Characterizing wave induced forces on the WEC during operation conditions.** Morisons equation is used to characterize the wave induced excitation loads. Then comparison is made between the estimates of the coefficients in experiment and numerical models. Using a modification by Faltinsen to take into account the relative motion of the device, the contributions from drag, excitation and body motion are determined.

2 **Determining the peak pressure on the surface on the device during extreme events and in freak conditions.** A great deal of work has been done to determine peak pressures on mono-piles worldwide, but only very little on spherical structures. In order to shed more light on the wave induced loads on a hemisphere the peak pressures are measured with the traditional drop test and during impact of so-called freak waves.

3 **Implementation and comparison of sub-optimal control in both simulation and experiments.** A long list of control schemes for wave energy devices has been presented in the past. After outlining some of these methods a non-predictive proportional and differential controller is selected for implementation in the laboratory experiments. Through simulation the maximum extractable power is determined and the corresponding control gains are used in the experiments.

4 **Ensuring a high comparability of the experiments and with numerical models. Herein also accurately determine the waves produced in the tank.** Scaling effects, unwanted cross waves, reflected waves and other disturbances may affect the results when comparing experiments with other experiments and numerical models. Methods are presented that reduces the influences in these comparisons. This includes work in determining the waves in the tanks accurately.

5 **A practical and reliable method to run experiments with combined waves and current.** Loads on a WEC's are affected by currents both directly and indirectly. The current adds to the particle velocity around the device and affects the shape of the waves. Work is carried out to find a way to make experiments that combines waves and current in a meaningful way. The method needs to be inexpensive, easy to implement and reduce the turbulence without distorting the incident waves in a detrimental way.

Resumé

Vi står over for en væsentlig udfordring når det angår sikring af den energi vi skal bruge til at sikre vores levestandard i fremtiden. Med øgede globale temperature og stigende kuldioxid i vores atmosfære er det nødvendig at reducere vores udslip af fossile brændstoffer. De vedvarende energi teknologier vil spille en væsentlig rolle i at opnå dette. Den vedvarende energi sektor består af en bred vifte af teknologier, men til trods for dette er den med den største energi koncentration stadig urørt. At trække energi ud af havet har vist sig at være både dyrt og svært.
Denne afhandling omhandler udviklingen af en bølge energi maskine ved at bestemme laster på konstruktionen. Lasterne på en bølge energi maskine spiller en væsentlig rolle i optimering af energi udvindingen, reducering af strukturelle omkostninger, og forbedring af overlevelses egenskaberne. Eksperimenter er udført i både lille og stor skala og er sammenlignet med simuleringer og empiriske funktioner. Bølgemaskinen der er brugt i case studierne er en duvende punkt-absorber maskine (Wavestar).
Den centrale del af afhandlingen fokuserer på udfordringerne, valgene og de indsamlede erfaringer gennem Ph.D. forløbet. De tekniske detaljer og resultater er præsenteret i fagfællevurderede artikler og i tekniske rapporter. Udfordringerne er opsummeret som:

1 **Karakterisering af bølgeskabte laster på bølgemaskinen under almindelig operation.** Morison's ligning er brugt til at karakterisere bølgeskabte eksitationslaster. Sammenligning er derefter lavet mellem estimatet af koefficienterne fra eksperimenter og fra den numeriske model. Bidrag fra friktion, eksitation og bevægelse bestemmes ved brug Faltinsens modifikation af ligningen, som tager den relative bevægelse med i betragtning.

2 **Bestemmelse af spidslaster (tryk) under ekstreme forhold og i såkaldte "freak-waves".** Der er allerede lagt et stort arbejde i at bestemme spidslaster fra tryk på monopæle på verdensplan, derimod er kugleformede bøjer beskrevet i et meget begrænset omfang. For at sprede mere lys på bølgeskabte laster på en kugleform er der lavet både traditionelle drop

forsøg og forsøg med såkaldte “Freak-waves”.

3 **Implementering og sammenligning af sub-optimal kontrol i både simulering og eksperimenter.** En lang liste af kontrol strategier for bølgeenergianlæg er blevet præsenteret gennem tiden. Efter at have præsenteret nogle af disse metoder er en ikke forudsigende proportional og differentiel kontrol strategi implementeret i laboratorieforsøg. Den maksimale energi der kan trækkes ud af bølgerne findes fra simulering og de tilhørende kontrol parametre er derefter brugt i eksperimenterne.

4 **Sikre en høj sammenlignelighed i eksperimenterne og med numeriske modeller. Herunder præcis bestemmelse af bølger produceret i bølgetanken.** Skalerings effekter, uønskede tværgående bølger, reflekterede bølger og lignende forstyrelser kan påvirke resultaterne når de sammenlignes med andre eksperimenter og med numeriske modeller. Metoder er præsenteret der reducerer inflydelsen i disse sammenligninger. Dette inkluderer arbejde med præcis bestemmelse af bølgerne i basinerne.

5 **En praktisk og pålidelig metode at udføre eksperimenter på med kombinerede bølger og strømning.** Laster på en bølgeenergimaskine er påvirket af strømning både direkte og indirekte. Strømning forøger partikelagtigheden omkring maskinen og påvirker ligeledes formen af bølgen. I forsøg er der fundet frem til en metode til at kombinere bølger og strømning på en meningsfuld måde. En metode der er både billig, nem at implementere og som reducerer turbulens uden at nedbryde den indkommende bølge unødigt.

Contents

Curriculum Vitae iii

Summary v

Resumé vii

Thesis Details xi

Acknowledgments xiii

1 Introduction 1
- 1.1 Renewable energies . . . 2
- 1.2 Overview of the main projects during the Ph.D. . . . 3
- References . . . 6

2 Wave Energy Concepts 7
- 2.1 Device development and overview . . . 7
- 2.2 Device characterization . . . 8
- 2.3 Challenges and prospects . . . 10
- 2.4 The Wavestar device . . . 11

3 Wave-Body Interaction 13
- 3.1 Introduction . . . 13
- 3.2 Wave fundamentals . . . 13
  - 3.2.1 Wave-body excitation . . . 15
  - 3.2.2 Impact pressure loads . . . 16
  - 3.2.3 Loads on moving bodies . . . 17
- 3.3 WEC control . . . 17
  - 3.3.1 Pitching buoy case . . . 18
  - 3.3.2 Other control schemes . . . 20
- References . . . 22

4 Experiments conducted **25**
4.1 Introduction 25
4.1.1 The pitching point absorber 25
4.2 Experiments in Aalborg 31
4.3 Large-Scale Experiments 35
4.3.1 Setup 35
4.3.2 Expteriments 36
4.3.3 Results and discussion 37
References 40

5 Conclusion **41**
5.1 Summary 41
5.2 Original Contribution 41
5.3 Future Work Recommendation 42

I Papers **43**

A Characterization of loads on a hemispherical point absorber wave energy converter. **45**

B Damping of unwanted turbulence in wave-current experiments **69**

C Practical Performance of Control Strategies for Point Absorbers **107**

D Experimental Study of Forces on Point Absorber **115**

E Layout of Wave Gauge Array for Estimation of 3D Waves **127**

I Appendices **137**

F Water-Structure Interactions on a Point Absorber **139**

G MARINET Infrastructure Access Report **177**

H Manual for open wave generation and analysis software **199**

Thesis Details

Thesis Title:	Wave-Structure Interactions on Point Absorbers - an experimental study
Ph.D. Student:	Morten Møller Jakobsen
Supervisor:	Assoc. Prof. Morten Mejlhede Kramer, Aalborg University

This thesis is submitted to the International Doctoral School of Technology and Science at Aalborg University in a partial fulfilment of the requirements for the degree of Doctor of Philosophy. The work was carried out in the period spanning from July 2012 to July 2015 at the Department of Civil Engineering at Aalborg University.

The main body of this thesis consist of the following peer-reviewed papers.

[A] Morten M. Jakobsen, Scott Beatty, Gregorio Iglesias, Morten M. Kramer, "Characterization of loads on a hemispherical point absorber wave energy converter," *International Journal of Marine Energy*, in review (submitted Dec. 2014).

[B] D. Markus, M.M. Jakobsen, K.-U. Bletzinger, P.B. Frigaard, "Damping of unwanted turbulence in wave-current experiments," *Coastal Engineering*, vol. 96, pp. 38–48, 2014.

[C] Morten M. Jakobsen, Francesco Ferri and Morten M. Kramer, "Practical Performance of Control Strategies for Point Absorbers," *European Wave and Tidal Energy Conference*, no. 11, accepted for publication in 2015.

[D] Morten M. Jakobsen, Gregorio Iglesias, Morten M. Kramer and Enrique Vidal, "Experimental Study of Forces on Point Absorber," *International Conference on The Application of Physical Modelling to Port and Coastal Protection*, vol. 2, no. 5, pp. 15–25, 2014.

[E] Morten M. Jakobsen and Peter Frigaard, "Layout of Wave Gauge Array for Estimation of 3D Waves," *International Conference on The Application*

of Physical Modelling to Port and Coastal Protection, no. 4, pp. 400–407, 2012.

Other publications included in the thesis.

[F] Morten M. Jakobsen, "Water-Structure Interactions on a Point Absorber," *DCE Technical Report*, no. 183, p. 26, 2015, ISSN 1901-726X.

[G] Morten M. Jakobsen, "MARINET Infrastructure Access Report," *Marine Renewables Infrastructure Network, MARINET*, `http://www.fp7-marinet.eu/access_user_projects_AAUWS.html`, last visited June 15th 2015.

[H] Morten M. Jakobsen, "Wave Generation and Analysis software," *Method of publication TBA*, `civil.aau.dk`, last visited June 15th 2015.

In addition to the main papers, the author has also co-authored the following publications.

[1] Carlos Pérez-Collazo, Morten M. Jakobsen, Julia F. Chozas and Hannah Buckland, "Synergies for a Wave-Wind Energy Concept," *The European Wind Energy Association*, 2013.

[2] Thomas V. Hansen; Morten T. Andersen, Morten M. Kramer, Morten M. Jakobsen, "Excitation Forces on Point Absorbers Exposed to High Order Non-linear Waves," *European Wave and Tidal Energy Conference*, no. 10, 2013.

[3] E. Ransley, M. Göteman, J. Engström, M. M. Jakobsen, M. Leijon, M. Hann, D. Greaves, A. Raby, D. Simmonds, "RANS-VOF Modelling of Wave Energy Converters," *Partnership for Research In Marine Renewable Energy*, no. 2, 2015.

This thesis has been submitted for assessment in partial fulfillment of the PhD degree. The thesis is based on the submitted or published scientific papers which are listed above. Parts of the papers are used directly or indirectly in the extended summary of the thesis. As part of the assessment, co-author statements have been made available to the assessment committee and are also available at the Faculty. The thesis is not in its present form acceptable for open publication but only in limited and closed circulation as copyright may not be ensured.

Acknowledgments

This Ph.D. was partially funded by a number of projects that not only provided financial support, but from which I have learned so much.
Specifically these projects are the FLOAT2 project, which is seeking to determine the applicability of high-performance concrete in wave energy converters. The Digital Hydraulic Power Take Off for Wave Energy project, testing a full-scale digital hydraulic Power Take-Off (PTO). The Cost Effective Foundation and Installation of Wave Energy converters (CEFIWE) project, which sought to reduce structural expenses of the foundation of the WEC. The Structural Design of Wave Energy Devices project (SDWED), which sought to harness the energy potential in wave energy at competitive costs.
I would like to thank the organizations, research groups and individuals that have helped me throughout the years of my Ph.D.
To the Wave Energy Research Group at Aalborg University and individuals in the department that has been helping me throughout the years. To Morten Kramer for his continual guidance, inspiration and complete support paving the way for my research. To Peter for steering me in the right direction up to my Ph.D. and for creating unique opportunities during it. To the people in the laboratory and especially Nikolaj, for all the help both in Denmark and during the experiments in Plymouth. To Francesco for putting up with all my impromptu questions through the years, and to Vivi for her valuable corrections to my past and present work.
To Wavestar for the willingness to support my work and openness to let me share my findings and work with fellow researchers within the sector. To Enrique and Mikael for their extensive and meticulous work on the Plymouth device.
And to the Coastal, Ocean and Sediment Transport (COAST) research group and technical staff in Plymouth for their full support both before, during and after the experiments carried out in their basin.
To all the great people in the International Network on Offshore Renewable Energy (INORE). I have learned so much of the renewable energy sector through this network. The year in the committee for INORE has been one of the most memorable experiences during my Ph.D.

Chapter 1

Introduction

This past decade has enlightened our society on the threat of global warming and the depletion of fossil fuels. The key is security. In order to maintain our standard of living we need to ensure a steady energy supply. However, as fossil fuel resources are slowly depleting we will reach a peak supply capacity. Optimistic estimates for this peak is 2030, but may be reached before 2020. With an increasing worldwide demand, this supply will be our main challenge in the coming years. One way to solve this problem is by increasing unconventional extraction methods by 10% yearly over the next 20 years [8]. But these extractions methods are more damaging to our environment and may not be available in the amounts needed in time [6].
The effect of burning fossil fuels is a very clear increase in CO_2 in the atmosphere. From a near constant 280 ppm before we first started affecting the atmosphere in the 18th century to a staggering 400 ppm in the atmosphere today [12]. The effect of this increase is the evident loss of mass at the ice caps. If we continue on this path, the CO_2 concentration will reach more than 600 ppm before it will decline [10], [13]. This is well past the 450 ppm critical limit set at the UN Framework Convention on Climate Change (UNFCCC) in 2010 [16].
In order to secure a sustainable future we need to look into every alternative to fossil fuels. While nuclear fission is a viable solution to bridge an energy supply gap in the short run, it is a depleting source as well. The only long-term solution is to use every feasible and safe source of energy we can. This includes all the expensive renewable energies, even the modest contributions from tidal and wave energy.

1.1 Renewable energies

Changing our energy source from fossil fuels to renewable energy is a substantial challenge on its own. The supply must meet the demand. This means that when the demand is large, so must the supply be and vice versa. Today this is done on the supply side by simply reducing or increasing production and storing/exporting excess [11]. With the exception of hydroelectric facilities, the renewables are only able to increase production when the source is available and nuclear power plants needs hours to increase or decrease the production of electricity. There is a number of solutions to this, with the smart grid being a significant part of this solution. Other options are to create storages and adjust the consumption. David JC MacKay has done a great job on highlighting some of these options [12].

The fluctuations in the available natural resources is a strong motivator towards diversifying the renewable energy. Put simply, when the sun is absent there may still be strong winds. Similarly, wind and wave resources may complement each other due to the inherent relation between the two. Creating combined renewable energy parks would provide the additional advantage of smoothing the production. This means better utilization of the limited capacity in the cabled connection. These and other symbiotic effects are discussed in the literature [4, 14].

Another key issue with renewables as a whole is the cost of energy and the availability of the natural resources. The typical benchmark is the Levelized Cost of Energy (LCOE)[1] of brown coal, which is about 50 EUR/MWh [2]. Fig. 1.1 shows an overview of the renewables. Excluding incentives and subsidies, only onshore wind and hydroelectricity are economically competitive using our current technology and only in regions with a high potential. As it is now solar photovoltaics (utility scale), offshore wind, wave and tidal energies need significant incentives to be economically feasible solutions. But common for these four technologies is that they are still under heavy development. And with increasing coal price. This may change dramatically in the foreseeable future.

Within the smaller tidal and wave energy sectors, several issues have prevented any significant commercial breakthroughs. The first issue is finding investors willing to invest the substantial amount of money needed for the full-scale devices. Poor performance based on high expectations and mishaps has made it even more unappealing to new investors.

In order to bring wave energy back on track, Jochem Weber [17] proposed a so-called TRL-TPL matrix. The Technology Readiness Level (TRL), being how close the device is to commercialization and the Technology Performance

[1] LCOE is a measurement of the systems expected lifetime cost. This includes construction, fuel, operation and maintenance, and normally also incentives and subsidies.

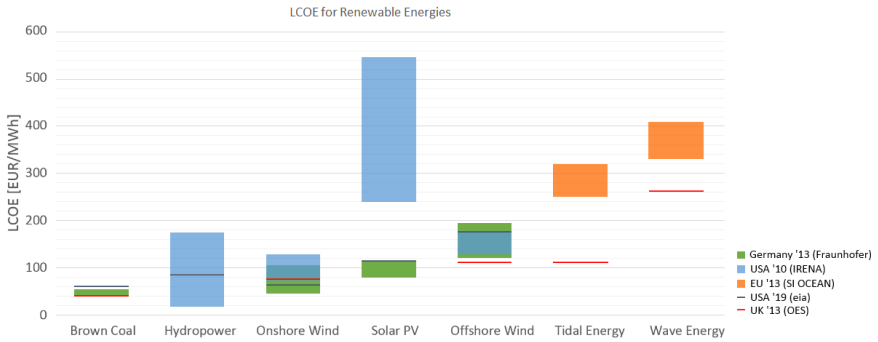

Fig. 1.1: Levelized Cost of Energy for Renewable Energies. Green boxes are based on 2013 numbers for Germany [5]. Blue boxes are for 2010 in the USA [9]. Orange boxes are early array estimates at locations with high resources [15]. Black lines are 2019 estimates in the USA [3]. Red lines are estimates for the UK in 2013 [1, 2].

Level (TPL) being the economic viability of the device, i.e. by estimating the LCOE. The idea is to ensure that the device development attempts to follow an optimized development trajectory towards commercialization.
The TRL was established by NASA to help characterize the maturity level of a technology. It has been widely used in engineering and scientific research. Within the wave energy field the nine levels in the TRL were later redesigned into five phases customized for the development of Wave Energy Converters (WECs) [7].
Several initiatives have been started through the years to help developers bring their devices through the TRLs. The Marine Renewables Infrastructure Network (MARINET) was initiated in Europe as part of a larger framework funded by the European Commission. The project provided access to both laboratories and testing sites under the condition that the users applied for transnational access to promote international collaboration.
As with all laboratory work, it is essential to ensure reliable, accurate, and reproducible results. This includes taking into account the effects of the boundaries in the experiments. Specifically, this means ensuring that the wave-makers are producing the waves requested. The produced waves in the far field in the general vicinity of the device location should be well formed. Reflections and re-reflections from walls and beaches may also be of significant importance in that aspect.

1.2 Overview of the main projects during the Ph.D.

The work presented in this thesis is primarily the results of working on the Wavestar. Wavestar is a point absorber that extracts energy from ocean waves

through pitching motions of the device. The primary focus is on the estimation of loads on the WEC during operation. The wave-induced loads were determined through both laboratory experiments and numerical simulation. Experiments were carried out in the local facilities at Aalborg University where a 1:40 scale device was tested with an electro-magnetic PTO (Phase 1, TRL 1-3 equivalent). To decrease the influence of scaling effects and to get more accurate measurements, a 1:10 scale device was tested in a large wave basin in Plymouth (Phase 2, TRL 4).
Complexity to the estimation of loads stems from the motion of the device. To extract energy this motion is controlled in a way that will generate as much power as possible. This control of the device affects the behavior of the float and leads to higher loads compared to a freely floating device. The examined controls are basic damping using proportional control of the device and the more advanced proportional, integral controller that is shown to give a greater yield. In Aalborg, the so-called floats were tested on multiple occasions with progressively more advanced setups and better equipment to increase the quality of the measurements, cf. Fig. 1.2. Throughout the experiments it became clear that the small scale of the device (1:40) was becoming a hindrance when looking at pressure distributions and peak loads. To overcome this it was decided to do large-scale laboratory experiments. Through the MARINET program, it became economically feasible to apply for access to the Ocean Wave Basin in Plymouth.

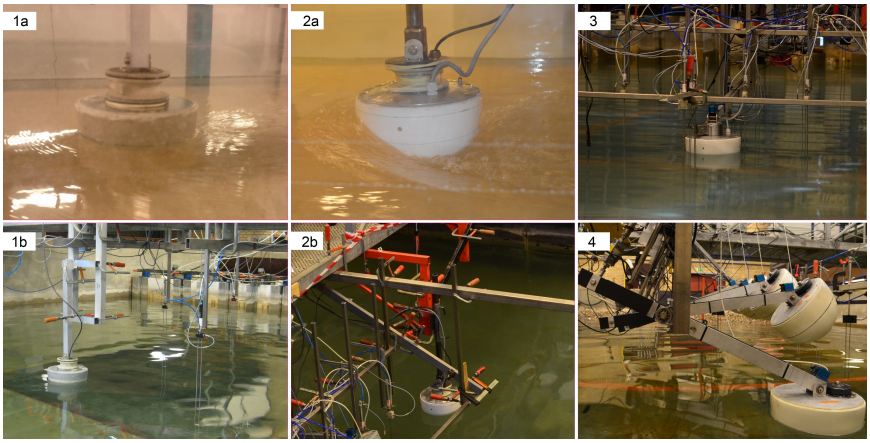

Fig. 1.2: 1a and 1b shows the styrofoam float with a 6-axis load cell from experiments in May 2012. The float is kept in place using fixed support. 1a is from a current flume and 1b is in the wave basin. 2a and 2b shows the glass fiber float with embedded pressure sensors in the shell from February 2013. The rigid support is replaced with one able to rotate about the vertical axis. 2a shows experiments in stream canal with the new fiberglass shell. 2b is from the basin. 3 is from experiments with new waterproof load cell in April 2013. The float is connected to an actuator, pivoting about ball bearings. 4 is from experiments in 2015 with the second edition of the fiberglass float.

References

[1] G. Allan, M. Gilmartin, P. McGregor, and K. Swales, "Levelised costs of wave and tidal energy in the uk: Cost competitiveness and the importance of "banded" renewables obligation certificates," *Energy Policy*, vol. 39, no. 1, pp. 23–39, 2011.

[2] G. Dalton, "Why Wave Energy – Market Driver Analysis for Investors and Policy Makers," Ocean Energy Systems, OES, 2010. [Online]. Available: http://www.ocean-energy-systems.org/what-is-ocean-energy/in-depth-articles/market-driver-analysis/

[3] eia, "Levelized Cost and Levelized Avoided Cost of New Generation Resources in the Annual Energy Outlook 2014," U.S. Energy Information Administration, 2014, url: http://www.eia.gov/forecasts/aeo/electricity_generation.cfm.

[4] J. Fernández-Chozas, M. M. Kramer, H. Sørensen, and J. Kofoed, "Combined Production of a full-scale Wave Converter and a full-scale Wind Turbine – a Real Case Study." 4th International Conference on Ocean Energy, 2012.

[5] Fraunhofer, "Levelized Cost of Electricity Renewable Energy Technologies," Fraunhofer-Institut für Solare Energiesysteme ISE, 2013, url: http://www.ise.fraunhofer.de/en/publications/studies/cost-of-electricity.

[6] D. Goodstein, *Out of Gas: The End of the Age of Oil*. W. W. Norton & Company, inc., 2004.

[7] B. Holmes, "OCEAN ENERGY: Development & Evaluation Protocol - Part 1: Wave Power," HMRC - Marine Institute, Tech. Rep., 2003.

[8] M. Höök and X. Tang, "Depletion of fossil fuels and anthropogenic climate change – a review," *Energy Policy*, vol. 52, pp. 797–809, 2013.

[9] IRENA, "Renewable Energy Technologies: Cost Analysis Series ," International Renewable Energy Agency, IRENA, 2012.

[10] P. A. Kharecha and J. E. Hansen, "Implications of "peak oil" for atmospheric CO2 and climate," *Global Biogeochemical Cycles*, vol. 22, 2008.

[11] H. Lund, "Energyplan advanced energy system analysis model," *Aalborg University, Denmark*. [Online]. Available: http://www.energyplan.eu/getstarted/

[12] D. J. MacKay, *Sustaineble Energy - without the hot air*. UIT Cambridge Ltd., 2009.

[13] OECD, "OECD Environmental Outlook to 2050: The Consequences of Inaction," OECD Publishing, 2012, doi:10.1787/9789264122246-en.

[14] C. Perez-Collazo, M. M. Jakobsen, H. Buckland, and J. Fernandez-Chozas, "Synergies for a wave-wind energy concept," in *The European Wind Energy Association, EWEA*.

[15] SI OCEAN, "Ocean Energy: Cost of Energy and Cost Reduction Opportunities," The Strategic Initiative for Ocean Energy (SI OCEAN), 2013.

[16] UNFCCC, "Report of the Conference of the Parties on its Sixteenth Session, held in Cancún from 29 November to 10 December 2010," UNFCCC, Bonn, Germany, 2011.

[17] J. Weber, "WEC Technology Readiness and Performance Matrix – finding the best research technology development trajectory," 2012.

Chapter 2

Wave Energy Concepts

2.1 Device development and overview

The following section will have a discussion on the process from initial assessment and design criteria to future prospects as well as an overview of the development and activities around the Wavestar WEC.
During the design phase of the WEC, there are a wide range of issues and considerations to consider. Some of these are outlined in the following based on [27, 33–35, 45, 56].

- **Extraction of the energy resource.** The highest concentration of extractable energy from ocean waves is near the surface, but this is also where the most destructive forces are located. To extract energy from these waves the devices absorb a percentage of the incident waves, the performance of which is commonly rated using the wave damping coefficient. As sea conditions changes so must the device in order to maintain a high damping coefficient.
  The short- and long-term fluctuations in the intensity of ocean waves (and the other renewables) create a significant challenge, not only for the individual devices but for the energy farms connected to the utility network as well. To optimize utilization of the expensive power cables it may be beneficial to think energy smoothening into the design of the device as well.
  The multi-directionality of the wave resources is another issue that needs to be addressed as it may reduce the overall production of a device. If the performance of a device is depends on the direction the device is facing it should be able to freely turn with the waves.

- **Survivability in extreme conditions.** During extreme events the wave

energy devices must have a strategy for survivability. Simply increasing the durability of the device to withstand these extreme sea conditions is generally considered a poor choice as this increases the structural cost and often reduces the efficiency of the device during normal sea conditions. Instead developers focus on putting the device into a survival mode, where production is either significantly reduced or halted completely.

- **The Power Take-Off System.** The oscillatory motion of ocean waves is slow but highly energetic. In order to extract energy a system using auxiliary fluid is commonly used (air, oil or water). The efficiency of wave-to-wire conversion of energy is highly influenced by the choice of these physical components, including those of the PTO systems (motor, generator and inverter). In order to have a high yield, the components are rated for the most energetic wave with a common occurrence. The problem with ocean waves is the large variation in both wave period and amplitude, which may reduce the efficiency significantly, regardless of the control strategy chosen.

- **Maintenance and serviceability.** Operation and maintenance is a significant expenditure for all offshore structures. There is a number of considerations to take into account. These includes making the design accessible for inspection for the longest practical duration of the year and ensuring that components with shorter life cycles (i.e. due to fatigue, corrosion, etc.) are replaceable.

As the device is being developed, there will be more considerations to take into account to bring down the LCOE. The list of these criteria is extensive and will not be delved into here, refer instead to e.g. [51, 56].

2.2 Device characterization

The common characterization of the various offshore WECs are split into three groups: the point absorber, the attenuator, and the terminator. The point absorber is usually a buoy-like structure with a diameter less than a wavelength. Riding on or near the surface with the waves, it is either moored by cable to the seabed or connected to a platform, see fig. 2.1a. The attenuator is a longer device (half the wave length and up) that generates energy from relative motion in the device, see fig. 2.1b. The terminator is a wider device that extracts energy from a wider area.
A wide range of extraction techniques has been proposed and tested for each type of WEC. To highlight the diversity of these devices, 11 of them are listed here.

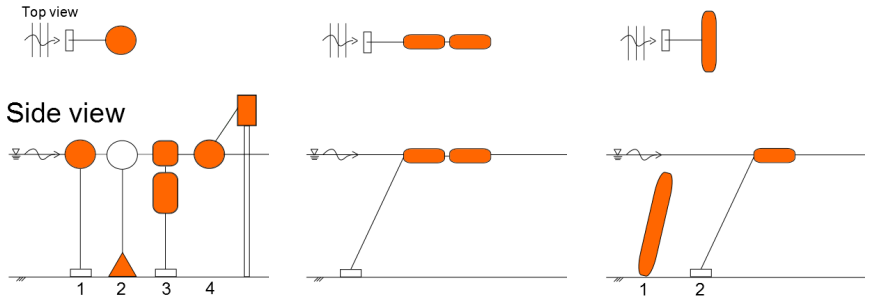

(a) Point absorbers **(b)** Attenuator **(c)** Terminator

Fig. 2.1: WEC classifications by structure composition. The orange coloration indicates the location of the PTO system. For point absorbers in (a), concepts 1-3 are slack moored to the seabed while 4 is connected to a fixed platform. For the terminators in (c), concept 1 is connected directly to the seabed and two is slack moored to the seabed.

Point Absorbers

- CorPower Ocean(SE), linear mechanical actuator (pneu-mechanical drive train) in the buoy with taut mooring line connected to the seabed. (Fig. 2.1a1) [23].
- GyroWaveGen(USA), a Gyroscopic PTO where energy is extracted from the relative motion of the two frames in the gimbal. One connected to mooring line, the other to the buoy. (Fig. 2.1a1).
- OE Buoy(IE), oscillating water column driving a Wells turbine using trapped air in the buoy (Fig. 2.1a1) [43].
- Seabased(SE), marine substations connected by line to a buoy. It extracts energy using a linear mechanical actuator with stator and translator (Fig. 2.1a2) [48].
- WaveBob(IE), a two-body, self-reacting converter with a linear hydraulic actuator extracting energy from the relative motion of the two bodies (Fig. 2.1a3).
- Wavestar(DK), extracts energy from the pitching motion of buoys connected to the main platform using linear hydraulic actuators (Fig. 2.1a4).

Attenuators

- Pelamis(UK), a multibody device using the relative motion of each section to extract energy using linear hydraulic actuators.
- Bulge Wave Anaconda(UK), a floating bulging tube that accumulates pressure at the end of the tube. The pressure buildup drives a hydraulic turbine [21].

Terminators

- Oyster(UK), seabed hinged flaps send high-pressure water through pipes to an onshore hydro-electric turbine (Fig. 2.1c1) [18].
- Weptos(DK), uses pear-shaped "ducks" (known as Salter's ducks) to drive a common axle. The axle drives a mechanical generator to extract the energy (Fig. 2.1c2) [57].
- Wavedragon(DK), collects overtopping water in a reservoir. This water is funneled through turbines built into the device (Fig. 2.1c2) [55].

2.3 Challenges and prospects

Examples of 11 different types of devices are listed to describe some of the diversities of WECs. From an engineer's perspective it is fascinating to look through the many ways of extracting wave energy. To some extent this has also been healthy to the sector, as many extraction methods have been explored. Unfortunately the resources (both intellectual and economical) have been spread thin. Another issue is that projects have been pushed into large expensive demonstrators in early stages of development making the development more rigid for those devices. With bold performance projections in attempts to garner more funding than the competition and not meeting these claims, investors are still loosing faith in the sector.
There are many parallels to be drawn between the wind and wave industry, and drawing from the experience of this sector seems prudent. But in therms of development and small-scale feasibility, the two sectors differ greatly. The Danish wind industry of the 1980s had two significant drivers: governmental support and the interest of the agricultural industry due to the energy crisis. This created a market for small wind turbines that was met by the crane manufacturer Vestas [38, 49]. While the wave energy sector has and will benefit from the wind sector, there are several key differences slowing the development of WECs.
One of the major differences is that wave extraction is done at the ocean or in coastal regions. This means that small devices will likely never become economical feasible to supply the market. There is also little incentive for private individuals to invest in these projects, as there are good alternatives even to those living along the coasts (solar or wind). This all means that the prototypes are €5 millions and up.
Fortunately some projects are starting to include wave energy in the budgets. One of these, the EU-FP7 funded MERMAID project, is seeking developers to install an array of 5 MW wave energy converters within allotted wind energy parks. Projects like these could potentially create a foundation for a front runner within wave energy to help the sector forward. In the long run the

synergies of combining renewables in parks could lead to more reliable and economically feasible energy as proposed in the EU-FP7 funded H2OCEAN project and others [22, 44, 50].

2.4 The Wavestar device

The focus in this thesis is the laboratory experiments with the Wavestar device from 2012 onward. As the device has been under development for 15 years, the focus has moved from design decisions (shape and dimensions) into reducing the LCOE. The notes of the 15 years of experience and development are outlined here:

2001 Initial concept. The "Tusindben"(caterpillar) Machine. Experiments carried out at the Aalborg University wave basin. Device consists of 20 floats with ⌀20cm spheres. Mechanical PTO solution with ratchet mechanism and weight lifting system.

2004-2005 Float optimization. Also carried out at Aalborg University on a device with up to 40 floats. The float shape, size and weight are adjusted. Mechanical PTO solution with ratchet mechanism and disk brake system.

2006-2011 First sea trial. The Nissum Machine, cf. Fig. 2.2a. On the coast of Nissum Bredning. Device with 38 floats, ⌀1m. Hydraulic PTO and single generator system.

2011 PTO control development. Nissum Mini Hydraulic Machine. Open sea trials in Nissum Bredning with single float device, ⌀1m. Hydraulic PTO with real time control.

2009-2013 Full-scale sea trial. The Hanstholm Machine, cf. Fig. 2.2b. Open sea trial in the North Sea, with 2 floats, ⌀5m. Hydraulic PTO and individual generator systems.

2012-2013 PTO development in small-scale experiments. Wave basin tests at Aalborg University, device with 1 to 3 floats ⌀25cm. Detailed tests regarding extreme forces, control strategies and power output in small waves. Magnetic PTO with linear electrical actuators.

2013 Large-scale laboratory experiments. Plymouth device. Experiments at Plymouth University in ocean wave basin, device with a single float ⌀1m. Detailed tests regarding forces on bearings and pressures on float shell. Hydraulic PTO with real time control (the PTO system used previously for the Nissum Mini Hydraulic Machine).

(a) Nissum Machine **(b)** Hanstholm Machine

Fig. 2.2: The Wavestar machines used in sea trials.

2013-2014 PTO test bench. Dry test of a full-scale, digital hydraulic PTO system at Aalborg University. A hydraulic cylinder simulates the motion of a single float. Size for use with a single ⌀5m float.

2015 Study of array interactions. Wave basin tests at Aalborg University, device with 5 floats ⌀25cm. Detailed tests regarding array interaction. Magnetic PTO with linear electrical actuators.

To reduce the LCOE the focus has been structural cost reduction and optimization of the power extraction. The work has been focused into projects such as: the FLOAT2 project, seeking to determine the applicability of high-performance concrete; the Digital Hydraulic Power Take Off for Wave Energy project, testing a full-scale digital hydraulic Power Take-Off (PTO); and the Cost Effective Foundation and Installation of Wave Energy converters (CEFIWE) project, seeking to reduce structural expenses of the foundation of the WEC.

Chapter 3

Wave-Body Interaction

3.1 Introduction

To determine the performance and loads on a wave energy device it is first necessary to characterize the waves and determine the power potential available. Typically the waves used in the models and experiments are based on scatter diagrams showing the significant wave heights and periods from the desired location. Then a set of representative sea states are chosen from the scatter diagrams and used in the experiments and numerical models. Then estimates can be made for the forces, pressures, electrical power production, etc.

3.2 Wave fundamentals

The total energy in mono-chromatic (linear regular) waves is characterised in an equal contribution from the potential and kinematic energy. The average energy per unit surface area can be written as Eq. 3.1.

$$E = E_p + E_k = \frac{1}{8}\rho g H^2 \tag{3.1}$$

Where ρ is the density of water, g is the gravitational acceleration, and H is the wave height. The wave energy is, in other words, proportional to the wave height squared and independent of the water depth h.
As the waves propagate, energy is transported. The energy is transported with the speed of the group velocity, cf. Eq. 3.2

$$P_w = E\ c_g \tag{3.2}$$

in which the speed of the transmitted energy for waves is referred to as the group velocity c_g. The group velocity is Eq. 3.3 for intermediate water depth

and linear waves.

$$c_g = \frac{c}{2}\left(1 + \frac{2kh}{sinh\ 2kh}\right) \tag{3.3}$$

Where c is the phase velocity of the wave, and k is the wave number. The phase velocity can be found from the dispersion relation Eq. 3.4.

$$c = \sqrt{\frac{g}{k\ tanh\ kh}} \tag{3.4}$$

In deep waters where $h \to \infty$ the group velocity simplifies to $c_g = c/2$, and $c = \sqrt{g/k}$.

For real sea approximations the linear regular waves with different wave heights and periods are superposed. In order to decide which waves to superpose, research in the past has been carried out. For the North Sea the most significant work was done under the Joint North Sea Wave Project (JONSWAP) [36]. By measuring the wave spectra during 10 weeks in the late 1960s, the group came up with a modification to the existing Pierson-Moskowitz spectrum, adding peak shape parameters to better fit with the measurements. This JONSWAP spectrum is written in the parameterized form in Eq. 3.5.

$$\begin{aligned} S_\eta(f) &= \frac{1.4}{\gamma}\frac{5}{16}{H_s}^2{f_p}^4 f^{-5}\gamma^\alpha exp\left(-\frac{5}{4}\left(\frac{f_p}{f}\right)^4\right) \\ \alpha &= exp\left(-\frac{(f-f_p)^2}{2{\sigma_f}^2{f_p}^2}\right) \\ \sigma_f &= \begin{cases} \sigma_a\ for\ f \leq f_p \\ \sigma_b\ for\ f > f_p \end{cases} \end{aligned} \tag{3.5}$$

Where H_{m0} is the significant wave height and f_p the frequency of the spectral peak (peak frequency). σ_f and γ control the width and height of the spectrum respectively. As the shape parameters are the only difference between the two spectra, the Pierson-Moskowitz spectrum is obtained by selecting $\gamma = 1$. Fig. 3.1 shows the Pierson-Moskowitz compared to the JONSWAP spectrum with $\gamma = 3.3$. The choice of these parameters should reflect the target sea state and may be bi-modal to account for both swell and wind generated waves. To account for directionality of the waves a spreading function can be included in Eq. 3.6, using the constraint in Eq. 3.7 to ensure that no additional energy is added. A commonly used example being the Cosine 2S spreading function [37].

$$S_\eta(f,\theta) = S_\eta(f) \cdot D_\eta(\theta|f) \tag{3.6}$$

$$\int_{-\pi}^{\pi} D_\eta(\theta|f)d\theta = 1 \tag{3.7}$$

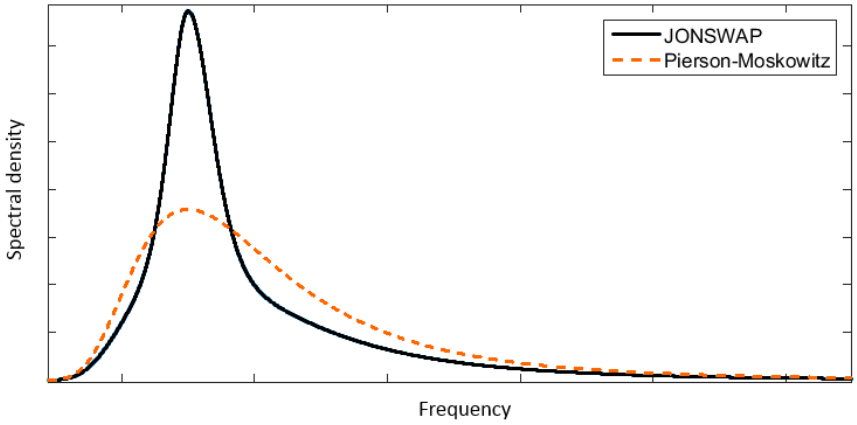

Fig. 3.1: JONSWAP spectrum with $\gamma = 3.3$ compared to the Pierson-Moskowitz using the same significant wave height and peak period.

Then the energy transport can be calculated from Eq. 3.8 for uni-directional (long-crested) waves and Eq. 3.9 for multi-directional (short-crested) waves.

$$P_w = \frac{1}{2}\rho g^2 c_g \int_0^\infty S_\eta(f)df \tag{3.8}$$

$$P_w = \frac{1}{2}\rho g^2 c_g \int_0^\infty \int_{-\pi}^{\pi} S_\eta(f,\theta)df d\theta \tag{3.9}$$

3.2.1 Wave-body excitation

By introducing a point absorber and locking the position, the excitation forces can be determined by calculating the contributions from Froude-Krylov and diffraction forces [31, 39]. Alternatively the excitation forces can be determined from the excitation response in Eqs. 3.10 and 3.11.

$$F_e(f) = H_e(f)\eta(f) \tag{3.10}$$

$$F_e(t) = \int_{-\infty}^{\infty} h_e(t-\tau)\eta(\tau)d\tau \tag{3.11}$$

In which H_e and h_e are the frequency and impulse response functions of the excitation force respectively. The excitation forces can be determined either numerically from an element method (e.g. WAMIT [40]) or from experiments with a stationary float. The two response functions can be interchanged using Eq. 3.12.

$$H_e(f) = \int_{-\infty}^{\infty} e^{i2\pi ft} h_e(t)dt \tag{3.12}$$

Alternatively the excitation forces can be obtained directly by measuring the forces propagating from the device through the fixed support in experiments. The instantaneous forces are assumed to be added contributions from drag and inertia. This leads to Morison's equation Eq. 3.13.

$$F_e = \frac{1}{2} C_D \rho A U |U| + C_M \rho V \dot{U} \tag{3.13}$$

In which C_D and C_M are drag and inertia coefficients that can be determined from the experiments. A is the projected area of the plane normal to the direction of the water particle movement and V is the volume of the body. U and $\dot{U}$ are the particle velocity and acceleration. Due to the particle motion of waves there is a contribution in both vertical and horizontal directions that should be considered. The Morison coefficients can be determined by minimizing the variance between the measured forces and Eq. 3.13. This method only produces one set of coefficients, which are reflecting the most energetic part of the waves. Dean and Dalrymple suggested a least squares method in which the wave(s) are divided into bins based on particle velocity. This produces a set of coefficients for each bin that can be weighed using the mean squared error [26].

3.2.2 Impact pressure loads

Slamming force is a third contribution that needs to be determined for offshore structures. While the devices can be put in a protected state during severe sea conditions, there may be cases where waves coincide to create breaking waves that are not covered by the previous defined equations. The waves are characterized by a steep wave front with a particle velocity larger than the phase speed that can potentially damage the structure. These occurrences, termed freak (or rogue) waves, can be created in a wave tank by controlling the phases of the linear wave components [28, 46]. Fig. 3.2a shows an example of one of these freak waves a fraction of a second before impact. As the velocity can be difficult to measure accurately in the location of impact, it can be advantageous to determine the relation between force/pressure and velocity by dropping the device into the water as seen in Fig.3.2b.

The slamming forces on a cylinder can be calculated by Eq. 3.14 [58].

$$F_s = \rho C_s R U_b^2 \lambda \eta_b \tag{3.14}$$

Where C_s is the slamming coefficient, R is radius of the cylinder, U_b is the celerity of the breaking wave, λ is the curling factor and η_b is the maximum surface elevation. For a vertical cylinder $\lambda = 0.46$ and $\eta_b = R - \sqrt{R^2 - x^2}$ with x being the distance from the center of the cylinder.

For a shell structure it may be more relevant to look at the maximum pressure. The peak pressures coefficients on the shell can be estimated using

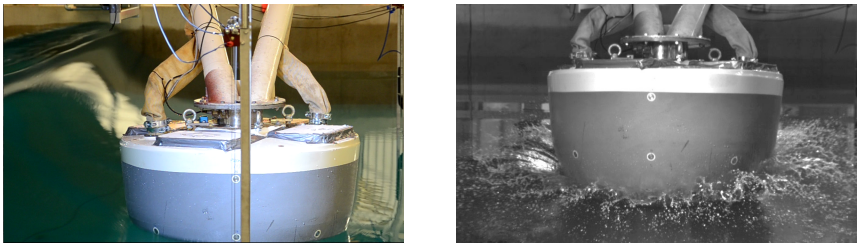

(a) Breaking wave **(b)** Drop

Fig. 3.2: Wave-structure impacts. In (a), the so-called freak wave creates a plunging breaker, that impacts the side of the float. In (b), the float is released from a height and impacts with the water surface.

Eq. 3.15 [32].

$$p_s = 0.5\rho C_p U_b^2 \tag{3.15}$$

Where C_p is the slamming pressure coefficient and p_s is the pressure on the float.
Empirical models are used to calculate these pressure coefficients [53, 54, 58]. While these models are based on cylindrical shaped structures, they have been shown to produce reasonably good approximations for hemispherical devices as well, cf. Paper A and others [25].

3.2.3 Loads on moving bodies

For moving bodies the relative motion of the body is included in Morison's equation Eq. 3.13. The resulting expression is shown in Eq. 3.16 [32].

$$F = \frac{1}{2}C_D\rho A(U - U_0)|U - U_0| + C_M\rho V\dot{U} - \rho(C_M - 1)V\dot{U}_0 \tag{3.16}$$

It should be noted that C_D and C_M in Eq. 3.16 might not correspond with Eq. 3.13 as U and $\dot{U}$ change with the displacement of the device.

3.3 WEC control

In order to extract energy from waves, a WEC needs a control strategy. Adjusting the weight of the device to make the natural frequency coincide with the incident wave will increase the motion of the device due to resonance. Part of the energy can then be extracted by damping the motion using a so-called proportional control or simply P control (A force controller, proportional to the velocity).

Adjusting the weight of the device can be effective only to a limited extent. In real sea (or the irregular waves produced in the lab), adding or removing physical mass is difficult and costly. An alternative is to add or subtract stiffness by sending energy back into the actuator controlling the float. This control is referred to as proportional and integral (PI) control, as it includes a control gain on the integral of the velocity (the displacement). Tuning the device to each sea state to bring it into resonance can be rewarding for efficient PTOs. The wave-to-wire efficiency of the PTO should be accounted for when using this controller.

3.3.1 Pitching buoy case

For the pitching point absorber, the load and positional measures refer to an angular position and moments. With the motion of the float the device is subjected to additional moments. This includes the restoring hydrostatic moment M_h, and hydrodynamic radiation damping and inertia (added mass) moments M_r. Including the control moment M_c to extract energy the equation is expressed using Newton's 2nd law as Eq. 3.17, with the definition of the forces shown in Fig. 4.8a.

$$J\ddot{\theta}(t) = -M_c(t) - M_r(t) - M_h(t) + M_e(t) \tag{3.17}$$

With the excitation defined in Eq. 3.11 and the remaining linearized coeffi-

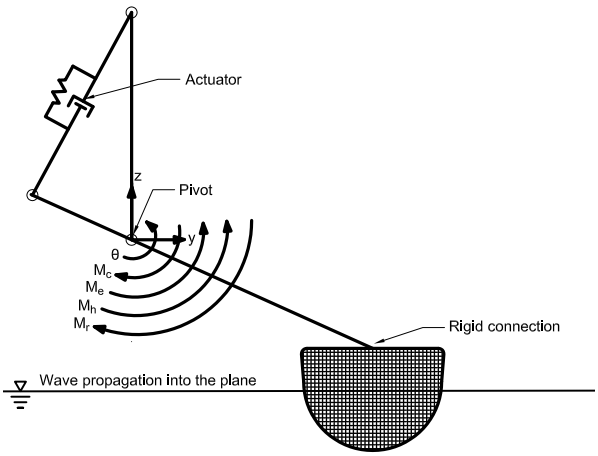

Fig. 3.3: The point absorber and sensors used in experiments.

cients in Eqs. 3.18-3.20.

$$M_c(t) = c_c\dot{\theta}(t) + k_c\theta(t) \tag{3.18}$$

$$M_r(t) = A_\infty\ddot{\theta}(t) + \int_{-\infty}^{t} h_r(t-\tau)\cdot\dot{\theta}(\tau)d\tau \tag{3.19}$$

$$M_h(t) = k_h\cdot\theta(t) \tag{3.20}$$

The added mass tending to infinity A_∞ and radiation impulse response h_r are again obtained from either potential theory or by numerical calculation. When working with laboratory experiments the hydrostatic stiffness k_h and moment of inertia J should preferably be obtained from the experiments. The damping coefficient c_c is used for the P controller, and stiffness k_c is included for the PI controller.
Inserting Eqs. 3.18-3.20 into Eq. 3.17, the expression can be written in terms of the excitation moment in Eq. 3.21.

$$(A_\infty + M)\ddot{\theta}(t) + c_c\dot{\theta}(t) + \int_{-\infty}^{t} h_r(t-\tau)\cdot\dot{\theta}(\tau)d\tau + (k_c + k_h)\theta(t)) = M_e(t) \tag{3.21}$$

The absorbed power is calculated from the control moment Eq. 3.22.

$$P_a(t) = M_c(t)\dot{\theta}(t) \tag{3.22}$$

To calculate the electrical power the efficiency of the PTO needs to be considered. For PI and other controllers where energy is fed back into the system, it is imperative that the efficiency is taken into account, as it will affect the optimization of the chosen controller. The efficiency of a PTO depends on the components used and changes with the sea state [27, 34].
When extracting energy the efficiency reduces the output, and when feeding energy back into the system the efficiency increases the energy input needed. This is expressed in the conditional expression in Eq. 3.23.

$$P_e(t) = \begin{cases} \beta M_c(t)\dot{\theta}(t) : M_c(t)\dot{\theta}(t) \geq 0 \\ \frac{1}{\beta} M_c(t)\dot{\theta}(t) : M_c(t)\dot{\theta}(t) < 0 \end{cases} \tag{3.23}$$

To compare the WECs on efficiency the capture width is used in Eq. 3.24.

$$\kappa = \frac{P_m}{P_w B} \tag{3.24}$$

In this thesis the PTO efficiency is denoted β and the capture width κ to not confuse it with the wave elevation η. B is the dimension of the device, which is typically chosen as the width (or length) of the device. As κ takes into account the location (resource) and size of the device, it is useful for the initial assessment and comparison of a device (as done by [20] and others). As power density should be a concern when planing offshore energy parks, it is easily justified to include capture width alongside the LCOE.

3.3.2 Other control schemes

There are many other control schemes that are regularly considered when developing wave energy devices. Here a brief non-critical overview will be given. Extensive work has been done to outline and compare the different techniques on this topic [33, 35, 47].
The distinction made here is between the causal control, which does not require prediction, and non-causal control. Optimal control is inherently non-causal in irregular waves [30, 42], so some compromise needs to be made. The options are to either go for a sub-optimal causal controller or to try predicting the incident waves in real-time in order to determine wave excitation.

Causal control

- **PI Controller.** As the impulse response from radiation damping in Eq. 3.19 is causal, the PI controller is causal.
- **Latching (Treshold unlatching).** By latching and unlatching the device it is possible to tune the device to the waves (when they are longer than the natural frequency). The advantage compared with a reactive controllers such as the PI controller is that latching can be done without feeding much energy into the system. Traditional latching is non-causal, but by making unlatching nearly instantaneous and using a threshold the method can work with no prediction. In threshold unlatching, the hydraulic pressure is monitored, and when it reaches a predefined threshold the device is unlatched. [29, 41].
- **PID.** The PID controller is an extension of the PI controller that includes a control gain of the acceleration. In optimal control the integral term is non-causal, but a deterministic sub-optimal control was developed that does not require future knowledge [42].
- **OCIR.** The Oscillation Control Implemented Resistively controller is a modified PI controller that changes Eq. 3.23 to not add negative control stiffness to the system [35].

Non-causal control

- **Clutching (Declutching).** Similar to latching, the (de)clutching usually works by disconnecting the PTO to bring the device in phase with the incident waves [19]. To present author's knowledge causal clutching controller has yet to be presented.
- **MPC.** The Model Predictive Control attempts to determine future states to asses the optimal control. The performance of the MPC relies on

accurate and adequate information from sensors (similar to wave prediction models) to accurately predict the future states. Both linear and non-linear MPCs have been developed [24, 52].

References

[18] Aquamarine Power, "Oyster," Aquamarine Power, 2015. [Online]. Available: http://www.aquamarinepower.com/

[19] A. Babarit, M. Guglielmi, and A. H. Clément, "Declutching control of a wave energy converter," *Ocean Engineering*, vol. 36, no. 12, pp. 1015–1024, 2009.

[20] A. Babarit and J. Hals, "On the maximum and actual capture width ratio of wave energy converters," in *Proc. 10th European Wave Energy Conference*, 2011.

[21] Bulgewave, "Anaconda: Wave Power Bulging Snake," Bulgewave, 2015. [Online]. Available: http://www.bulgewave.com/

[22] J. F. Chozas, H. Soerensen, and M. Korpås, "Integration of wave and offshore wind energy in a european offshore grid," *Proc. ISOPE 2010*, 2010.

[23] Corpower Ocean, "Compact high-efficiency Wave Energy Converter," Corpower Ocean, 2015. [Online]. Available: http://www.corpowerocean.com/

[24] J. A. Cretel, G. Lightbody, G. P. Thomas, and A. W. Lewis, "Maximisation of energy capture by a wave-energy point absorber using model predictive control," in *Proceedings of the 18th IFAC World Congress, Milano, Italy, Aug*, 2011, pp. 3714–3721.

[25] G. De Backer, "Hydrodynamic design optimization of wave energy converters consisting of heaving point absorbers," Ph.D. dissertation, ugent, 2009.

[26] R. G. Dean and R. A. Dalrymple, *Water wave mechanics for engineers and scientists*. Prentice-Hall,, 1984.

[27] B. Drew, A. Plummer, and M. N. Sahinkaya, "A review of wave energy converter technology," *Proceedings of the Institution of Mechanical Engineers, Part A: Journal of Power and Energy*, vol. 223, no. 8, pp. 887–902, 2009.

[28] K. Dysthe, H. E. Krogstad, and P. Müller, "Oceanic rogue waves," *Annu. Rev. Fluid Mech.*, vol. 40, pp. 287–310, 2008.

[29] A. F. D. O. Falcão, "Phase control through load control of oscillating-body wave energy converters with hydraulic PTO system," *Ocean Engineering*, vol. 35, pp. 358–366, 2008.

[30] J. Falnes, "On non-causal impulse response functions related to propagating water waves," *Applied Ocean Research*, vol. 17, no. 6, pp. 379–389, 1995.

[31] ——, *Ocean waves and oscillating systems: linear interactions including wave-energy extraction*. Cambridge university press, 2002.

[32] O. M. Faltinsen, *Sea Loads on Ships and Offshore Structures*, ser. Ocean Technology. Cambridge Univ Press, 1990.

[33] J. Hals, "Modelling and phase control of wave-energy converters," Ph.D. dissertation, Norwegian University of Science and Technology, NTNU, 2010.

[34] R. H. Hansen, T. O. Andersen, and H. C. Pedersen, "Model based design of efficient power take-off systems for wave energy converters," in *The 12th Scandinavian International Conference on Fluid Power, May 18-20, Tampere, Finland*, 2011.

[35] R. H. Hansen, "Design and Control of the PowerTake-Off System for a Wave Energy Converter with Multiple Absorbers," Ph.D. dissertation, Videnbasen for Aalborg Universitet,VBN, Aalborg UniversitetAalborg University, Det Teknisk-Naturvidenskabelige FakultetThe Faculty of Engineering and Science, 2013.

[36] K. Hasselmann, T. Barnett, E. Bouws, H. Carlson, D. Cartwright, K. Enke, J. Ewing, H. Gienapp, D. Hasselmann, P. Kruseman, A. Meerburg, P. Müller, D. Olbers, K. Richter, W. Sell, and H. Walden, "Measurements of wind-wave growth and swell decay during the Joint North Sea Wave Project (JONSWAP)," *Ergnzungsheft zur Deutschen Hydrographischen Zeitschrift Reihe*, vol. A(8), no. 12, p. 95, 1973.

[37] S. Hughes, "Directional wave spectra using cosine-squared and cosine 2s spreading functions," *Coastal Engineering Technical Note. Coastal Engineering Research Center, Coastal and hydraulics Laboratary*, 1985.

[38] IRENA, "30 Years of Policies for Wind Energy: Denmark," International Renewable Energy Agency, IRENA, 2012. [Online]. Available: https://www.irena.org/DocumentDownloads/Publications/GWEC_Denmark.pdf

[39] C. H. Kim, *Nonlinear waves and offshore structures*. World Scientific, 2008, vol. 27.

[40] C.-H. Lee, *WAMIT theory manual*. Massachusetts Institute of Technology, Department of Ocean Engineering, 1995.

[41] M. Lopes, J. Hals, R. Gomes, T. Moan, L. Gato, and A. d. O. Falcao, "Experimental and numerical investigation of non-predictive phase-control strategies for a point-absorbing wave energy converter," *Ocean Engineering*, vol. 36, no. 5, pp. 386–402, 2009.

[42] S. R. Nielsen, Q. Zhou, M. M. Kramer, B. Basu, and Z. Zhang, "Optimal control of nonlinear wave energy point converters," *Ocean Engineering*, vol. 72, pp. 176–187, 2013.

[43] OceanEnergy, "OceanEnergy: A world of power," OceanEnergy, 2015. [Online]. Available: http://oceanenergy.ie/

[44] C. Pérez-Collazo, D. Greaves, and G. Iglesias, "A review of combined wave and offshore wind energy," *Renewable and Sustainable Energy Reviews*, vol. 42, pp. 141–153, 2015.

[45] H. Polinder and M. Scuotto, "Wave energy converters and their impact on power systems," in *Future Power Systems, 2005 International Conference on*. IEEE, 2005, pp. 9–pp.

[46] E. Ransley, M. Hann, D. Greaves, A. Raby, and D. Simmonds, "Numerical and physical modeling of extreme waves at wave hub," in *Proceedings 12th International Coastal Symposium*, 2013.

[47] J. Ringwood, G. Bacelli, and F. Fusco, "Energy-maximizing control of wave-energy converters: The development of control system technology to optimize their operation," *Control Systems, IEEE*, vol. 34, no. 5, pp. 30–55, 2014.

[48] Seabased, "Seabased wave energy," Seabased, 2015. [Online]. Available: http://www.seabased.com/

[49] K. Smith, "The danish wind industry 1980-2010: Lessons for the british marine energy industry," *Underwater Technology-Journal of the Societyfor Underwater Technology*, vol. 30, no. 1, p. 27, 2012.

[50] E. D. Stoutenburg, N. Jenkins, and M. Z. Jacobson, "Power output variations of co-located offshore wind turbines and wave energy converters in california," *Renewable Energy*, vol. 35, no. 12, pp. 2781–2791, 2010.

[51] The European Marine Energy Centre Ltd., "Marine Renewable Energy Standards," 2014, url: http://www.emec.org.uk/standards/.

[52] N. Tom and R. W. Yeung, "Nonlinear model predictive control applied to a generic ocean-wave energy extractor," *Journal of Offshore Mechanics and Arctic Engineering*, vol. 136, no. 4, p. 041901, 2014.

[53] T. von Karman, "The impact of seaplane floats during landing," Tech. Rep. Technical note no. 321, 1929.

[54] H. Wagner, "Über Stoß- und Gleitvorgänge an der Oberfläche von Flüssigkeiten," *ZAMM - Journal of Applied Mathematics and Mechanics*, vol. 125, pp. 193–215, 1932.

[55] Wavedragon, "Wavedragon: For a better future," Wavedragon, 2015. [Online]. Available: http://www.wavedragon.net/

[56] J. Weber, R. Costello, and J. Ringwood, "Wec technology performance levels (tpls)-metric for successful development of economic wec technology," in *Proc. 11th European Wave Energy Conference. Aalborg, Denmark*, 2013.

[57] Weptos, "Weptos: Innovating in Wave Energy," Weptos, 2015. [Online]. Available: http://www.weptos.com/

[58] J. Wienke and H. Oumeraci, "Breaking wave impact force on a vertical and inclined slender pile–theoretical and large-scale model investigations," *Coastal Engineering*, vol. 52, pp. 435–462, 2005.

Chapter 4

Experiments conducted

4.1 Introduction

Laboratory experiments are not perfect representations of reality, and neither are numerical models for that matter. The essential part in this is to understand the limitation of the models and the reliability and accuracy of the results. In this, the numerical and experimental models are codependent. For both fields it boils down to a compromise between cost and quality.
The experiments are presented individually with comparison to empirical functions and numerical models to the extent possible. It is rounded off by looking into the validation of the results between the experiments and numerical models.

4.1.1 The pitching point absorber

Fig. 4.1 shows the laboratory versions of the Wavestar point absorber. It consists of a hemisphere shaped float with a stub-shaped top part above water. The float is pivoting about a set of ball bearings, which are connecting it to the support frame. A lever arm connects the wave-induced forces on the float to the linear actuator that extracts the energy. In small-scale experiments it has been convenient to extend the arm past the ball bearings and have the actuator attached there, as seen in Fig 4.1a. For the full-scale devices seen in Fig. 2.2 and the large-scale experiment seen in Fig. 4.1b, the actuator is located on the same side as the float due to the hull of the main structure.

To measure the mean absorbed power, the control moment and angular velocity was measured (cf. Eq. 3.23). The control moment was determined using force and displacement sensors on the cylinder. To get an accurate angular velocity in Paper C, a Kalman filter [64] was used with the displace-

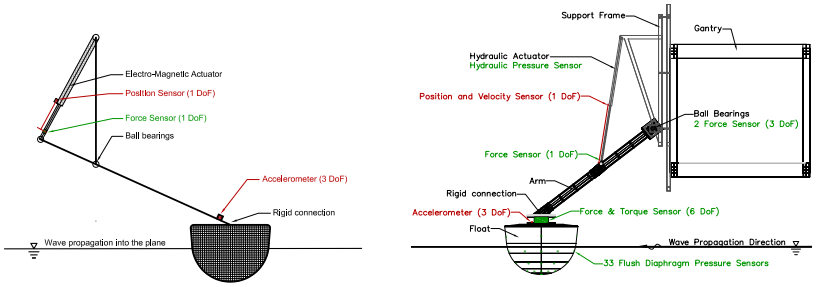

(a) Setup in Aalborg (1:20) **(b)** Setup in Plymouth (1:5)

Fig. 4.1: Laboratory setups for small- and large-scale experiments.

ment sensor and the accelerometer.
When comparing with simulations in Paper C the excitation forces measured were used directly in the simulations. A comparison was made between the measured mean absorbed power and simulations using two different approaches. The first approach used the undisturbed wave elevation series, and the second approach used the excitation forces measured. The undisturbed wave elevation series are obtained by running each wave series with no device in place.

The drag and inertia contributions were determined by measuring the excitation forces on 10-15 regular waves. This was determined to be enough to get a good estimate and not being adversely affected by reflections and cross waves. Two methods was described and used to determine the coefficients from the measurements in Paper A. These results were compared to a numerical model (WAMIT). The particle velocity of the incident waves was measured using the elevation obtained from the wave gauges and directly using an Acoustic Doppler Velocimeter (ADV). The particle velocity was also determined using the using stream functions wave theory from the measured wave elevation [62].
A compound was added to the water to use the ADV. To ensure that the results were reliable it was ensured that the Signal-to-Noice Ratio SNR $> 15dB$ and the correlation was greater than 70%. The measurements were despiked in post-processing as unphysical spikes occurred in the measurements [68]. A more thorough explanation is available in Paper B and the literature [65].
The ADV was used to verify that the velocities obtained from the wave gauges were accurate. By having wave gauges and ADV in line with the float (perpendicular to wave propagation direction), the only thing needed was to determine the undisturbed velocity at the location of the float.
To get measurements from undisturbed experiments a synchronizing signal is sent to the data acquisition unit (DAQ) when the wave maker starts a new

wave series. This ensures that each series starts at the same instance. And by including a diode the synchronizing can be visually inspected in video recordings as well. The synchronization signal was essential in Plymouth where three DAQ systems were needed to measure all the signals in Fig. 4.1b and 4.3b.

All of the experiments carried out has been in the traditional wave basins. That is, fully reflecting/impermeable sidewalls, beach and wave generators along opposing sides. The reflecting sidewalls are in general useful in generating oblique waves thanks to the corner reflection method [60, 63], but an adverse effect is that it may add to the unwanted disturbances in the testing area due to reflections and re-reflections. This can be an issue when testing long duration irregular waves series on devices that diffracts and radiates waves, such as a wave energy converter.
This issue cannot be avoided in this type of basin, but by properly measuring the waves around the device it can be accounted for. The alternative is to use the undisturbed wave measurements (where no device is in the water) and use these as reference for the calculation and numerical models. As the primary focus has been on comparing the experiments with the results of the numerical model the later method has be preferred. Fig. 4.3 shows the wave gauge and ADV for both the small scale setup in Aalborg and the large-scale in Plymouth. In all the experiments carried out the incident waves are measured both in front, behind, and on the side of the device. To distinguish the incident and reflected waves, a three-wave gauge combination is chosen with the separation in accordance with the suggested separation distances in Eq. 4.1. [66]

$$\begin{aligned} x_{12} &= L_p/10 \\ L_p/6 < x_{13} &< L_p/3 \\ x_{13} \neq L_p/5 \text{ and } x_{13} &\neq 3L_p/10 \end{aligned} \tag{4.1}$$

Where x_{nm} is the distance between gauges and L_p is the length of the shortest significant wave.
To measure the short-crested waves in experiments, an array of wave gauges were placed in front of the device, cf. Fig. 4.3b. By placing the wave gauges properly and using an appropriate wave analysis method, the directionality of the waves can be determined. Some of these methods are listed and explained in Appendix H. The configuration of six sensors in a pentagonal shape was chosen as it has shown to produce accurate directional spectra when conducting analysis. The five-gauge CERC array [67] is sufficient in most cases, but the 6th sensor to make a pentagon is slightly better, cf. Paper E. With the additional senor in front of the array the three wave gauges reflection analysis can be done properly.

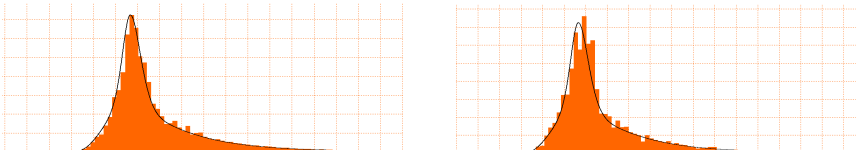

(a) Random Phase Method **(b)** White Noise Method

Fig. 4.2: Comparison of deterministic and non-deterministic wave generation methods in small samples <<1000 waves. Lines are reference JONSWAP spectrum and bars are the distribution of generated waves. With increasing sample size the white noise method will converge to fit the spectrum similar to the random phase method.

To ensure that results of irregular wave series are comparable, a reference series is made. The irregular wave series is then made by adjusting the sampling rate and scaling the elevation. The reference wave is generated in Wavelab and is made by either using the non-deterministic White Noise Method (WNM) or the deterministic Random Phase Method (RPM) [59]. The WNM is used with long wave series ($\approx$ 1000 waves) as the fit of the spectral distribution is ensured through statistical probability. With the shorter irregular wave series the RPM is usually used instead as this method ensures that the spectral distribution is sound, cf. Fig. 4.9. It can be argued that a non-deterministic method is better for short series as well. The argument being that if a short sample of the real sea is collected it would likely not have the correct spectral shape, so the non-deterministic method would better represent this. The generated wave series are post processed to ensure that the wave heights of the reference wave series are close to Rayleigh distributed. This is not guaranteed for the largest waves with $(H/H_m)^2$ exceedence probability of $\sim$2% or less.

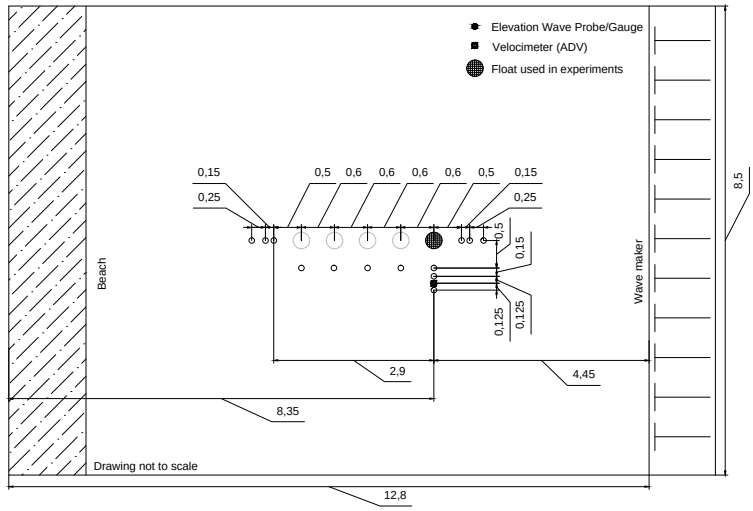

(a) 2015 setup in Aalborg (1:20)

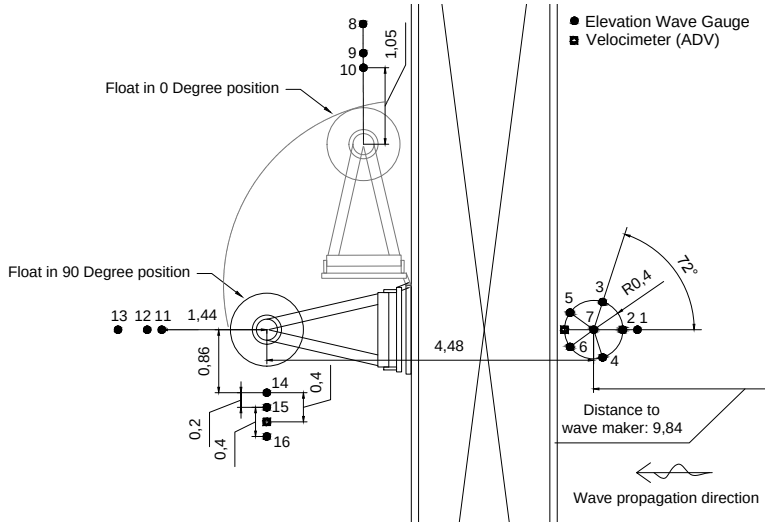

(b) Setup in Plymouth (1:5)

Fig. 4.3: Laboratory setups for small- and large-scale experiments.

4.2 Experiments in Aalborg

Fig. 4.4 shows the setup of the first experiments. For a more in-depth explanation of the experiments carried out see the technical report in Appendix F. The setup used a six-axis force sensor that was selected to be able to obtain both the vertical and horizontal force components with a fine accuracy. The float was placed in the current channel to determine the drag coefficient, as this was anticipated to be difficult to obtain in dominated waves ($H/D \leq 1$) [61]. With constant velocity the Morison Equation reduces to a pure drag. A moulinet propeller, ultrasonic velocimeter and a Laser Doppler Velocimeter (LDV) were used to determine the velocity. Fig. 4.5 shows the results of the experiments that seemed to support the results found in precious studies.

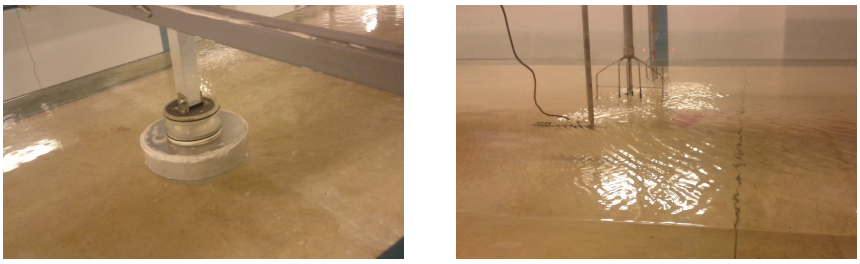

(a) Float in current flume **(b)** Current measurement equipment

Fig. 4.4: Setup of experiment in stream canal. (a) shows the float and water sensitive 6-axis load sensor. In (b), the moulinet propeller is closest with the ultrasonic velocimeters behind.

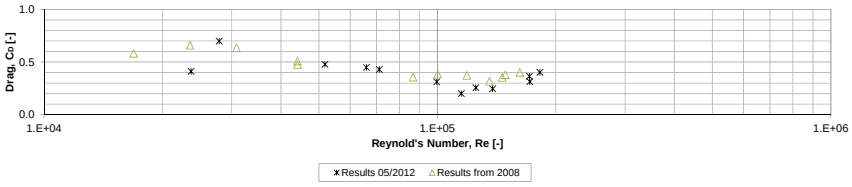

Fig. 4.5: Horizontal drag components from experiments compared to past results.

In later experiments it was decided to switch to a glass fiber shell instead of the old styrofoam float, cf. Pic. 4.6. This made it possible to include pressure sensors in the shell for the next round of experiments.

Using the six-axis force sensor and a newly acquired ADV it was finally possible to determine the inertia coefficient with a satisfactory accuracy. The results of both drag and inertia from these experiments are shown in Fig. 4.7. Then using Figs. 4.5 and 4.7, Morison's equation, and wave theory the inertia

(a) Current flume **(b)** Wave Basin

Fig. 4.6: Fixed glass fiber float with 11 pressure sensors. The translucent water is due to the seeding compound used for the ADV. (a) shows one of the highest current velocities achievable.

and drag forces can be determined on the float for any combination of wave height and period.

Unfortunately the pressure sensors were not as accurate as hoped for and suffered with a high thermal hysteresis. So with the experiences from Aalborg it was decided to increase the scale of the experiments. Colleagues at the department had successfully managed to use larger pressure sensors to measure breaking waves, so these were included in the considerations for the new setup.

Section 4.3 covers the experiments that followed in Plymouth. With only three weeks of testing it was not possible to do all the tests that could be interesting. So the focus was on the experiments that could not be carried out in Aalborg. This could be either due to scaling effects or hardware issues such as those of the pressure sensors. That included measuring the pressures from wave slamming and incident waves impacting from various directions. Unfortunately that meant that only the P controller was thoroughly tested, and the PI control was limited to a single configuration.

Fig. 4.8b shows the setup used for the final set of experiments focused on testing the PI controller in a laboratory setting. The results were presented in Paper C and showed a good correspondance between a boundary element model and the measurements from the experiments.

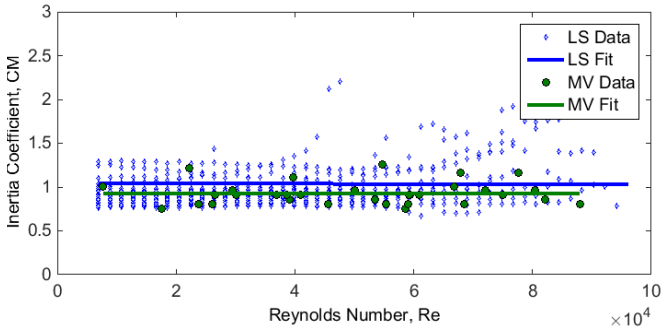

(a) Wave propagation direction (surge)

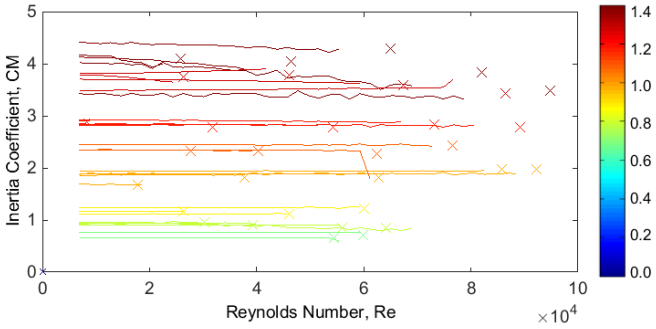

(b) Vertical direction (heave)

Fig. 4.7: Drag and inertia coefficients obtained from the regular wave series in the wave propagation direction. Data point are shown with best fitting tendency lines. (a) has the least squares method in blue and minimum variance in green. In (b) the solid lines are least squares estimates and crosses uses minimum variance. The color of the line is the wave period with values found in the color bar.

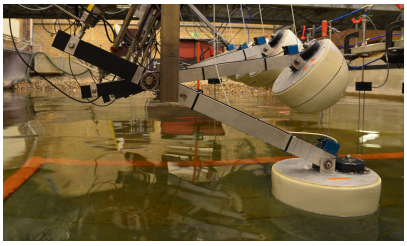

(a) Profile of float and arm.

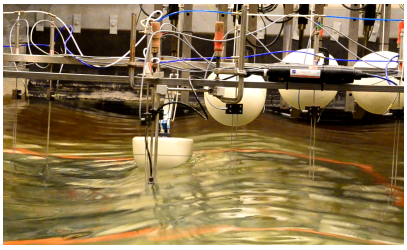

(b) Operation in regular waves.

Fig. 4.8: Experiments with PTO in Aalborg 2015.

4.3 Large-Scale Experiments

Based on the experiences in Aalborg it was decided to increase the scale of the experiments. A suitable model had already been used previously in the real sea testing site at Nissum Bredning, Denmark. In order to make the plans economically viable it was necessary to get external funding. Applying for the MARINET program seemed like the best option. The Ocean Wave Basin at Plymouth University was part of this program and fit the specifications required. The application was accepted providing four weeks of access to the facility.
The purpose of the Plymouth project was to investigate the wave-body interactions on a large-scale model. As there was no do-over in the project and limited time, it was important to select the tests carefully and have a sufficient sensor coverage.
Working together with the staff at the facility the preparation of the device was undertaken in Denmark. As the device was being prepared a 3D model was made (cf. Fig. 4.9a) to make sure that the frame fit, that there was room for the hydraulic and electrical station, etc. Using the option to study abroad with the doctoral school in Aalborg, the author went to Plymouth on September 15, 2013 to see the facility, equipment and meet the staff. The device was shipped to Plymouth on November 1 and was installed during the first week of testing. Fig. 4.9b shows the setup.
The MARINET application and infrastucture access report is included in Appendix G. The initial results are presented in Paper E and in greater detail later in Paper A.

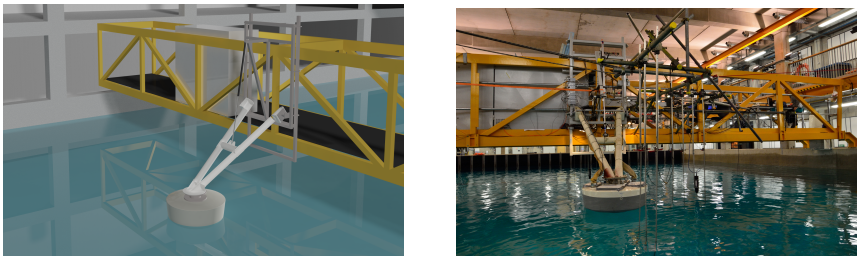

(a) Visualization from 3D model **(b)** Photo taken from the facility

Fig. 4.9: Setup in the Plymouth Ocean Wave Basin.

4.3.1 Setup

From the Nissum Bredning device the arm and hydraulic control station were reused. The selected float was an unused spare. Holes were cut in it to fit

pressure sensors[1] and provide access through hatches in the top, as seen in Fig. 4.10a. As indicated in Fig. 4.3b it was possible to turn the setup by rotating the frame, shown by example in Fig. 4.10b. Experiments were carried out with the frame rotated to 0, 45 and 90 degree angles respectively. At 0-degree rotation the results are comparable to the new experiments in Aalborg presented in Paper C. When it is turned 90 degrees it is comparable with the older experiments in Appendix F.

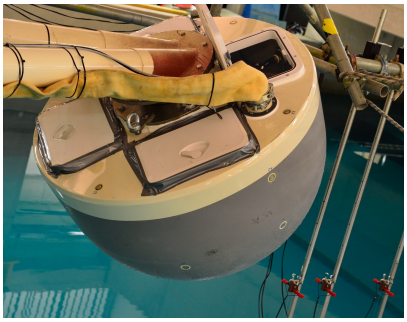

(a) Pressure sensors in shell

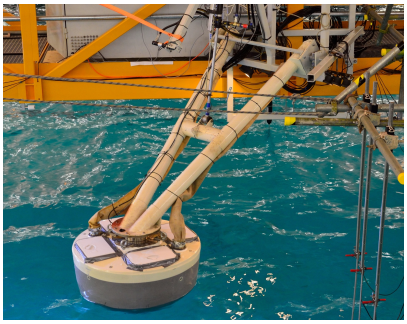

(b) Experiment at 45 degree angle

Fig. 4.10: The float was equipped with a number of sensors. (a) shows some of the pressure sensors. Three pressure sensors were placed around the device 45 degree apart. An additional sensor was place above the water level with 90 degrees of separation. Four sensors were placed in the lid to measure over topping.

4.3.2 Expteriments

During the three weeks of testing the experiments carried out could be divided into three groups: The calibration and characterisation phase A, the operation test phase B, and the extreme condition phase C.

A1. Environmental sensor equipment, generation software, DAQ and cameras are tested. Simple wave and current time series are initiated, measuring the characteristic of the basin with the environmental sensors.

A2. Slow motion in air (static test) to determine centre of gravity and weight. Fast motion in air (dynamic test) to determine mass inertia moment. Decay test to determine the eigen frequency.

A3. Slow submergence in water (static test) to determine hydrostatic stiffness.

[1]GE, UNIK 5000, ± 5 mH2O, pmp5036-TA-A3-CC-H0-PHGA with modification for flush mounting

B1. Fast sinusoidal motion in still water (dynamic test) to determine wave radiation moments (hydrodynamic added mass and damping).

B2. Fixed float in waves to determine wave excitation moments.

B3. Freely moving float in waves and experimentation with different control settings.

C1. Bottom-slamming in still water. Float is released from high position and hits the water with a high velocity, and the impact pressures on the shell are measured (estimation of slamming coefficient).

C2. Wave slamming (Freak waves composed of an optimized set of waves).

To finish the experiments within the allotted time, some compromises were made. Fortunately this mostly meant reducing the duration of the irregular waves. As significant noise from cross waves was anticipated in the long (30-60 min.) irregular time series it would be necessary to do undisturbed experiments as well. With seven selected sea states and all the different scenarios in B2 and B3, it was decided to use the shorter samples instead (100 waves). The plans to do the regular wave experiments with current were dropped as the turbulence intensity and temporal fluctuation were deemed too great.
It was decided to do experiments with both bottom-slamming and freak waves to get a more comprehensive insight into the impact loads on the device. The device was dropped with and without the hydraulic oil and from different heights to get a range of velocities and peak pressures. The first experiments were sampled at 500 Hz, which turned out to be too low and it was increased to 4000 Hz in the later drops. The freak waves, designed by the staff in Plymouth were made as both long- and short-crested plunging waves.

4.3.3 Results and discussion

Keeping the float completely sealed was a challenge, and it started to take in water in the four weeks of testing. With so many pressure sensors in the shell this was an anticipated risk, and in the end this change in weight was accounted for and included in the numerical WAMIT model. As seen in Fig. 4.11 the inertia coefficients were determined for both vertical and horizontal loads and compared to the numerical model. While the horizontal inertia coefficient is close to constant in the experiments, the vertical coefficient changed with the wave period and should be taken into account when calculating the inertia forces.

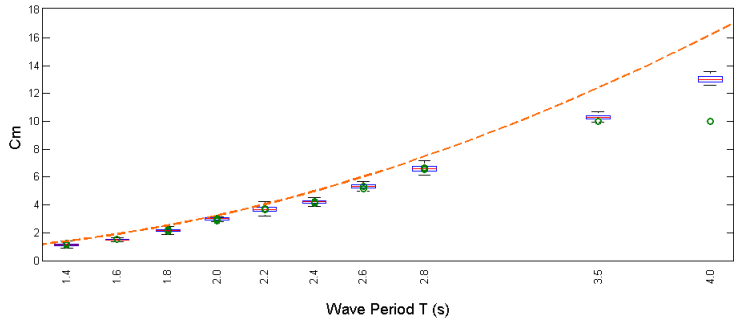

(a) Wave propagation direction (surge)

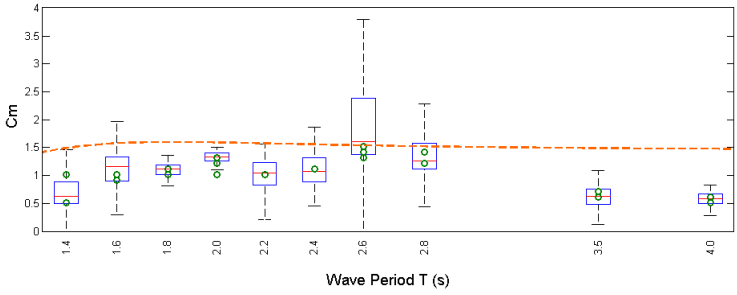

(b) Vertical direction (heave)

Fig. 4.11: Inertia coefficient for both heave and surge. The results of the least squares method are displayed using the red line as the median, the blue edges are the 25th and 75th percentiles, and the black whiskers are extreme data (not considered outliers). The green circles are values obtained from the minimum variance method and the blue dashed line is from WAMIT.

The operating range of the pressure sensors was exceeded by a great margin in some of the drops. Fortunately a few of the drops damped by the hydraulic oil were within measuring range. The successful tests led to a good comparison with the empirical expressions for piles presented in Fig. 4.12. The 5 kHz frequency response of the sensor and the 4 kHz sampling rate seemed sufficient to detect the general shape of the peaks[2].

[2]Suitable studies on sampling frequency convergence could not be found. The studies found has not taken into account the scaling effects, i.e. the surface subjected to the impact, the impact velocity etc.

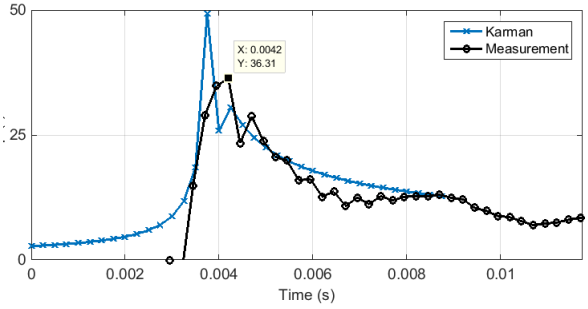

Fig. 4.12: Slamming pressure coefficient during sensor impact with water surface.

References

[59] T. L. Andersen, *WaveLab*, 2010, version 3.0 and 3.34. Download: 03-05-2010. [Online]. Available: http://hydrosoft.civil.aau.dk/wavelab/index.htm

[60] T. L. Andersen and P. Frigaard, "Wave Generation in Physical Models: Technical documentation for AwaSys 6," Department of Civil Engineering, Aalborg University, Tech. Rep., 2014.

[61] S. Chakrabarti, *Hydrodynamics of Offshore Structures*. WIT press, 1987.

[62] J. R. Chaplin, "Development of stream function wave theory," *Journal of Coastal Engineering*, no. 2, pp. 179–205, 1980.

[63] R. A. Dalrymple, "Directional wavemaker theory with sidewall reflection," *Journal of Hydraulic Research*, vol. 27, no. 1, pp. 23–34, 1989.

[64] R. E. Kalman, "A new approach to linear filtering and prediction problems," *Journal of Fluids Engineering*, vol. 82, no. 1, pp. 35–45, 1960.

[65] B. Khorsandi, L. Mydlarski, and S. Gaskin, "Noise in Turbulence Measurements Using Acoustic Doppler Velocimetry," *Journal of Hydraulic Engineering*, vol. 138(10), pp. 829–838, 2012.

[66] E. Mansard and E. Funke, "The Measurement of Incident and Reflected Spectra Using a Least squares Method," *Coastal Engineering Proceedings*, vol. 1, no. 17, pp. 154–172, 1980.

[67] N. . N. Panicker and L. E. Borgman, "Directional Spectra From Wave-Gage Arrays," 1970, pp. 117–136.

[68] T. L. Wahl, "Discussion of "Despiking acoustic doppler velocimeter data" by Derek G. Goring and Vladimir I. Nikora," *Journal of Hydraulic Engineering*, vol. 129, no. 6, pp. 484–487, 2003.

Chapter 5

Conclusion

5.1 Summary

First and foremost the presented work has been focused on determining loads on a point absorbing WEC and then secondly on optimizing the electrical power output. This has included the study and characterization of loads in normal operation and extreme conditions. It has also been a look into the pressure distribution and, to a larger extent, the peak pressure during extreme conditions.
The initial work was done in small-scale experiments with a device fixed in place. During the three years of the project the models and methods were progressively refined. This eventually led to the large-scale experiments in Plymouth and the refined model in Aalborg.
The large-scale model was used to characterize the loads in a wide range of scenarios. One of the reasons being to compare the model with small-scale experiments and the data acquired from experiments from the Hanstholm machine. Only limited work was done with regards to control of the device. Instead this was done later in Aalborg using a smaller model. Here the traditional P and PI controllers were examined thoroughly both with experiments and simulation.

5.2 Original Contribution

The following is considered the main contributions of the work carried out:

- Characterisation of wave-body interactions for wave energy device. Herein publishing useful methods and procedures to determine the hydrostatic

and hydrodynamic coefficients and concrete values for the hemispherical point absorber.

- Calculation of drag and inertia contributions both with and without relative motion of the wave energy device. Including the highlight of useful methods and reference values.
- Results from drop tests that supports the use of empirical cylinder models in determining the peak pressures on hemispheres.
- Implementation and comparison of experiments and simulations using proportional and derivative control in both regular and irregular waves. Suggestions on how to properly compare control strategies.
- Assessment and recommendation on inexpensive physical filter to be used in flumes when conducting experiments with combined wave and current.
- Data and documentation from measurement in small- and large-scale experiments.
- Open source GUI based wave generation with array layout generator and analysis tool for both 2D and 3D.

5.3 Future Work Recommendation

With the large amount of recorded data in both small- and large-scale experiments (and from the Hanstholm device) it is possible to do an in-depth study of scaling effects.
The data from the Plymouth experiments could serve a wide variety of purposes, as possible scaling effects should be limited compared to previously obtained measurements. It could be useful to compare more advanced numerical models.
Much more work could be done in determining the pressure distribution during operation and in the drop and freak wave scenarios. It would also be interesting to go into greater depth with the comparison between the pressure buildup during the drop and the freak waves.

Part I

Papers

Paper A

Characterization of loads on a hemispherical point absorber wave energy converter.

M.M. Jakobsen, Scott Beatty, G. Iglesias, M.M. Kramer

The paper has been submitted to the
International Journal of Marine Energy Under review, since Dec. 2014.

The layout has been revised.

Characterization of loads on a hemispherical point absorber wave energy converter.

M.M. Jakobsen[a,*], Scott Beatty[b], G. Iglesias[c], M.M. Kramer[a]

[a] *Department of Civil Engineering, Aalborg University, Sofiendalsvej 11, 9000 Aalborg, Denmark*

[b] *University of Victoria, Victoria, BC V8P 5C2, Canada*

[c] *School of Marine Science and Engineering, Plymouth, Devon, PL4 8AA, United Kingdom*

Abstract

Large-scale experiments were carried out using a hemispherical shaped point absorber with a diameter of one meter, equivalent to scale 1:5 of the Wavestar North Sea prototype. The purpose of the experiments is to determine the hydrodynamics and dynamic loads on the Wavestar wave energy converters. The set-up consists of the hemisphere connected through a rigid arm that pivots on non-moving main structure, which in this case is the gantry of the wave basin. The pitch motion of the hemisphere arm assembly is controlled using a linear hydraulic actuator. Wave and motion induced loads on the floating point absorber in regular waves as well as extreme conditions are presented. Drag, inertia and slamming pressure are determined directly from the experiments. Radiation, diffraction and excitation moments are determined by inviscid boundary element numerical models.

Keywords: Wave energy converter, Point absorber, Experimental, Linear actuator.

1. Introduction

In the past few decades harvesting wave energy has been and still is of significant interest to the marine sector, but very little progress has been achieved towards commercialisation. Wave energy must compete with the well established sectors on the cost of energy (CoE). In order to compete on CoE, the wave energy sector can benefit from the work spearheaded by existing industries, especially the offshore oil/gas and wind sectors. Doing so

*Corresponding author. Tel.: +45 9940 8567

Email address: mmj@civil.aau.dk (M.M. Jakobsen)

has accelerated and structured the development and will hopefully help reach a point where wave energy will be competitive with other offshore renewables. Reducing CoE can be done either by optimizing the absorbed power of the wave energy converters (WEC) or by reducing expences. [1] focused on the former and compared eight different types of devices on the mean annual power absorption. And for the Wavestar device of this study, [11] presented an optimization of the PTO to maximize the generated electrical energy.

In this paper the focus will be to reduce costs by getting a better understanding of the loads on the device. To get closer to this goal it is essential to get a strong understanding of the underlying hydrodynamics and dynamic loads on WEC. Any WEC device failure at this nascent stage of the WEC industry can prove detrimental to not only the device but the sector in general. As improving the survivability of the WECs is in direct conflict with the need to reduce the structural expenses in order to be competitive, it is necessary to obtain a detailed understanding of the loads on the structure. Achieving an optimum between safety and a low CoE must start with the first principles. In this paper the goal is to reduce the assumptions and increase the accuracy when determining the hydrostatic and hydrodynamic loads. This is done by testing a large scale model in a controlled laboratory environment. After determining the wave kinematics from the laboratory results, an inviscid boundary element method (BEM) model is made to estimate the hydrodynamics. The set-up used in the experiments is a single Wavestar WEC, which is a hemispherical point absorber attached to a rigid structure fixed in the seabed. The PTO control is extracting energy through a linear actuator. Experiments with small-scale devices have shown that it is possible to obtain reasonable results in terms of device behaviour and force readings of the actuator, when comparing to numerical models. Examples of this have been achieved in-house using a combination of efficient magnetic actuators and compensating for the friction in the actuator using advanced control schemes, see [14]. However, small-scale physical models are likely sensitive to scaling issues and practical instrumentation problems, particularly when measuring surface pressures and loads during non-linear control of the float. The small pressure sensors needed are less accurate and suffer more from the thermal shock during submergence. To determine the hydrostatic and hydrodynamics, a sub-set of the experiments carried out are used, namely the regular long-crested waves and various step and free decay tests.

2. Experimental Set-up

The large-scale WEC testing was carried out at the COaST Ocean Wave Basin at Plymouth University in November 2013. The COaST Ocean Wave Basin is a 35 m by 15 m wave and current basin with a water depth of 3 m when the adjustable floor is at the lowest position. The device used in the experiments in Plymouth is from the old 38-float testing rig which was deployed in Nissum Bredning for real-sea testing for four years until replaced by the 1/2 scale device outside Hanstholm harbour in 2009, see [8]. The set-up seen in Figs. 1 and 2 consists of a one meter hemisphere with a carbon fiber arm attached in a fixed angle on top of the float. The arm is attached through ball bearings to a large support frame attached to the gantry of the basin.

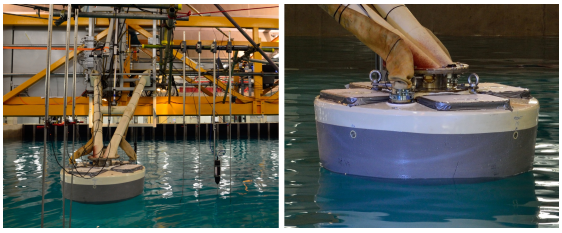

Figure 1: Setup of experiment in Plymouth Ocean Wave Basin.

The support frame has hinges built-in to allow the device to be rotated and locked into 0, 45 and 90 degree positions, see Fig. 3. The primary direction of the float, and the only direction presented in this paper, is referred to as the 90 degree set-up, defined by the arm being perpendicular to the wavefront. Only a select subset of the experiments are repeated for the other directions. The motion of the device is constrained to pitch by ball bearings at the main structure. The pitch of the device is controlled by a hydraulic based piston attached to the support frame and roughly halfway down the arm, cf. 2.
In terms of instrumentation, sensors are located throughout the structure. Two force sensors measuring the three force components are located at the ball bearings, one single degree of freedom sensor is located by the hydraulic

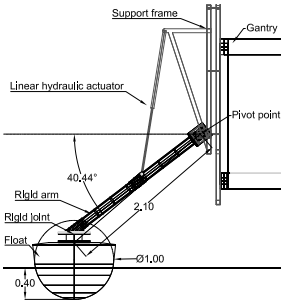

Figure 2: Device geometry as seen from the side, measurements in meters.

actuator near the connection to the arm, and a force and torque sensor measuring all six components (referred to as the 6-axis sensor) is located at the joint between the float and the arm. The pressure exerted on the surface of the float is measured by flush diaphragm pressure sensors, which are distributed in eight discrete directions at five heights including additional four sensors on top of the float. Position and velocity of the float are measured at the cylinder together with an accelerometer on top of the float. The wave and current characteristics are measured using wave elevation gauges and acoustic doppler velocimeter/profilers (ADV) as seen in Fig. 3. Both velocity and elevation are measured in line with the float position and directly in front of it. The ADVs require a seeding material (Potters hollow micro-spheres) dissolved into a liquid solution and added to the water.

2.1. The Wavestar Device

Due to the pitching motion of the device, it is more convenient to define the loads in terms of moments and the motion as angular position, velocity and acceleration. The moments attributing to the loads on the device are defined in terms of the linearized equation of motion in Eq. 1 and shown in Fig. 4.

$$J\ddot{\theta}_A = M_{hs} + M_r + M_e - M_c \tag{1}$$

Where the moment of inertia, J, of the device, is defined in terms of the angular acceleration about the pivot, $\ddot{\theta}_A$. M_{hs} is the hydrostatic stiffness

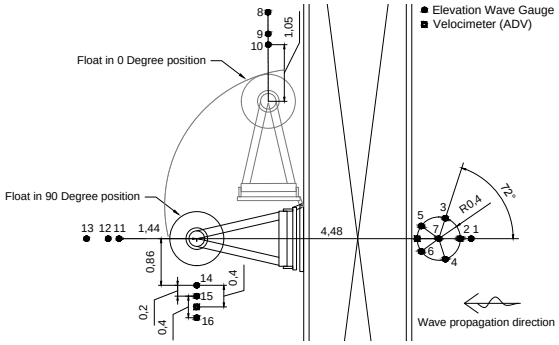

Figure 3: Locations of wave elevation gauges and velocity profilers, measurements in meters.

moment from eigenweight and buoyancy loads, and M_r, M_e and M_c are the radiation, excitation and control moment from the PTO respectively.

Using Eq. 1 the hydrodynamic and hydrostatic coefficients are determined

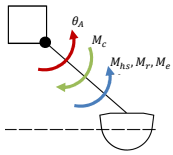

Figure 4: Definition of direction of moments affecting body.

from the set-up of the experiment and used in the numerical model. When determining Morison's coefficients the loads are calculated in the traditional way using forces, leading to Eq. 2 for excitation and Eq. 3 in later cases where the float is moving freely in pitch based on [6].

$$F = \frac{1}{2} C_D \rho A U |U| + C_M \rho V \dot{U} \tag{2}$$

$$F = \frac{1}{2} C_D \rho A (U - U_0) |U - U_0| + C_M \rho V \dot{U} - \rho (C_M - 1) V \dot{U_0} \tag{3}$$

With the particle velocity of the wave, U, the float velocity, U_0, the water plane area and volume, A and V and the drag and inertia coefficients C_M and C_D.

2.2. Selection of sea conditions

The decision on the regular wave characteristics are optimized empirically by gradually approaching the limitations of the facility, by ensuring that the waves created are comparable with the stream function theory and that there are no significant residual energy outside the selected frequencies. A total of 46 regular waves were selected within the limitations as seen in Fig. 5. The largest regular waves achieveble during testing were 0.7 m at wave periods around 2.0 s. The duration of each regular wave condition was set based on the wave number to minimize reflections. After each regular wave, the basin was left to calm so the proceeding wave would not be affected. The samples used in the experiments were most densely populated in the lower range of wave periods, as the recorded wave series showed signs of unbound waves in the higher range.

3. Numerical Estimation of Loads During Body Motion

In this section, the experimental and numerical approaches used to calculate the loads are presented. The goal is to use the results of the inviscid BEM to compare with the results found in the experiments presented in the following section.

3.1. Hydrostatic Stiffness

Because the cross-sectional area at the waterline changes as a function of θ, the hydrostatic force is nonlinear. The hydrostatic stiffness, centre of gravity and gravitational moment are determined using an experiment where the device is slowly lowered from the upper limit of the arm position down into the water to equilibrium, then pushed further into the water until the lower limit of the arm position is reached. The float is then retracted back to the surface and to the upper arm position again. Fig. 7 shows the arm position and the measured loads during a hydrostatic stiffness test. The

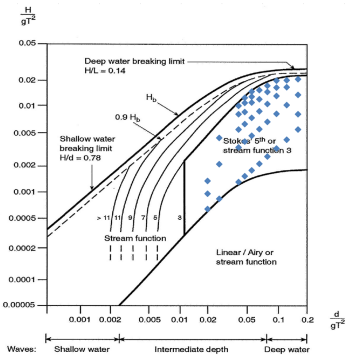

Figure 5: Range and distribution of regular waves. Diamonds indicates each regular wave experiment carried out. [3].

hydrostatic stiffness is determined from the slow submersion and ascension of the device using Newton's second law of motion in Eq. 4. As the velocity $\dot{\theta}_A$ and acceleration $\ddot{\theta}_A$ are low, the contribution from inertia of the device, the radiation moment M_r and the wave excitation moment M_e are negligible leading to Eq. 4.

$$M_{hs} = M_c \tag{4}$$

As the hydrostatic moment is equal to the control moment, the hydrostatic stiffness coefficient k_h is determined using the best linear fit $M_{hs}(\theta_A) = k_h \cdot \theta_A$ in the range $\theta \in [-0.2; 0.2]$, cf. Fig. 6, with resulting coefficients listed in Tab. 1.

3.2. Gravitational Moment

The centre of gravity and gravitational moment are determined using the section of the sample where the device is lowered from storm protection until it reaches the water surface. Again the gravitational moment is assumed to be equivalent to the control moment $M_g = M_c$, and the unknown polar coefficients, θ_g and the angular position θ_A are determined from Eq. 5.

$$M_g(\theta_A) = a_g \cdot cos\,(\theta_A + \theta_g) \cdot F_g \tag{5}$$

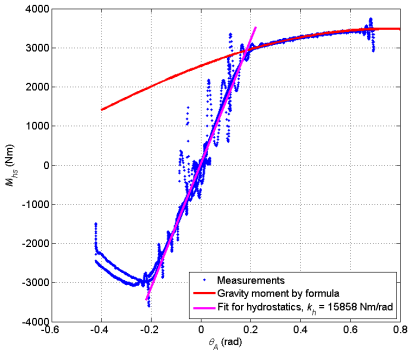

Figure 6: Nonlinear hydrostatic moment from hydrostatic experiment. The linear estimate for the coefficient from $\theta_A \in [-0.2; 0.2]$ and the gravitational moment from Eq. 5 in the range $\theta_A \in [0.2; 0.7]$.

Where F_g is the constant gravitational force determined from the combined vertical components of the bearings and cylinder, see Fig. 7. The resulting coefficient estimates are shown in Fig. 1 and listed in Tab. 1.

3.3. Moment of Inertia

The moment of inertia was determined from two methods. First, a step test, in which the device is released from a suspended position in the air and stopped mid-air by closing a valve of the hydraulic circulation rapidly decelerating the float. While the duration of the decaying vibrations is a fraction of a second, the damped oscillation is useful for analysis if a sufficiently high sampling frequency is used. For this experiment, $f_s = 4kHz$, the angular acceleration can be determined using the accelerometer and derived from the cylinder velocity. However, a significant scatter was prevalent, so a second method was used to determine the moment of inertia using the geometry and the known masses of the device. The two methods showed good agreement with a deviation of less than 2%, so the value found by the first method is used in Tab. 1.

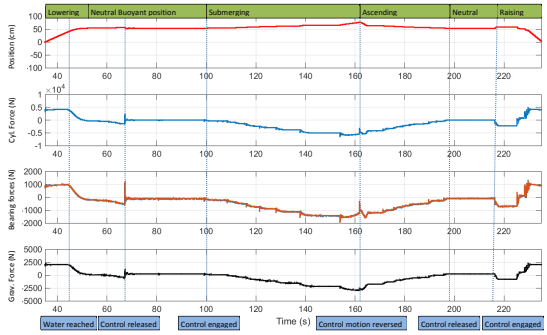

Figure 7: Time series of cylinder position, cylinder force, bearing forces and gravitational force in experiment to estimate hydrostatics.

3.4. Radiation and Excitation Loads

The radiation damping and added mass are first determined from the experiment. To determine the raditaion coefficients, decay tests are used, in which the device is suspended at various heights and release into the water. To achieve the best possible free decay, the hydraulic oil is removed from the cylinder to reduce the friction as much as possible while still monitoring the cylinder position. From the average of three decay tests, the eigenfrequency is found to be $\omega_0 = 3.26\text{Hz}(T_0 = 1.927\text{s})$. The added mass estimate is then determined using $A_{33} = k_h/\omega_0^2 - J = 669$ kgm^2. In Fig. 8 the damping ratio ζ is estimated using exponential Eq. 6, then the damping $B_{33} = 1265$ Nm/(Rad/s) is found using Eq. 7, and included in Fig. 10 for comparison.

$$\theta_\zeta = ae^{-\zeta\omega t} - b \tag{6}$$

$$B_{33} = 2\zeta\sqrt{(m + A_{33}(\omega)) \cdot k_h} \tag{7}$$

Using WAMIT the damping and added mass was determined, using a mesh with 860 polygons and the hydrostatic coefficients found. The mesh shown in Fig. 9 is reduced in size to depict only the submerged section. The section is closed to avoid numerical irregular frequencies in the solutions. The assumption here is that the change in inclination of the float in buoyancy is

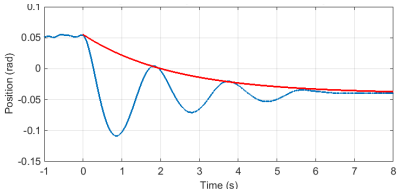

Figure 8: Exponential fit to estimate the damping ratio from decay test.

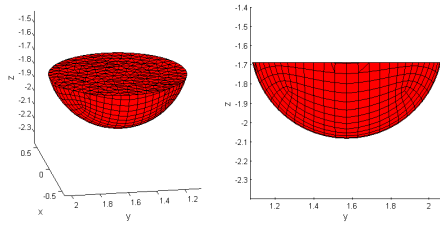

(a) Top view. (b) Side view.

Figure 9: Mesh used in BEM model.

negligible. Fig. 10 shows the added mass and radiation damping as a function of wave period. Fig. 11 shows the amplitude and phase of the wave excitation moments.

3.5. Overview of Hydrostatic estimates

The results of this section are summarized in Tab. 1.

4. Estimation of Loads from Experiments

Using measurements from the experiments, the peak pressures from drop tests are compared with the asymptotic theory. Moving up from the surface of the float to the rigid joint between float and arm, the excitation forces are estimated and compared to the results of the numerical model from the preceeding section. Then the found coefficients are used to calculate and compare with a so-called "free float" case.

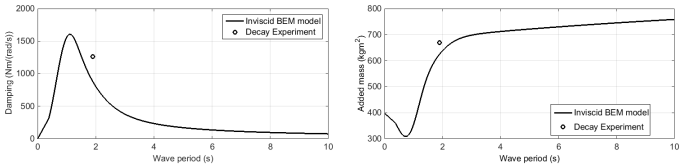

(a) Damping. (b) Added mass.

Figure 10: Radiation damping and added mass from BEM analyses and decay test as a function of wave period.

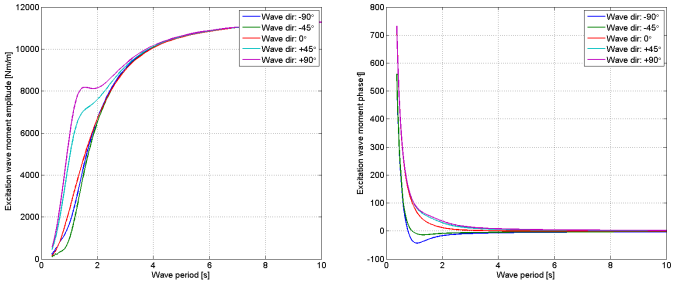

(a) Excitation moment, amplitude. (b) Excitation moment, phase.

Figure 11: Wave excitation moments, amplitude and phase as a function of wave period. The directionality of the waves changed in increments of 45.

4.1. Slamming Pressure Coefficient

As a breaking wave impacts on the float, a characteristic pressure spike occurs, which lasts for a fraction of a second. In spite of the short duration, the slamming forces have caused substantial damage to a float at the prototype installation in the North Sea. To estimate the pressure coefficient the velocity of the impact needs to be high, and while the freak waves are likely, leading to high velocities the best estimate of the velocity is still very crude. So to achieve a more controlled environment, the device is dropped in near free fall to the water surface, see Fig. 12.

Sensors 1 and 6 examined here are highlighted in Fig. 13a, as the tra-

Table 1: Hydrostatic coefficients.

Coefficient description	Symbol	Value
Hydrostatic stiffness coefficient	k_h	15858Nm/rad
Center of gravity from bearings (Polar)	θ_g,a_g	-0.7552rad, 1.848m
Center of gravity from bearings (Cartesian)	x_g,y_g	1.3456m,-1.2667m
Gravitational force of arm and float	F_g/m_g	1885.4N/192kg
Moment of inertia	J	823Nm/(rad/S^2)
Eigenfrequency/period	ω_0/T_0	3.26Hz/1.927s

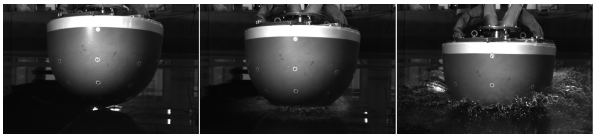

Figure 12: Experiment where hemisphere is released from suspended position and drops into calm water. The drops are captured with highspeed camera.

jectory of the hemisphere is inclined due to the pitching motion. The first sensor to reach the water surface is sensor 6 as seen in Fig. 13b.

The pressure sensors are carefully mounted so the diaphragm is completely flush with the shell surface of the hemisphere. The sample rate of the experiments was set to $f_s = 4$ kHz, and the velocity was deemed to be sufficiently accurate using the velocity and position sensor at the cylinder, and translating the velocity to the vertical component at the pressure sensors. Unfortunately, the pressure sensor range ($\pm$5 mH2O) limited the measureable pressures of the float, creating cut-offs in the high-velocity experiments. To reduce the maximum velocity, free float exsperiments with the hydraulic oil still flowing are used, in which the maximum velocities are roughly a factor four lower. The pressure coefficients from the experiments are determined using Eq. 8, see [6], where C_p is the slamming pressure coefficient and p is the pressure on the float. Fig. 14 shows the results of the two sensors closest to the water surface during impact together with the velocity of the float at the moment of impact. As expected, sensor 6 is the first sensor to hit the water surface and measures a higher value than sensor 1 at the bottom of the float, cf. Fig. 14. The asymptotic theories used in Fig. 14b are derived

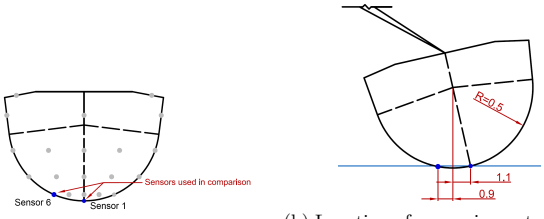

(a) Sensor position and selection.

(b) Location of sensor impact on free surface.

Figure 13: Sensor size and position comparison, scaled based on radius of hemisphere.

for the pressure coefficient from [6] and [9] using the values from Fig. 13b.

$$Cp = p/(0.5\rho U^2) \tag{8}$$

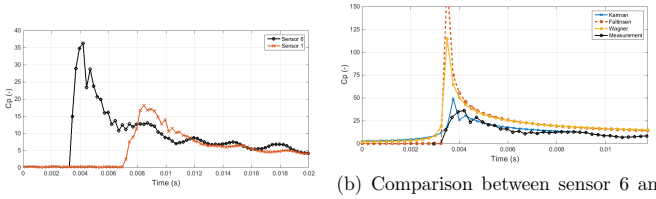

(a) Pressure coef. for sensors 1 and 6.

(b) Comparison between sensor 6 and theory.

Figure 14: Slamming pressure coefficient and velocity during sensor impact with water surface. The peaks of the coefficients being $C_{p,1} = 18$ and $C_{p,6} = 36$.

4.2. Inertia and Drag Excitation Loads

The inertia loads on the device are estimated by analysing data from the force sensor located between the float and arm. To limit uncertainties, the float was locked in place and subjected to $k = 20$ regular waves in order to have as much data as possible while limiting reflections from walls and beach. In regular waves, the direct ADV measurement of fluid particle velocity is compared to esitmates of the velocities using the stream function potential theory [4]. Since there is a good agreement between the velocities

from the theory and the measurements, the stream function waves are used in the calculations to get the velocity at the center of the float. The wave regimes selected for testing the contribution from drag is expected to be low relative to the inertia contribution. To determine the contributions from drag and inertia in both horizontal (heave) and vertical (surge) direction, the wave excitation forces are determined using Morison's equation in Eq. 2. However, as the experiments are all carried out in inertia dominated regime ($H/D < 1.5$), the uncertainties are too high to extract sufficiently accurate values for the drag coefficient through these experiments. Two methods are used to calculate the drag and the inertia coefficients. First, a brute force method where the measured force from the F/T sensor is compared to the predicted force using minimum variance (MLM) and a second method, see [5], where the two coefficients are calculated by a least squares optimum fit approach (LSQ) seen in Eq. 9, where the mean squared error ϵ^2 is minimized with respect to C_M and C_D.

$$\begin{aligned} \epsilon^2 &= \frac{1}{I}\sum_{i=1}^{I}\left(F_{mi} - F_{pi}\right)^2 \\ \frac{\partial \epsilon^2}{\partial C_D} &= \frac{2}{I}\sum_{i=1}^{I}\left(F_{mi} - F_{pi}\right)\frac{\partial F_{pi}}{\partial C_D} = 0 \\ \frac{\partial \epsilon^2}{\partial C_M} &= \frac{2}{I}\sum_{i=1}^{I}\left(F_{mi} - F_{pi}\right)\frac{\partial F_{pi}}{\partial C_M} = 0 \end{aligned} \tag{9}$$

An advantage of the method in Eq. 9 is that it estimates the coefficients from the entire sample and not only the peaks and troughs. The first step is determining the undisturbed elevation and velocity at the location of the float in the following process (with no float). Then using the stream function approximations of the velocities and the force components from the 6-axis sensor at the float, the drag and inertia coefficients are determined for all the regular wave series. Fig. 15 shows the results of both the horizontal (flow direction) and vertical coefficients with respect to wave periods.

Fig. 16 shows the root-mean-squarred (RMS) error between numerical estimations and measured values of the elevation, velocities and forces. Looking at the inertia coefficients from Morison's equation, the horizontal forces appear be constant, cf. Fig. 15a, while there seems to be a quadratic relation with the wave period for the vertical component in Fig. 15b.

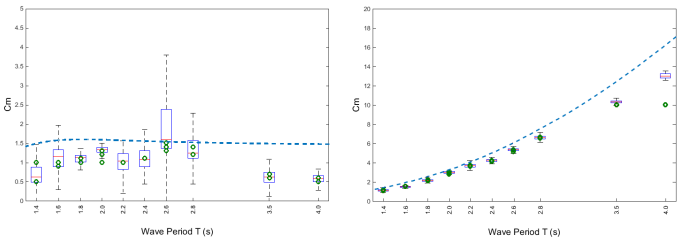

(a) Horizontal inertia coefficient (b) Vertical inertia coefficient

Figure 15: Inertia coefficient as a function of wave period for both heave and surge. The results of the LSQ method are displayed using the red center line as the median, the blue edges indicates the 25th and 75th percentiles, and the black whiskers indicates the extreme data not considered outliers. The green circles are values obtained from the MLM, and the blue dashed line is the inviscid BEM numerical model.

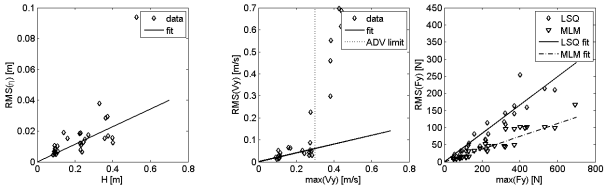

(a) Wave elevation. (b) Horizontal velocity and force.

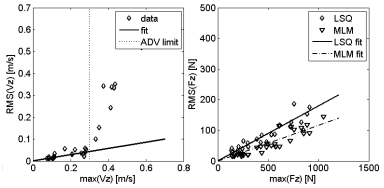

(c) Vertical velocity and force.

Figure 16: RMS error between numerical estimates and measurements.

5. Relative Importance of Loads During Operation.

Using the coefficients found in section 4.2, the forces are calculated for the freely pitching float using Eq. 3. Here, the free motion is carried out

by setting damping and stiffness of the system to zero, but leaving the oil to circulate through the system. As explained in the previous section, it has been necessary to use the wave velocity and acceleration from the stream function approximation. The motion of the device is used from the experiment which is measured redundantly by the accelerometer and by measuring the cylinder position and velocity. By translation and rotation, the forces, velocities and accelerations are calculated for the inertial coordinate system of the float center. The forces shown in Fig. 17 are based on two regular waves, a small and smooth wave within normal operation range and a second wave pushing the limits of the stroke length of the actuator.

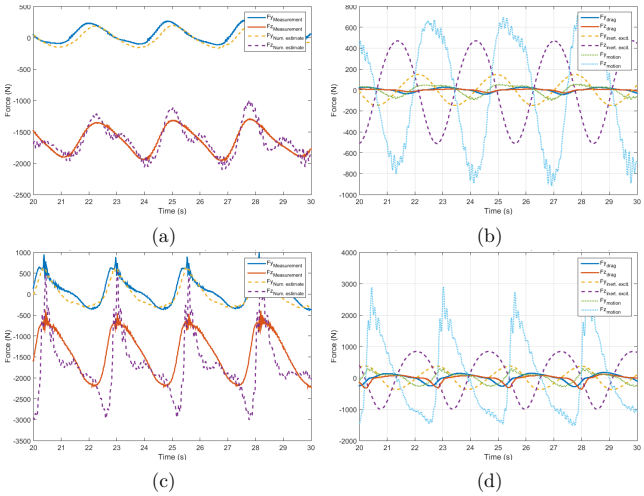

Figure 17: Forces from regular wave experiments with coefficients from section 4.2 and drag contribution $C_D = 1$ based on upper limit values found in past experiments. In (a,b) using a wave with $H = 0.25$ m and $T = 2.8$ s, in (c,d) the largest and steepest wave possible for the set-up, $H = 0.55$ m and $T = 2.2$ s. Figures (a,c) showing the calculated forces compared to measurements. Figures (b,d) showing the drag force and the inertial force divided in excitation and the reduction due to body motion.

6. Discussion & Conclusions

This paper has presented experimental and numerical methods to characterize loads on a large-scale point absorber with hydraulic power take-off. The hydrostatic coefficients for the device were calculated, and an inviscid numerical model was used to determine the hydrodynamics of the device. The Morison coefficients were determined from excitation experiments and showed good correspondance with the results found in the numerical model. Finally, the paper presented application of the found coefficients for a wave within normal operation conditions and one at the limits of the device.

In Fig. 10, the radiation damping and added mass is shown and compared to the result of the decay test of the experiment. The damping in Fig. 10a and added mass in Fig. 10b vary with 31% and 6% between experiment and numerical model. The significant deviation in the former is likely partly due to mechanical damping.

Fig. 14b shows a comparison between pressure coefficients in measurements and theory, using the same sampling frequency. The comparison could suggest that the methods by Faltinsen [6] and Wagner [12] lead to overestimating not only the peak pressures (as suggested in [2]) but also the accumulated energy that needs to be absorbed and distributed by the shell. The method in [7] and [13] is more agreeable with the results found. There are a few explanations that may explain the differences in peak values, one being the sampling frequency and entrapment of air as also suggested in [9], another being the influence of the flexibility of the hemisphere as suggested by Sarpkaya, see [10]. Rather than just seeking the highest possible sampling rate and focusing on the impact force, it might be just as important to look into the material strength of the shell and dynamic response of the system.

Fig. 15 shows the inertia coefficients obtained from both numerical and experimental methods. Comparing the measurements and the numerical model in Fig. 15a, the numerical method appears to reach a higher value of the coefficient, particularly around the higher and lower frequencies, the tendency to use a constant value for the coefficient is justifiable for horizontal loads. For vertical loads, it is apparent from Fig. 15b that a constant value is inadvisable and using one derived from theory of horizontal loads would significantly underpredict the loads for longer period waves. In these experiments, a rule of thumb for the coefficient C_M could be approximated using $C_M \approx 0.5T^{2.5}$. Drag induced loads could not be determined accurately enough from the wave excitation experiments, but as the regime of the waves

was in an inertia dominated regime this was not unexpected.

Fig. 16 shows the RMS error for the numerical estimates of the elevation and velocities. In Fig. 16a, the RMS error is about 5% on average for wave elevation, where the primary deviation is in slight phase shifts and deformations in the shapes of the waves. The reason for the minor phase shift is mostly due to the data being aquired using different DAQs. A synchronization signal was recorded when the wave generation software sent signal to the wave paddles, but this was delayed slightly. Steps were taken to reduce this delay, by taking into account the measured pressures from the shell, and this has reduced the error to an acceptable range.

Several issues arose using the ADVs as seen in Fig. 16b and 16c. For the lower section, the seeding was problematic in such a large basin. It was sought to keep with the Signal-to-noise ratio (SNR) above the recommended 15 dB, though this proved to be difficult at times in spite of the near neutral buoyancy of the seeding material. But a more significant issue occured with wave run-up and overtopping of the sealed ADV power supply that would make the ADV stop recording. This means that for most experiments the actual waves were not measured properly and the numerical results were used instead. With a RMS error of about 15%, the fact that the numerical approximations have been used has probably affected most of the results, but it has not had an detrimental effect as there are reasonably good agreements between measurements, theoretical and numerical models.

The final results using the coefficients from the excitation experiments to determine loads on the freely floating device seen in Fig. 17 were satisfying. The coefficients in Fig. 17a were $C_M(y,z) = (1.5, 6.0)$ and $C_M(y,z) = (1.5, 4.1)$ for Fig. 17c. The fluctuation in F_z is likely due to simplifications in the numerical model, particularly in the decision to keep the submerged volume constant. The spurious peaks in Fig. 17c could be due to unbound second order waves occuring with the steep wave. These unbound waves are not accounted for in the calculation of the velocity and acceleration of the waves, but they are included indirectly in the measurement of the body motion through the measurements. As seen in Figs. 17b and 17d, the drag contribution is small as could be expected. It may be observed that the vertical and horizontal acceleration components of the float are in phase due to the pitching motion. The vertical forces from wave excitation will be in counter phase whereas the horizontal forces are partly in phase contributing to an increase in the combined horizontal load on the device.

Acknowledgements

The authors wish to express their sincere gratitude to the technical staff and research group at the COaST facility. They also acknowledge the financial support of, MARINET, a European Community - Research Infrastructure Action under the FP7 Capacities Specific Programme. Additional acknowledge goes to the Danish ForskEL-programmes by Energinet.dk and partners in FLOAT2, "New Flexural UHPC Application for Wave Converters 2" and "Digital Hydraulic Power Take Off for Wave Energy".

References

[1] Babarit, A., Hals, J., Muliawan, M.J., Kurniawan, A., Moan, T., Krokstad, J., 2012. Numerical benchmarking study of a selection of wave energy converters. Journal of Renewable Energy 41, 44–63.

[2] de Backer, G., Vantorre, M., Beels, C.,de Pre, J., Victor, S.,de Rouck, J., Blommaert, C.,van Paepegem, W., 2009. Experimental investigation of water impact on axisymmetric bodies. Journal of Applied Ocean Research 31, 3, 143–156, 10.1016/j.apor.2009.07.003.

[3] Chakrabarti, S. K., 1987. Hydrodynamics of Offshore Structures. WIT press, Plainfield, Illinois 978-0905451664.

[4] Chaplin, J. R., 1980. Development of stream function wave theory. Journal of Coastal Engineering 2, 179–205.

[5] Dean, R. G., Dalrymple, R. A., 1984. Water wave mechanics for engineers and scientists. Prentice-Hall, Englewood Cliffs, NJ 07632 0-13-946038-1.

[6] Faltinsen, O. M., 1990. Sea Loads on Ships and Offshore Structures. Cambridge Univ Press, Cambridge, UK Ocean Technology, 0-521-45870-6.

[7] von Karman, T., 1929. The impact of seaplane floats during landing. National Advisory Committe for Aeronautics, Washington, Technical note no. 321,

[8] Marquis, L., 2014. Wavestar - 4 years of continuous operation in the North Sea, in: Proceedings of the the 5th International Conference on Ocean Energy (ICOE), Halifax, Nova Scotia Canada.

[9] van Nuffel, D., 2014. Experimental Study of the Slamming Induced Pressures, Forces and Deformations of Quasi-Rigid and Deformable Bodies during Vertical Water Entry. Dissertation. Ghent University. Faculty of Engineering and Architecture, Ghent, Belgium, 9789085786832.

[10] Sarpkaya, T., 2010. Wave Forces on Offshore Structures. Cambridge Univ Press, Cambridge, UK, 978-0-521-89625-2.

[11] Vidal, E., Hansen, R., Kramer, M. M., 2012. Early Performance Assessment of the Electrical Output of Wavestar's prototype, in: Proceedings of the the 4th International Conference on Ocean Energy (ICOE), Dublin, Ireland.

[12] Wagner, H., 1932. Über Stoß- und Gleitvorgänge an der Oberfläche von Flüssigkeiten. Journal of Applied Mathematics and Mechanics (ZAMM) 125, 193–215.

[13] Wienke, J., Oumeraci, H., 2005. Breaking wave impact force on a vertical and inclined slender pile–theoretical and large-scale model investigations. Journal of Coastal Engineering 52, 435–462.

[14] Zurkinden, A., Ferri, F., Beatty, S., Kofoed, J. P., Kramer, M. M., 2014. Non-linear numerical modeling and experimental testing of a point absorber wave energy converter. Journal of Coastal Engineering 78, 11–21.

Paper B

Damping of unwanted turbulence in wave-current experiments

D. Markus, M.M. Jakobsen, K.-U. Bletzinger, P.B. Frigaard

The paper has been published in the
Coastal Engineering Vol. 96, pp. 38–48, 2014.

The layout has been revised.

Damping of Unwanted Turbulence in Wave-Current Experiments

D. Markus[☆a,*], M.M. Jakobsen[☆b], K.-U. Bletzinger[a], P.B. Frigaard[b]

[a] *Lehrstuhl für Statik (Structural Analysis), Technische Universität München, Arcisstr. 21, 80333 Munich, Germany*
[b] *Department of Civil Engineering, Aalborg University, Sohngaardsholmsvej 57, 9000 Aalborg, Denmark*

Abstract

Laboratory testing of structures placed in combined wave-current flows is a valuable source of information for the fulfillment of offshore engineering related tasks and the development of ocean energy devices. In recirculating wave-current flumes, one of the problems encountered during such experimental studies is the occurrence of undesirable current induced velocity fluctuations. These fluctuations often result in significant disturbances of the generated wave profiles. In this paper, a physical flow filter is introduced that significantly reduces fluctuations in the current profile while permitting wave passage. This is achieved by passing the wave-current flow through a setup of perforated net tubes that allows for both horizontal and vertical flow motion. An in depth investigation of the properties of different filter configurations is presented, focusing on the reduction of turbulence intensities in the flow field as well as the influence of the setup on waves.

☆These authors contributed equally to this paper.
*Corresponding author. Tel.: +49 89 289 22422; fax: +49 89 289 22421
Email address: d.markus@tum.de (D. Markus☆)

The filter characteristics are quantified in terms of its deflection, absorption, and transmission properties. It is shown that the overall setup effectively reduces velocity fluctuations, resulting in stable wave-current conditions and allowing for high quality laboratory testing.
Keywords: filtering, turbulence, flow-smoothing, waves, wave-current interaction, flume

1. Introduction

Ocean environments relevant to offshore engineering applications are often encountered as a combination of waves with an underlying current. Such combined conditions are of high interest in various fields: They play a vital role in the development of ocean energy devices, such as tidal turbines or wave energy converters, or in fundamental studies of sediment transport and scouring, to name a few. As part of such studies, it is often desirable to carry out laboratory testing. However, an efficient and accurate generation of wave-current conditions remains to be a challenging task.

A number of experimental setups have been designed in order to model waves in combination with a current. In the design of a structure or device subjected to wave-current conditions, one approach is to utilize a wave towing tank. Previous experimental studies following this concept have for example been carried out by Barltrop et al. (2007), Galloway et al. (2010), as well as Faudot and Dahlhaug (2012). These experiments aimed at modeling tidal turbine behavior in wave-current conditions. Towing tank experiments do not require the generation of a current as part of the experimental setup. However, as discussed by Myers and Galloway (2011), the free stream

turbulence levels from the current are zero when carrying out a towing tank experiment, because the water in the free stream is only subjected to the wave motion. Furthermore, the boundary layer of the current is not represented in this approach, which is particularly problematic in the case of bottom mounted structures. Therefore, the physical characteristics of the flow are only partially considered in towing tank experiments.

The alternative is to utilize a recirculating water channel in combination with a wave maker. This approach was followed by de Jesus Henriques et al. (2013). In the suggested setup, the water is directed through a flow straightener at the inlet of the channel. Prior to entering the working section, the water flow passes under a hinged wave paddle located on the water surface. Using an electrical motor, the paddle generates waves by oscillating vertically. The resulting wave-current field generated with this setup agrees well with theoretical reference solutions and studies of tidal turbines were carried out on its basis. A trade-off with this type of wave-current flume is the inherent limitation in the wave height to water depth ratio.

This is likely part of the reason why a majority of flumes consist of a vertical wave paddle with the current typically entering the channel in front of the paddle, or below the paddle. Under such conditions, the current will have a strong circulatory motion in the inlet region, particularly when the inlet pipe is oriented vertically. As assessed by Nowell and Jumars (1987), these circulations propagate through the flume for about 20 times the inlet diameter. This distance is usually beyond the test section and thus the flow field will not consist of a simple boundary layer in the vicinity of testing.

Several approaches have been developed to unify and straighten flows

in pure current flumes. At present, this is usually achieved by passing the flow through a wire mesh screen and a honeycomb (Kulkarni et al., 2011). Flow distribution control using screens is well established and was analyzed in detail by Laws and Livesey (1978), including calculations that can be used to predict the effects of the screen on the flow field. Although screens can be used effectively to either suppress or generate turbulence in the flow, their functionality in essence is limited to flows that are already well developed, as pointed out by Nowell and Jumars (1987). The dissipation of large-scale motion in a flume is achieved more effectively using honeycombs. Here, the flow is passed through an assembly of horizontal ducts in order to break down large-scale motion. The characteristics of honeycombs and the optimal geometric dimensions to reduce turbulence in a flow were analyzed and documented by Mikhailova et al. (1994). Scheiman and Brooks (1981) analyzed both screens and honeycombs and concluded that a combination of the two setups is the most effective approach to reduce turbulence in a flow. This setup is specifically designed and optimized for pure current scenarios, while it is not intended to function in combination with waves. The closed chamber walls of a honeycomb serve to break down the vertical motion, which would also affect wave induced vertical velocities. This motivates the introduction of alternative experimental methods that are specifically geared towards wave-current scenarios.

In this paper, a physical flow filter is introduced that serves the purpose of diffusing undesirable velocity fluctuations in the current flow, while simultaneously allowing for the passage of waves. The filter consists of net tubes that permit fluid motion in both horizontal and vertical direction.

The setup consists of vertically placed tubes to diffuse turbulence from the current, as well as horizontally oriented sections that act as a flow straightener. A detailed description of the filter layout and experimental setup used to test the filter is given in the succeeding sections. Following, the results of an elaborate test series are documented, which describe the characteristics of different filter configurations in waves and currents. It is shown, that the setup allows for the generation of stable and well formed wave-current conditions. The filtering technique is a low cost approach to enhancing recirculating wave-current flumes consisting of vertical wave paddles, allowing for laboratory testing of devices and sea floor conditions in wave-current environments.

2. Filter Description

The basic concept of the filter setup is to diffuse turbulence in the flow field, while permitting a vertical flow through the setup. This is achieved by utilizing perforated net tubes. The flow is directed through an arrangement of vertical tubes that function similar to a flow screen. In this filter section, the water can move freely in the vertical direction. In addition, horizontally oriented tubes can be added to the setup to act as a flow straightener. These function similar to a honeycomb, with the distinct difference that a flow through the tube walls in the vertical direction is possible.

Prefabricated tube blocks, typically used in drainage systems and waste-water treatment plans, allow for a simple and quick assembly of the filter setup. In this study, the BIO-BLOK® 80 HD G produced by EXPO-NET Danmark A/S was used. The tubes are made of polyethylene

and are welded together to form square blocks of dimensions 0.54 m x 0.54 m x 0.55 m. The individual tubes have an inner diameter of 5.5 cm and the tube walls consist of a 0.2 cm thick mesh with a mesh size equal to 0.8 cm x 0.8 cm. This leads to a horizontal free flow area through the tubes equal to approximately 70%, a vertical free flow area through the tube walls of approximately 40%, and an overall void percentage is 95%. The individual blocks are lightweight (approximately 60 kg/m^3) and can be combined and cut easily to fit into the designated flume section.

For this experimental study, the filter blocks were cut in half and combined to span across the width of the flume. In the vertical direction, the blocks were stacked to a height of approximately 1 m. A total of four such segments were built: two segments, referred to as 'h', consisting of tubes pointing in flow direction (Fig. 1a), and two segments, referred to as 'v', with a vertical tube orientation (Fig. 1b). The four segments were combined to form different filter configurations (1v0h, 1v1h, 1v2h, and 2v2h), which were tested individually in order to determine an optimal setup configuration. The different arrangements are given in Tab. 1. An example of the installed filter for configuration 2v2h is shown in Fig. 2.

3. Experimental Setup

A detailed analysis of the introduced filtering concept was carried out in the Aalborg University (Denmark) wave-current flume. The flume consists of a piston wave maker as well as a recirculating water pump that drives a current from the outlet to the inlet of the flume through pipes located below the flume floor. A layout of the flume is given in Fig. 3. The flume bottom

is horizontal in the test section and slopes towards the wave paddle at an inclination angle of approximately 3°. In order to absorb the main part of the incident energy from waves at the outlet, an adjustable absorption beach was used, covered by porous absorption material. The water depth for all conducted tests was 0.35 m in the test section, corresponding to 0.70 m at the location of the wave paddle.

The overall aim of the study was to characterize the effects of the filter on the ensuing flow field. For this purpose, a total of eight resistance type wave gauges were installed in the flume, in order to measure the surface elevation and carry out a reflection analysis. Four of these wave gauges were situated between the wave paddle and the flow filter, while the remaining four wave gauges were installed in the test section between the flow filter and the absorption beach. In addition, a Nortek Acoustic Doppler Velocimeters (ADV) was installed in the test section. The sampling volume is a cylinder of 6 mm diameter and 5 mm height, measured 5 cm below the sensor head. Because the ADV measures acoustic signals reflected by particles in the flow, a seeding material (Potters hollow microspheres) is added to the water. By adding this compound, a signal to noise ratio (SNR) higher than 20 dB was ensured throughout the duration of the experiments. This ratio adheres to the manufactorers' suggested 15 dB minimum. Using the ADV, three dimensional flow velocities were measured 0.15 m below the water surface at a sampling rate of 25 Hz. The ADV recordings were also used to compute the turbulence intensity in the test section, an approach analyzed thoroughly by García et al. (2005) and previously applied successfully in various experiments, such as those carried out by Hendriks et al. (2006) and

Chamorro et al. (2013). Studies by Chanson et al. (2007) and Khorsandi et al. (2012) have shown that the data should be post-processed to remove unphysical noise, as discussed in the subsequent section. The precise wave gauge and ADV locations as well as the filter positioning in the flume is given in Fig. 3.

4. Filter Analysis

4.1. Current Scenario

In a first step, the effect of the flow filter on velocity fluctuations and turbulence intensity in a pure current scenario is demonstrated. Three current velocities are analyzed in a water depth of 0.35m, as given in Tab. 2. The flow velocities for each current are measured over a period of 3 minutes using the ADV positioned in the test section. The selection of a 3 minute sampling duration is the result of an unfiltered 60 minute sample analysis. The collected data was split into 3 minute sub-samples, which renedered a mean turbulence intensity variability of 7.3% compared to the full 60 minute sample, with a maximum deviation of 15.0%. Furthermore, when considering a 20 minute sample, the mean variability was only further reduced by 0.5%. Overall, the 3 minute sample was considered adequate for the performance analysis of the setup, and preferable beause it allowed for testing of a great number of setups and conditions. Examples of recorded 3 minute test data for selected filter configurations are shown in Fig. 4.

In order to evaluate the characteristics of each flow field, the mean three-dimensional velocities $\overline{U}$ are compared to the three dimensional velocity fluctuations U'. The latter is defined as the root mean square

(RMS) of the recorded horizontal velocity data. From these values, the turbulence intensity I can be computed based on the following definition:

$$I = \frac{U'}{\overline{U}} \tag{1}$$

Although ADV velocity recordings are a popular approach to determine experimental flow conditions, the recorded data may contain spurious peaks due to Doppler signal aliasing or air bubbles, as assessed by Voulgaris and Trowbridge (1998). These unphysical spikes in the data set are recorded together with the physical turbulence components of the flow, thereby distorting the true flow characteristics. In order to avoid incorporating these unphysical components in the computation of the turbulence intensity, a despiking algorithm is applied to the data set to remove the ADV spike noise. In this paper, phase-space threshold despiking is applied, as introduced by Goring and Nikora (2002) and modified by Wahl (2003). The basic concept of the method is to take advantage of the characteristic of good ADV data to be tightly clustered within an ellipsoid in 3D phase space, defined by the velocity recordings as well as approximations of their first and second derivative. In an iterative procedure, those points outside of the ellipsoid are eliminated, thereby despiking the data set. As discussed by Mori et al. (2007), the approach is very efficient, and has the advantage of not relying on empirical coefficients. It should be noted that Khorsandi et al. (2012) has pointed out that the method will likely overpredict the actual RMS value of the velocity and that doppler noise (white noise, uncorrelated with mean velocity) has the same negative effect on the RMS estimates. However, as the primary comparison made in this paper deals with the same mean

velocities, it is assumed that the effect is beningn when comparing the data.

The horizontal and vertical RMS velocity fluctuations u' and v' from the despiked ADV data recorded in the test section are plotted in Figs. 5a and 5b, respectively. The Reynolds stresses, turbulence kinetic energy, and turbulence intensity are all defined as a function of these velocity fluctuations, giving a measure of the flow turbulence. Overall, the filter setups have a similar affect on both the horizontal and vertical fluctuations, resulting in a significant reduction compared to the unfiltered configuration. This reduction is further assessed based on the turbulence intensities plotted in Fig. 5c and documented in Tab. 3. The relatively high intensities ranging from 7% to 9% in the case of the unfiltered flow, decrease dramatically even when only one filter section is positioned in the flume. Introducing additional filter sections further reduces the turbulence intensity, although the reduction is relatively small in comparison. In the case of higher flow velocities, all combinations of tested filters results in a turbulence intensity of 2% to 4%, which amounts to a reduction of 70% when compared to the unfiltered result.

The findings are further supported by injecting red dye into the flume through a narrow tube and recording the flow with an underwater camera. Care was taken, that equal amounts of dye were injected into the test section for each recording. The resulting images for the unfiltered and filtered 2v2h setup are compared in Fig. 6 for the C1 current case at a distance of approximately 25 cm from the dye-inlet. The noticeable spread of the dye filament in Fig. 6a is evidently a result of high turbulence in the flow. By introducing the flow filter, the flow becomes significantly more steady, allowing for a visualization of smaller eddies due to a more concentrated dye

propagation in Fig. 6b.

Overall, the tests show that an introduction of the flow filter into the setup results in a significant decrease in turbulence intensity and a unification of the flow field. As even the shortest tested filters results in low turbulence intensities (<4%) it is recommended that the filter-induced reduction in wave height is taken into consideration as well, an aspect assessed in the following section.

4.2. Pure Wave Scenario

The porosity of the flow filter allows for fluid motion in both horizontal and vertical direction. This characteristic of the device permits the penetration of waves through the filter and into the test section of the flume. As the wave passes through the filter, the wave field is influenced by the filter in the form of wave deflections as well as wave dissipation, resulting in a loss of wave energy. The degree of dissipation as well as its sensitivity to varying wave heights and wave periods is assessed in this section.

Data from a comprehensive parameter study is presented in this paper, incorporating 9 wave heights (ranging from 0.044 m to 0.171 m) and 3 wave periods (ranging from 1.00 s to 1.75 s) at a water depth of 0.35 m. The results for the various filter setups are summarized in Fig. 7. The given reference wave heights H_{ref} corresponds to the unfiltered, averaged wave heights measured in the test section.

The reference wave height includes reflections from the beach. This choice was made to better compare results with wave-current scenarios, where obtaining the incident wave height is complicated and likely to lead to equal or greater uncertainties. The explicit assumption is therefore that

the relationship between wave heights for different filter-configurations H_{filt} and the unfiltered wave heights H_{ufilt} are proportional to the ratio of filtered pure incident waves $H_{\text{inc,filt}}$ and unfiltered pure incident waves $H_{\text{inc,ufilt}}$:

$$\frac{H_{\text{filt}}}{H_{\text{ufilt}}} \propto \frac{H_{\text{inc,filt}}}{H_{\text{inc,ufilt}}} \tag{2}$$

Each curve given in Fig. 7 shows the relation between the measured wave height and the reference for all tested filters. As shown, the introduction of the first filter section results in a significant drop of the measured wave heights. As additional filter sections are introduced, the wave heights decreases further. The amount of wave damping for configuration 1v0h ranges from 20% to 35% while for the largest filter setup (2v2h) the damping range amounts to 40% to 70%. The degree of damping is both dependent of the wave height and wave period. This is demonstrated in Fig. 8, which gives damping curves for the different setups as a function of the wave period for a 0.10 m wave. The amount of wave damping is particularly pronounced at small wave periods and reduces steadily as the wave period is increased. This suggests that for the analyzed range of waves, the setup acts as a low pass filter, with a near linear damping ratio with respect to the wave period.

Based on the collected data, a damping estimation equation in the form of a polynomial function was derived, as given in Eq. 3. The polynomial coefficients for each filter setup are documented in Tab. 4. Exemplary, the fitted surface for filter set up 1v1h is shown in Fig. 9. Using the polynomial equation and the corresponding coefficients, the degree of damping D can be estimated.

$$D(H,T) = aHT + bH^2T + cHT^2 + dH^2T^2 \quad \forall \quad \begin{cases} H \in [0.04m, 0.20m] \\ T \in [1.00s, 2.00s] \end{cases} \tag{3}$$

To further characterize and generalize the filter damping properties, the recorded data is non-dimensionalized using the ratio between the filter width λ and the wave length L of the various tested wave scenarios. As seen in Fig. 10, the data can be approximated reasonably well with the exponential expression:

$$D\left(\frac{L}{\lambda}\right) = \hat{a} \cdot exp\left(\hat{b} \cdot \frac{L}{\lambda}\right) + \hat{c} \cdot exp\left(\hat{d} \cdot \frac{L}{\lambda}\right) \tag{4}$$

with $[\hat{a}, \hat{b}, \hat{c}, \hat{d}] = [0.2893, -0.0304, 0.7182, -0.5707]$.

Eq. 3 and 4 give a first indication of the amount of dissipation to be expected and the percentage by which to increase the wave height generated by the wave maker in order to compensate for the effects of the filter. It should be noted that the results are meant to give only a starting point for a systematic tuning of the input conditions until the desired wave height is reached.

To further analyze and quantify the source of damping of the wave field, reflection coefficients (C_r), absorbsion coefficients (C_a), and transmission coefficients (C_t) are determined using wave gauges positioned both in front and behind the filter (Fig. 3). In order to measure wave reflections from the filter between the wave paddle and the filter, the filter setup is positioned further downstream from the inlet[1]. The reflection and transmission

[1]This position of the filter is for experimental purposes only in order to determine the

are determined directly by measurements, whereas the remaining energy absorbed by the filter is determined based on the relation:

$$C_r{}^2 + C_t{}^2 + C_a{}^2 = 1 \tag{5}$$

Here, the transmission coefficient C_t is determined by computing the ratio of the wave heights measured in the test section for each filter setup, to the measured unfiltered wave height results. The overall reflection coefficient C_r for each filter setup is determined as the difference between the reflection coefficients computed with and without the filter. The method used to determine the reflection coefficients is based on Mansard and Funke (1980); where three wave gauges are used to separate incident and reflected waves using the least squares method to reduce the influence of noise in the measurements. The resulting coefficients for various wave heights and periods are shown in Fig. 11. For all tested wave conditions, the wave energy loss is dominated by absorbsion within the filter, while the the measured reflections are small in comparison, with a maximum reflection coefficient of approximately 0.2. The low reflective properties of the filter ensure that the incoming waves from the wave maker remain largely undisturbed. Therefore, the generation of a stable wave field is warranted even when carrying out long term testing.

In addition to analyzing the damping effect on the wave heights for each filter configuration, the wave profiles are verified after passage through the

reflections; under normal circumstances, the filter would be positioned close to the wave maker.

filters. In general, it was found that independent of the filter setup, the specified wave periods were preserved throughout all tests. Fig. 12 shows a comparison of waves with a large bandwidth of varying wave heights and wave periods for the smallest and largest filter setup. Each wave profile was derived by averaging the shape over three wave periods of the recorded wave-gauge data. The average shape of the wave is then compared to Dean's Stream Function theory (Dean, 1965) to determine if there are any significant bound components created by the filter. It becomes apparent that the shape of the waves very much resemble the expected distributions. Overall it can thus be concluded that when taking into account the damping effects of the filter, realistic wave conditions are retained for all setups.

4.3. Combined Wave-Current Scenario

After verifying the characteristics of the flow filter for pure wave and pure current flows in the previous sections, the two scenarios can be combined at will to generate stable wave-current flow conditions. To assess the quality of the ensuing flow field, ADV velocity recordings are analyzed in this section for the smallest (1v0h) and largest (2v2h) filter setup and compared to the unfiltered results.

The scenario chosen for the comparison consists of a 0.055 m high wave of period 1.5 s in combination with a 0.11 m/s current. Fig. 13a shows the horizontal velocity field over a time span of 15 s for the unfiltered flow. As can be seen, the variation of wave peaks and troughs is relatively high, as a result of the fluctuations in the underlying current. For the given scenario, this results in a relative standard deviation (RSD) of the wave heights equal to 12.6%.

After installing one vertical filter section, the fluctuation of the current and the resulting variations in wave peaks and troughs are reduced significantly, as seen in Fig. 13b. For this setup, the wave height RSD reduces to 2.1%. This value can be reduced further by installing further filter sections, as demonstrated in Fig. 13c. As expected, the difference in results for the two filter setups is relatively small, in accordance with the similar current turbulence intensities documented in Fig. 5c.

Overall, the recorded wave-current data shows the capability of the filter setup to reduce current-induced fluctuations and to render stable wave-current flow fields, thus allowing for a reliable experimental analysis of offshore structures subjected to such combined conditions.

5. Conclusions

This paper addressed challenges frequently encountered when performing combined wave-current testing in laboratory experiments. In particular, this concerns undesirable velocity fluctuations in current flows generated by a recirculating water pump, which are combined with waves generated by a vertical paddle wave maker. A novel physical flow filtering approach introduced in this study handles this problem by dissipating turbulence in the flow field, while permitting the generated wave motion to pass through the filter setup. The key to this approach is the utilization of perforated tubes that allow for water passage in both the horizontal and vertical flow direction.

Various filter configurations were analyzed, with different arrangements of vertical and horizontal tube sections. The analysis involved elaborate

testing in pure current, pure wave, and combined wave-current conditions. It was shown that even the smallest tested filter width (27.5 cm) results in a significant decrease of turbulence in the current flow, reducing fluctuations by approximately 70%. The incorporation of additional filter segments up to a total filter width of 109 cm allowed for a further reduction of the turbulence intensity. Overall, it was possible to reduce the turbulence in a pure current flow from approximately 8% in the unfiltered scenario down to 2% for the maximum filter width.

The properties of the filter with regards to its effect on wave flows were quantified in a series of dissipation tests. It was found that the largest tested filter setup results in a wave height damping ranging from 40% to 70% depending on wave height and period, when compared to the unfiltered scenario. The amount of dissipation is significantly lower for smaller filter configuration, amounting to approximately 15% to 20%. A reflection analysis of the wave field showed that the source of damping is mainly due to dissipation within the filter, while the wave reflections from the filter are relatively small in comparison. Consequently, only small alterations of the wave field between the wave paddle and the filter setup ensue. This characteristic of the filter accounts for the high quality of the measured wave profiles in the test section. Taking into account the damping effects of the filter, these profiles closely match computed theoretical reference solutions. Furthermore, the wave periods remain entirely unaltered by the filter setup. The overall amount of wave energy dissipation can be estimated using a polynomial expression derived as a function of the wave height and period.

Finally, the effectiveness of the filter setup in combined wave-current flows

was demonstrated. Current induced fluctuations are largely dissipated by the filter, allowing for the generation of stable wave-current flow conditions. Whereas disturbances in the unfiltered current field result in a relative wave height standard deviation of over 12%, the deviation in the filtered scenario reduce to below 2%. Based on the collected data, it can be concluded that even the smallest tested filter setup is sufficient to reduce turbulence in the flow significantly, at comparatively small wave dissipation rates. Therefore, the narrow setup is likely to be a good choice for most standard applications, while additional filter sections can be added when demanding an even more substantial stabilization of the flow field.

The filter system can easily be adjusted to and installed in an existing flume setup using lightweight prefabricated net tube blocks. Therefore, the introduced flow filter is a highly efficient approach to enhancing recirculating wave-current flumes. Overall, the physical filter setup can be effectively applied to in depth laboratory studies of offshore engineering applications involving combined wave-current flow conditions.

Acknowledgements

The authors wish to express their sincere gratitude to the International Graduate School of Science and Engineering (IGSSE) at TU München for supporting the research documented in this paper.

Table 1: Tested filter arrangements and corresponding total filter widths.

	1v0h	1v1h	1v2h	2v2h
Setup:	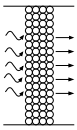	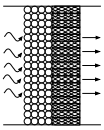	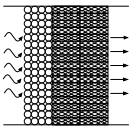	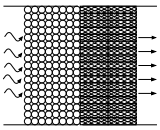
Width:	27.5 cm	54.5 cm	81.5 cm	109.0 cm

Table 2: Current velocities

case	velocity [m/s]
C1	0.11
C2	0.22
C3	0.36

Table 3: Turbulence intensity for each configuration.

case	unfiltered [%]	1v0h [%]	1v1h [%]	1v2h [%]	2v2h [%]
C1	7.1	3.7	3.4	2.8	2.7
C2	8.5	2.6	2.2	2.1	2.0
C3	8.1	2.6	2.7	2.1	2.3

Table 4: Coefficients for damping estimation.

filter	a [-]	b [-]	c [-]	d [-]
1v0h	7.33	-14.10	-3.23	4.88
1v1h	13.89	-49.24	-6.70	24.53
1v2h	18.67	-73.89	-9.20	37.99
2v2h	22.76	-102.40	-11.05	53.31

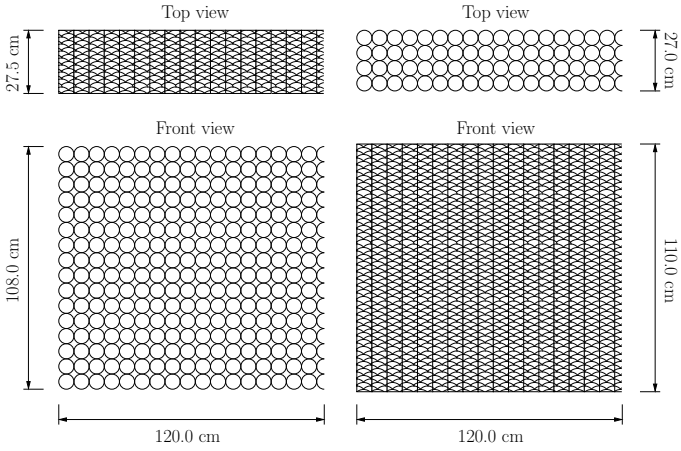

(a) Horizontal filter segment (1h) (b) Vertical filter segment (1v)

Figure 1: Dimensions of the individual horizontal and vertical filter segments.

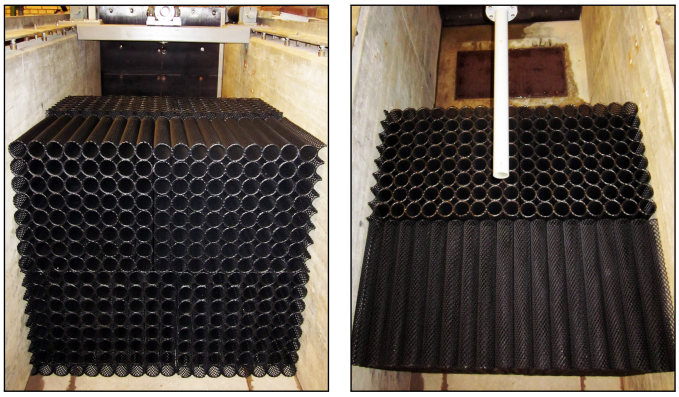

(a) Front view (b) Top view

Figure 2: Flow filter setup 2v2h installed in the inlet region of the flume.

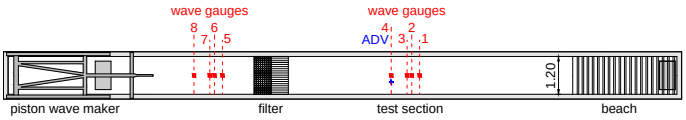

(a) Flume top view

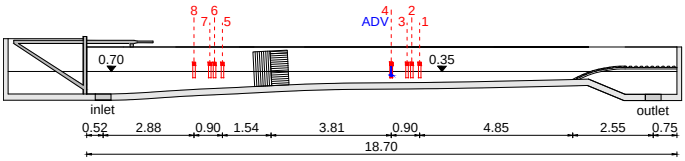

(b) Flume side view

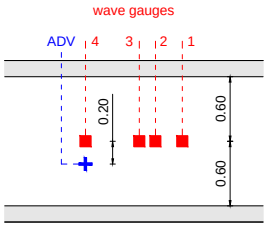

(c) Test section top view

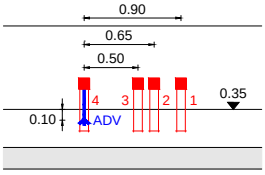

(d) Test section side view

Figure 3: Test setup in the Aalborg University recirculating wave flume. All measurements are in meters. The distances between wave gauges 5 to 8 correspond to the distances between wave gauges 1 to 4, respectively.

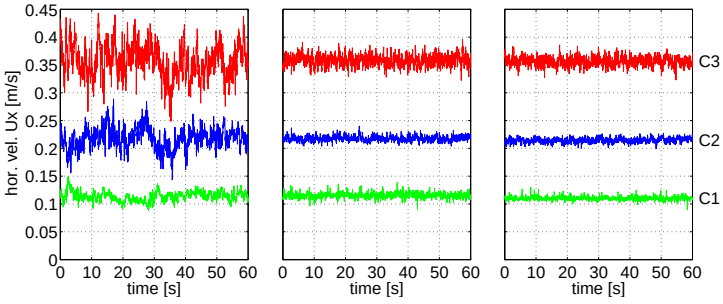

(a) Unfiltered (b) Filter 1v0h (c) Filter 2v2h

Figure 4: Comparison of horizontal velocity time series before and after flow filter installation.

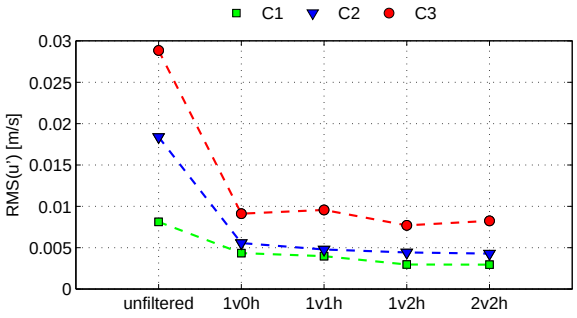

(a) Horizontal velocity fluctuations

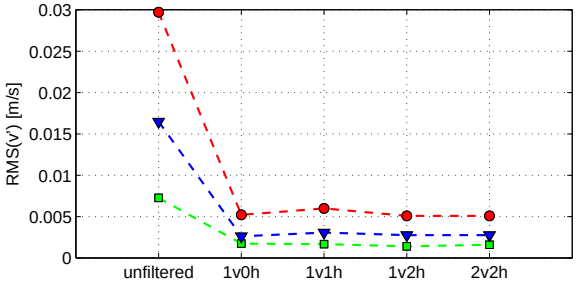

(b) Vertical velocity fluctuations

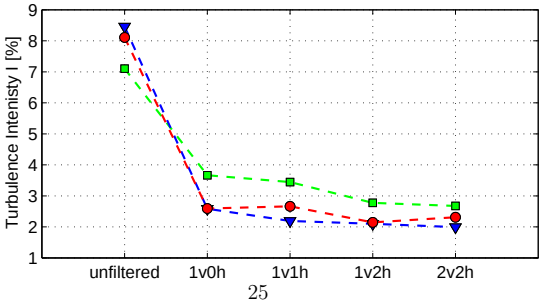

(c) Turbulence intensity

Figure 5: Filtering affect on the current velocity fields for each configuration.

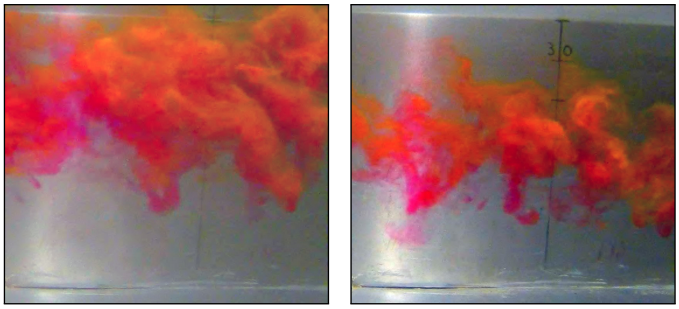

(a) Unfiltered (b) Filter 2v2h

Figure 6: Visualization of the C1 flow fields using dye injection.

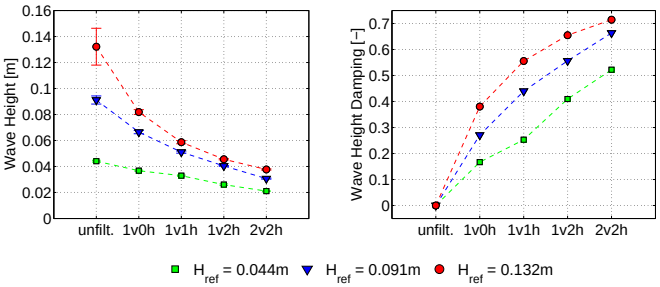

(a) Wave Period T=1.00s

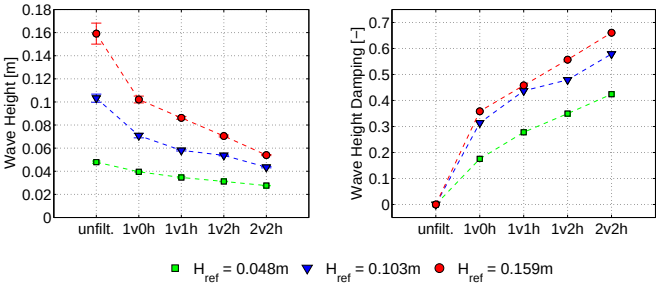

(b) Wave Period T=1.25s

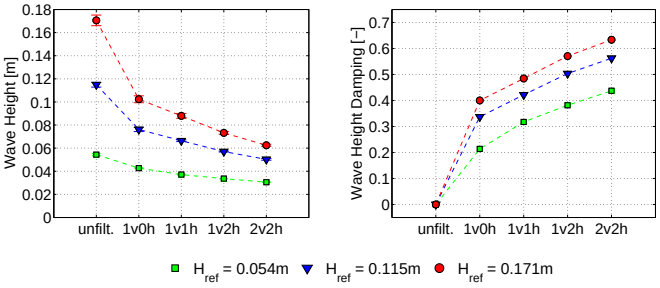

(c) Wave Period T=1.50s

Figure 7: Wave height comparison at different wave periods.

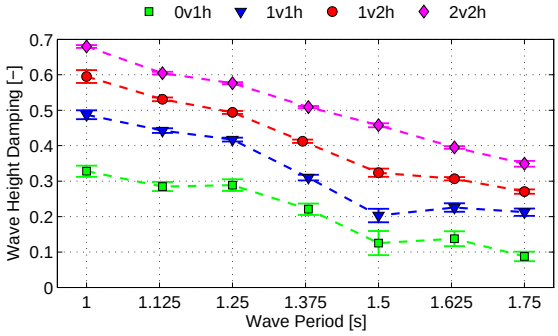

Figure 8: Amount of wave damping for a 0.10 m wave at various wave periods.

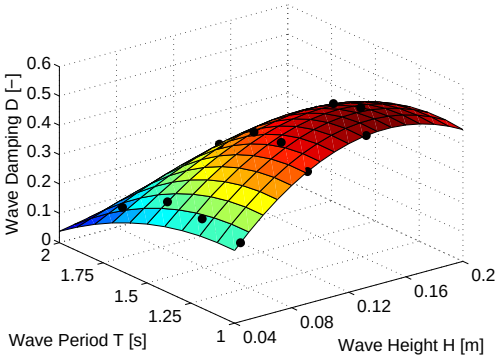

Figure 9: Polynomial damping fit for filter setup 1v1h.

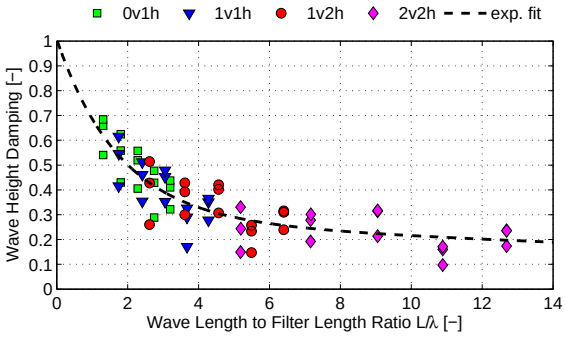

Figure 10: Exponential damping fit as a function of the wave by filter length ratio.

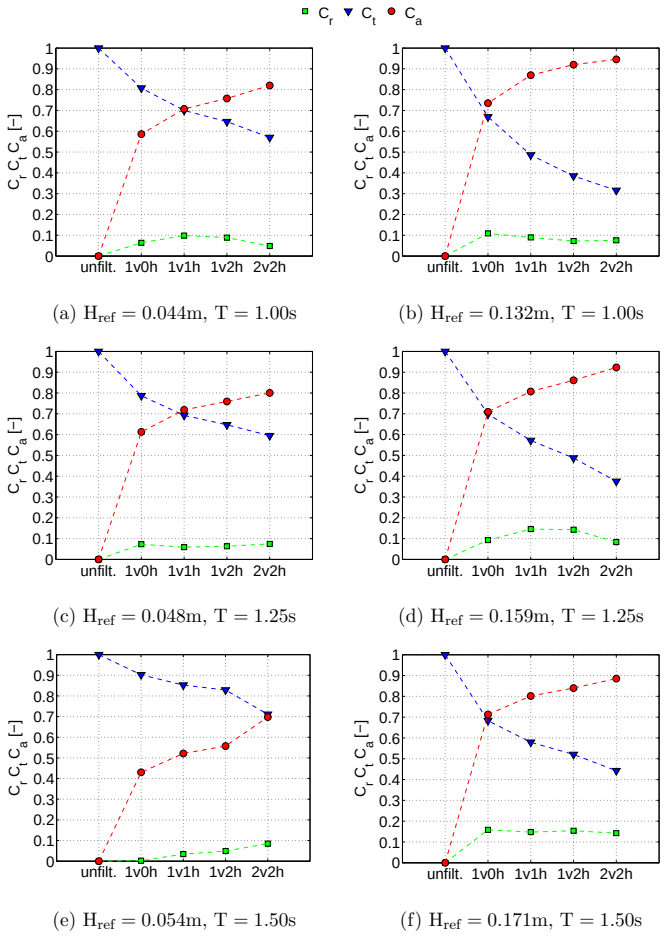

(a) $H_{ref} = 0.044$m, T = 1.00s (b) $H_{ref} = 0.132$m, T = 1.00s

(c) $H_{ref} = 0.048$m, T = 1.25s (d) $H_{ref} = 0.159$m, T = 1.25s

(e) $H_{ref} = 0.054$m, T = 1.50s (f) $H_{ref} = 0.171$m, T = 1.50s

Figure 11: Filter characteristics in terms of reflection C_r, transmission C_t, and absorbsion C_a.

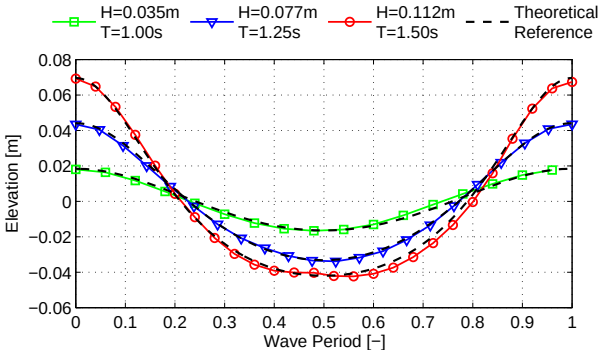

(a) Filter 1v0h

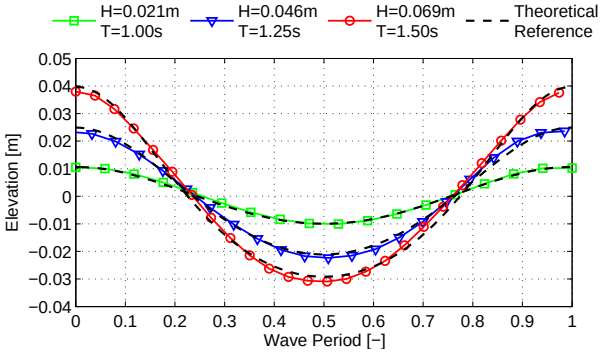

(b) Filter 2v2h

Figure 12: Measured and computed wave elevation over one period for various wave conditions passed through the 1v0h and 2v2h filter.

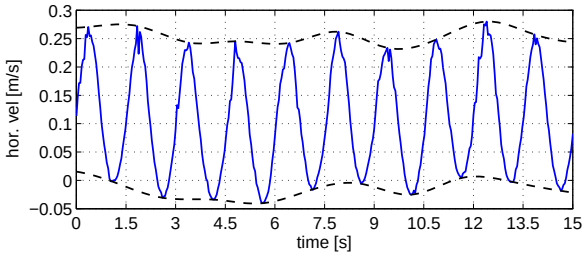

(a) Unfiltered (wave height RSD = 12.6%)

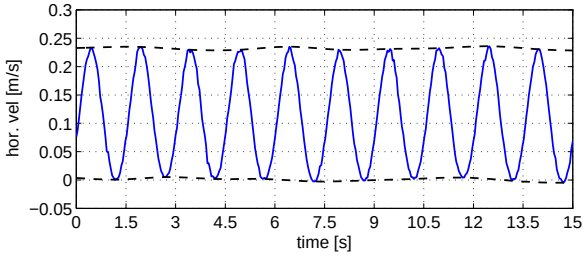

(b) Filter 1v0h (wave height RSD = 2.1%)

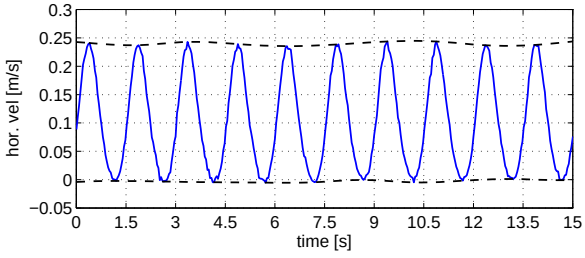

(c) Filter 2v2h (wave height RSD = 1.9%)

Figure 13: ADV horizontal velocity recordings for a 0.055 m wave of period 1.5 s with a 0.11 m/s current measured 0.15 m below the mean water level.

References

Barltrop, N., Varyani, K., Grant, A., Clelland, D., Pham, X., 2007. Investigation into wave-current interactions in marine current turbines. Proceedings of the Institution of Mechanical Engineers, Part A: Journal of Power and Energy 221, 233–242.

Chamorro, L., Hill, C., Morton, S., Ellis, C., Arndt, R., Sotiropoulos, F., 2013. On the interaction between a turbulent open channel flow and an axial-flow turbine. Journal of Fluid Mechanics 716, 658–670.

Chanson, H., Trevethan, M., Koch, C., 2007. Discussion of "Turbulence measurements with acoustic Doppler velocimeters". Journal of Hydraulic Engineering 133, 1283–1286.

Dean, R., 1965. Stream function representation of nonlinear ocean waves. Journal of Geophysical Research 70, 4561–4572.

Faudot, C., Dahlhaug, O.G., 2012. Prediction of wave loads on tidal turbine blades. Energy Procedia 20, 116–133.

Galloway, P., Myers, L., Bahaj, A., 2010. Studies of a scale tidal turbine in close proximity to waves, in: Proceedings of the 3rd International Conference on Ocean Energy, Bilbao, Spain.

García, C.M., Cantero, M.I., Niño, Y., García, M.H., 2005. Turbulence measurements with acoustic doppler velocimeters. Journal of Hydraulic Engineering 131, 1062–1073.

Goring, D.G., Nikora, V.I., 2002. Despiking acoustic doppler velocimeter data. Journal of Hydraulic Engineering 128, 117–126.

Hendriks, I.E., van Duren, L.A., Herman, P.M., 2006. Turbulence levels in a flume compared to the field: implications for larval settlement studies. Journal of Sea Research 55, 15–29.

de Jesus Henriques, T., Tedds, S., Botsari, A., Najafian, H., Sutcliffe, C., Owen, I., Poole, R., 2013. The effects of wave-current interactions on the performance of a model horizontal axis tidal, in: Proceedings of the 10th European Wave and Tidal Energy Conference, Aalborg, Denmark.

Khorsandi, B., Mydlarski, L., Gaskin, S., 2012. Noise in Turbulence Measurements Using Acoustic Doppler Velocimetry. Journal of Hydraulic Engineering 138(10), 829–838.

Kulkarni, V., Sahoo, N., Chavan, S.D., 2011. Simulation of honeycomb–screen combinations for turbulence management in a subsonic wind tunnel. Journal of Wind Engineering and Industrial Aerodynamics 99, 37–45.

Laws, E., Livesey, J., 1978. Flow through screens. Annual Review of Fluid Mechanics 10, 247–266.

Mansard, E., Funke, E., 1980. The measurement of incident and reflected spectra using a least squares method. Coastal Engineering Proceedings 1, 154–172.

Mikhailova, N., Repik, E., Sosedko, Y.P., 1994. Optimal control of

free-stream turbulence intensity by means of honeycombs. Fluid Dynamics 29, 429–437.

Mori, N., Suzuki, T., Kakuno, S., 2007. Noise of acoustic doppler velocimeter data in bubbly flows. Journal of Engineering Mechanics 133, 122–125.

Myers, L., Galloway, P., 2011. Operational issues surrounding the use of towing tanks for performance quantification of marine current energy converters, in: Proceedings of the 9th European Wave and Tidal Energy Conference, Southampton, UK.

Nowell, A.R., Jumars, P.A., 1987. Flumes: theoretical and experimental considerations for simulation of benthic environments. Oceanography and Marine Biology 25, 91–112.

Scheiman, J., Brooks, J., 1981. Comparison of experimental and theoretical turbulence reduction from screens, honeycomb, and honeycomb-screen combinations. Journal of Aircraft 18, 638–643.

Voulgaris, G., Trowbridge, J.H., 1998. Evaluation of the Acoustic Doppler Velocimeter (ADV) for Turbulence Measurements. Journal of Atmospheric and Oceanic Technology 15, 272–289.

Wahl, T.L., 2003. Discussion of "Despiking acoustic doppler velocimeter data" by Derek G. Goring and Vladimir I. Nikora. Journal of Hydraulic Engineering 129, 484–487.

Paper C

Practical Performance of Control Strategies for Point Absorbers

Morten M. Jakobsen, Francesco Ferri and Morten M. Kramer

The conference proceedings has been accepted for publication in the
11th European Wave and Tidal Energy Conference, EWTEC, 2015.

The layout has been revised.

Control of Point Absorbers and their Performance in Experiments

Morten M. Jakobsen, Francesco Ferri and Morten M. Kramer
Department of Civil Engineering, Aalborg University
Sofiendalsvej 11, 9200 Aalborg SV, Denmark,
*E-mail: mmj@civil.aau.dk

***Abstract*—Appropriate control of point absorbers is essential in order to increase the energy capture from waves. Optimal and near optimal numerical controllers has been presented in the past. In laboratory and real sea testing these methods are difficult to implement often due to the motion of point absorbers or the need to predict the future. The paper presents and compares numerical estimates and experimental measurements for different control strategies, and explains the benefits and drawbacks of these. Simulated estimates and experimental measurements are compared in regular and irregular waves and time series of motions, moments and power are presented for regular waves.**

***Index Terms*—Experimental, Numerical, PTO, PI control, optimization.**

I. Introduction

Power Take-Off (PTO) used for Wave Energy Converters (WEC) is a topic that has been studied extensively in the past. J. Falnes and K. Budal started optimizing the control by introducing latching as a way to tune the device to the incident waves [1]. However to optimize the latching controller a short term forecast of the incoming wave is needed to the non-causality of the system [2], [3]. A. Falcão presented a novel approach that did not need prediction, but instead relied on natural latching in hydraulic actuators [4]. Other control schemes such as real-time control [5]–[7], and model predictive control [8]–[11] has been suggested, but they too require knowledge of future waves and are hence non-causal. In this study only causal feed-back control laws are considered due to their relative simplicity and robustness. The first strategy examined is a proportional controller, i.e. a controller which only includes a gain factor for the control force component, proportional to the velocity of the motion. This type of control is also often referred to as linear damping control or resistive control, and is only effective in the eigenfrequency range of the device. The second strategy is a reactive control strategy which includes both a proportional and integral gain factor (PI control). It has been decided not to include a derivative part to the controller (PID). The added complexity and sensitivity to noise outweighs the benefit, which was shown to be limited in a numerical study [12].

The performance of the controllers are demonstrated in a case study on a single 1:20th scale Wavestar [13] point absorber see Fig. 1. The device is extracting energy using a linear actuator to control the pitching motion of the floating hemisphere.

A numerical optimization of the control gains has been completed using a traditional linear hydrodynamic model where realistic limits on maximum PTO-force and a PTO-efficiency of 70% is included. The results show that the benefit of the more advanced control strategies depends on the following practical implementation which is often neglected in traditional comparative performance studies. This includes friction losses in bearings, performance of PTO to accurately deliver the target force, non-linear hydrodynamics, sensor signal delays and noise.

The experiments and numerical simulations are carried out and compared in both regular and irregular waves. The comparison is made based on the electrical power output with the PTO limitations described.

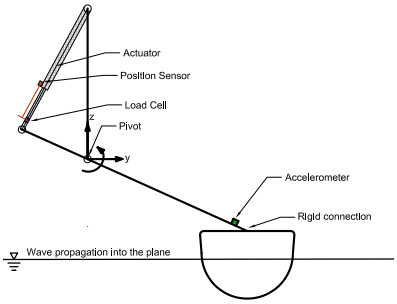

Fig. 1. The point absorber and sensors used in experiments.

II. Methods

Simulations to estimate the stiffness and damping coefficients are done in Matlab Simulink [14]. The simulations are run for ten regular and three irregular wave series. The irregular waves are based on a unitary wave series (scaling the amplitude and sampling frequency) using a Pierson-Moskowitz spectrum and appropriate sea states for the North Sea. The waves are generated using inverse Fourier transformation and optimized to have a good Rayleigh distribution of $(H/Hm)^2$. This should ensure that the waves in the series are well distributed and that the deterministic wave series are comparable. To account for any disparity between target waves and generated waves in the wave basin, each regular and

irregular wave series used in the simulations are from surface elevation measurements of the undisturbed waves from the wave basin, cf. Fig. 2.

Simulink is used in the experiments together with the remote

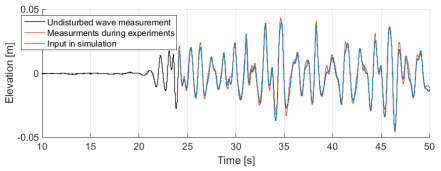

Fig. 2. Wave series surface elevation in simulation with measurements from the wave basin. Example shown for buildup of irregular wave series S2. As simulation input is the undisturbed wave signal the blue and black lines overlap within the range of the target wave.

xPC software, where the WEC and Wave block in Fig. 3 are measured from the experiments.

The found stiffness and damping coefficients are then used as candidates for the controller in the experiments to find the peak power outputs. For the experiments a 10 second wave buildup is used to account for the wave maker ramping up and down.

Constrains are then introduced to account for the more practical limitations similar to what was done previously by R. Hansen [15]. In both the experiments and simulations a torque limiter is included to constrain the actuator, limiting the performance to that of the prototype using Froude scaling. The instantaneous power is calculated using the moment from

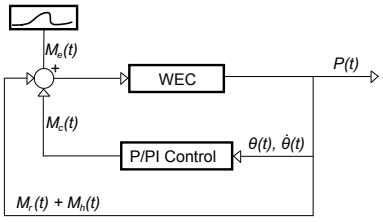

Fig. 3. Concept used in laboratory and in simulation.

the actuator about the pivot M_c and angular velocity $\dot{\theta}$. In the experiments this is obtained from the aforementioned Kalman observer. Including the efficiency of the PTO the electrical power is then calculated by $P_e = P - (1 - efficiency) \cdot |P|$. The implication on the P controller is purely a reduced net-power production and will not affect the choice of damping coefficient. The PI controller is affected in the choice of the stiffness coefficient and incidentally on the choice of damping as well.

A. Simulation

Using Newton's second law of motion and the definitions in Fig. 4, the fundamental equation used in the simulations is shown in Eq. 1.

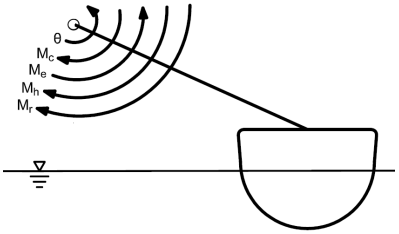

Fig. 4. Sketch of pivoting motions and moments.

$$J \cdot \ddot{\theta}(t) = -M_c(t) - M_r(t) - M_h(t) + M_e(t) \quad (1)$$

Where the control M_c, radiation M_r, excitation M_e, and hydrostatic moments M_h are defined in Eqs. 2-5.

$$M_c(t) = c_c\dot{\theta}(t) + k_c\theta(t) \quad (2)$$

$$M_r(t) = A_\infty\ddot{\theta}(t) + \int_{-\infty}^{t} h_r(t-\tau)\cdot\dot{\theta}(\tau)d\tau \quad (3)$$

$$M_h(t) = k_h \cdot \theta(t) \quad (4)$$

$$M_e(t) = \int_{-\infty}^{\infty} h_e(t-\tau)\cdot\eta(\tau)d\tau \quad (5)$$

Inserting the coefficients of Eqs. 2-4 in Eq. 1 leads to Eq. 6.

$$(m_c + A_\infty + M)\ddot{\theta}(t) + c_c\dot{\theta}(t) + \ldots$$
$$\int_{-\infty}^{t} h_r(t-\tau)\cdot\dot{\theta}(\tau)d\tau + (k_c + k_h)\theta(t) = M_e(t) \quad (6)$$

The added mass tending to infinity A_∞, the radiation H_r and excitation H_e frequency responses are obtained from a model in WAMIT [16] and transformed into impulse responses via inverse Fourier Transformation. The impulse responses functions (IRF) h_r and h_e are shown in Fig. 5(a) and 5(b) and A_∞ in Table I.

Table I also lists the hydrostatic stiffness k_h and moment of inertia J, which are obtained from the experiments.

B. Experiment

The experimental model consists of a glass fiber float connected with an arm to the PTO as seen in Fig. 6. The weight is adjusted to be proportional to the prototype using ballast attached to the lid. The force and displacement of the linear, electromagnetic actuator is measured using a force sensor and laser positioning. The angular velocity is obtained using a Kalman observer with the laser position sensor and an accelerometer. The wave gauge used to measure the surface elevation is located in parallel with the device, perpendicular

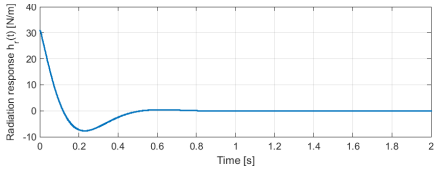

(a) Impulse response from radiation force

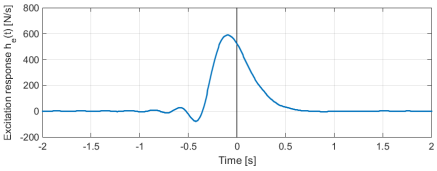

(b) Impulse response from excitation force

Fig. 5. Impulse response functions used in simulations, obtained from inverse Fourier Transform of the frequency response functions from WAMIT.

TABLE I
SETUP SPECIFCATIONS

Length of arm	l_A	0.68 m
Diameter of hemisphere	D	0.25 m
Draft	d	0.10 m
Hydrostatic stiffness	k_h	92.7 Nm/rad
Natural period	T_0	0.84 s
Added mass	A_∞	0.41 kg
Actuator constrain	$F_{cyl,sat}$	$\pm$6.25 Nm

to the flow direction.
The wave basin has the traditional layout, consisting of a line of wave makers and a permeable beach in the opposite end. The remaining two walls are impermeable. The dimensions are 15 m $\times$ 8 m with a water depth of 60 cm in the testing area, 4.45 m from the wave maker. The Awasys [17] wave generation software uses a deterministic random phase method to phase-shift the predefined irregular wave series to the location of the WEC [18]. To avoid spurious sub harmonics the regular waves are generated using a second order generation method.

For the simulation the natural period is obtained from a decay test by measuring the period of the oscillation. The float is released from a suspended state 0.1 radian above neutral buoyancy. From this slightly elevated state it was determined that the oscillations was still easily discernible while minimizing second order effects. To measure the decay the effect of the actuator should be negligible. Unfortunately the 70 ms response delay of the setup affects the measured period. To overcome this issue the actuator was disconnected. As the positioning is usually done with the laser measuring the extension and retraction of the piston rod of the actuator,

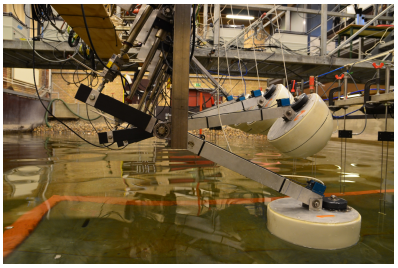

Fig. 6. Laboratory setup in the Aalborg University wave basin.

it was necessary to use another device for this measurement. The MTi xsens showed to be sufficiently accurate to determine the natural period and was used when the decay was repeated without the actuator, cf. Fig. 7.

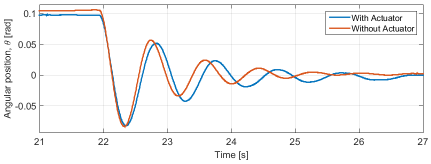

Fig. 7. Measurement of natural decay of motion with and without actuator.

The hydrostatic stiffness is determined by slowly submerging the float from neutral buoyancy. By assuming that radiation and excitation moments are negligible, then $M_h = -M_c$. In this paper k_h is determined by making a best linear fit to the $M_c(\theta)$ curve, cf. Fig. 8. The non-linearity occur when the device is submerged to a degree where the lid is submerged ($\theta < -0.1$ rad) and similarly when the float is pulled out of the water ($\theta > 0.1$ rad).

The moment of inertia is determined by forced sinusoidal oscillation of the float in air, again assuming that $M\ddot{\theta} = -M_g - M_c$.

III. RESULTS

Using the constrains of the PTO force and 70 % efficiency, the average power of the regular and irregular waves are calculated with regards to the damping and stiffness coefficients. The main point of the findings are driven by the following examples.

To determine how well the numerical WAMIT model, the implemented simulation, and the experimental setup fit with

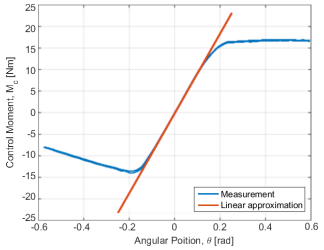

Fig. 8. Nonlinear hydrostatic moment. Best linear fit for measurements in range $\theta \in [-0.1; 0.1]$

each other the excitation moments are compared. For the experiments this is done by keeping the float locked in place with a physical lock on top of the actuator and with a high damping coefficient in the simulation. The excitation moments are shown in Fig. 9 for the six regular waves with the same wave height.

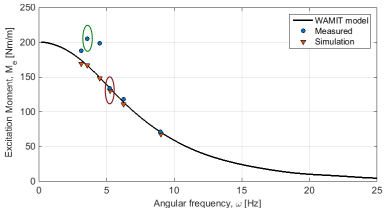

Fig. 9. Excitation moment used in the numerical model compared with measurements from experiments where the float is locked in place. Circles are measurements from the experiments, triangles are results from simulations. The solid line represents the coefficients calculated in WAMIT, used in the numerical model of the floater.

To study the magnitude of the power between simulation and experiments three regular waves are shown with the P control scheme in Fig. 10. These three experiments corresponds to the measurement marked with a red circle in Fig. 10. Both simulations (lines) and experiments (dots) are shown in the figure for comparison. The three regular waves shown in the figure has a common wave period with increasing wave height. Each wave series is repeated with variations in the damping coefficient. The damping coefficients producing the most power in the simulations has been chosen as the center node, and then additional nodes are picked on either side to outline a curve.

Following the findings in in Fig. 9, the time series of the angular position, control moment and electrical power are shown in Fig. 11. The experiment mark with a green circle in Fig. 9 is selected, which is a $H = 0.25$ m $T = 1.75$ s wave. The damping coefficient used is the found optimum for the

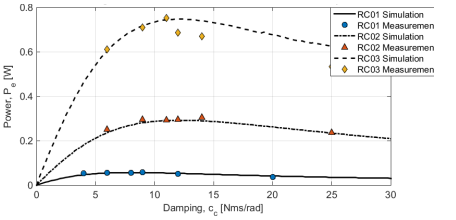

Fig. 10. Comparison of laboratory and simulation peak using variation in damping of the P control. The regular wave used has wave period of 1.2 s and wave heights 0.025, 0.0625 and 0.1 m.

P controller, $c_c = 17$ Nms/rad. The dashed, red lines shows the results based on the IRFs and wave elevation. The dotted, green lines are from the numerical model where the excitation moments measured from the experiments are used as input to the model.

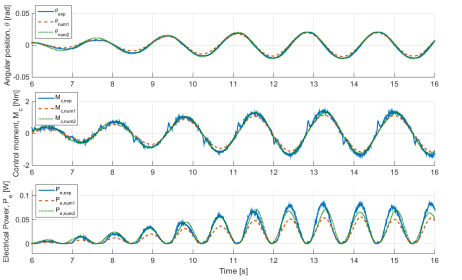

Fig. 11. Angular position, control moment and electrical power time series using P control. Blue lines are directly measured from experiments, red dashed lines are from numerical models using wave elevation as input, and green dotted lines are from the numerical model where the excitation moments from experiments is used as input.

Fig. 12 shows the contour plots of the electrical power for the PI control coefficient in the three irregular sea states. The initial value for both the damping and stiffness coefficients are chosen based on the simulations, in the same way it was done with regular waves. To limit the number of experiments carried out with two unknowns, only a select subset of experiments was carried out around the peak.

Fig. 13 shows the comparison between P and PI control for the regular wave series with the same wave height. 100% means that the two methods are equally efficient in extracting the wave energy, which happens when the waves are close to the natural frequency of the device ($\lambda/D \approx 3$).

IV. Discussion

Fig. 9 shows the excitation moments from experiments and simulation running the regular wave series. The frequency

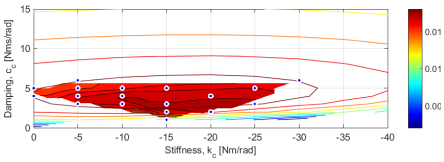

(a) S1: H_{m0} = 0.02 m, T_p = 0.99 s

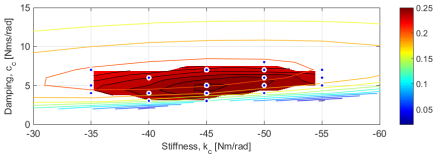

(b) S2: H_{m0} = 0.06 m, T_p = 1.41 s

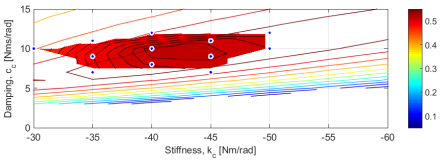

(c) S3: H_{m0} = 0.10 m, T_p = 1.84 s

Fig. 12. Comparison of extracted power P_e in laboratory and simulation for PI control. Blue dots are laboratory experiments. The opaque contours indicates the extracted power using linear interpolation between measurements. Simulations are shown as colored contour lines.

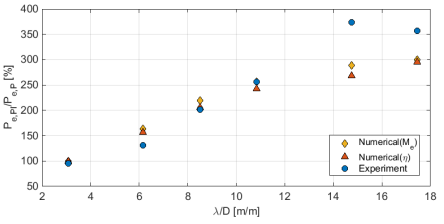

Fig. 13. P and PI control compared on extracted power from experiments and simulation of regular waves. Numerical(η) is with the unidisturbed wave series as input, numerical(M_e) is with excitation moments. λ is wave length and D is float diameter.

response function of the excitation moments from the WAMIT model is included as reference for the numerical simulation. The deviation between the two is attributed to the uncertainty in the wave height estimate and fluctuation of the undisturbed wave series used as input. Examining the results suggests that the model under-predicts the excitation moments. The issue is especially pronounced with longer waves, i.e. wave periods shorter than ca. 5 Hz.

Looking at the time series in Fig. 11 the simulations with the IRF from WAMIT (red dashed line) underestimates both θ, M_c, and P_e. By using the excitation moments from the measurements with the locked float, the IRF from excitation moments in Eq. 5 is bypassed (green dotted line). As this significantly improves the estimate with the measurements (blue solid line), this suggests that the issue is with incompatibility between the model used in WAMIT and the experimental setup. The model is based on a previous study with another hemisphere, and it was implicitly assumed that there was no significant change to the geometry. This seemed reasonable as the change in the model is a few millimeters in diameter. Judging by the results presented this is arguably not the case.

The efficiency varies with frequency and amplitude(stroke length) in wave-to-wire conversion. The assumption here of a constant 70% efficiency is made to simplify the procedure needed to calculate the electrical power output. This value is non-conservative using conventional components [19].

Fig. 10 shows the comparison of regular wave series with a wave period in the range where the IRF from excitation moments between model and experiment corresponds well. The reduction in measured power for the highest waves are expected to be due to over-topping in the experiments. The slightly higher power output from the experiments is attributed to the mismatch between the geometries mentioned previously. The same problem encountered in regular waves affects the magnitude of the measurements in the irregular waves. However, as seen in Fig. 12 the contours of laboratory measurements and simulation corresponds quite well, which means that the peaks are within about $\pm 1-2$ Nms/rad for c_c and $\pm 2-3$ Nm/rad for k_c.

V. Conclusion

This paper presented results from simulation and laboratory experiment using P and PI control strategies. A realistic PTO efficiency and cylinder force constraint was included in both experiments and simulation. This was done to account for the conversion loss and limitations of the PTO that affects the electrical power output in the wave-to-wire conversion.

In the experiments it is shown that:

- There is a good correlation between the performance of the controller in experiments and simulation.
- There is a clear benefit in using the PI controller over the P controller, particularly with longer waves.
- The PI controller is consistently superior in all the regular and irregular wave series used in the experiments outside the resonance frequency in spite of the loss from 70% efficiency.
- With a good agreement between numerical and experiment it is possible to use the numerical model for the rough parameter optimization and the lab for the fine tuning, and thereby reducing the time used in the lab.

REFERENCES

[1] J. Falnes and K. Budal, "Wave-power conversion by point absorbers," *Norwegian Maritime Research*, vol. 6, no. 4, pp. 2–11, 1978.

[2] K. Budal and J. Falnes, "Wave power conversion by point absorbers: a Norwegian project," *International Journal of Ambient Energy*, vol. 3, no. 2, pp. 59–67, 1982.

[3] A. Babarit and A. Clément, "Optimal latching control of a wave energy device in regular and irregular waves," *Applied Ocean Research*, vol. 28, no. 2, pp. 77–91, 2006.

[4] A. F. D. O. Falcão, "Phase control through load control of oscillating-body wave energy converters with hydraulic PTO system," *Ocean Engineering*, vol. 35, pp. 358–366, 2008.

[5] J. Falnes, *Ocean waves and oscillating systems: Linear Interactions Including Wave-Energy Extraction*. Cambridge Univ Press, 2002.

[6] M. Belmont, J. Horwood, R. Thurley, and J. Baker, "Filters for linear sea-wave prediction," *Ocean Engineering*, vol. 33, no. 17, pp. 2332–2351, 2006.

[7] J. Tedd and P. Frigaard, "Short term wave forecasting , using digital filters , for improved control of Wave Energy Converters," p. 2007, 2007.

[8] P. Gieske, "Model predictive control of a wave energy converter: Archimedes wave swing," *Master Thesis, Delft University of Technology, Delft*, 2007.

[9] G. Bacelli, J.-C. Gilloteaux, and J. Ringwood, "A predictive controller for a heaving buoy producing potable water," in *Proceedings of the European Control Conference*, 2009, pp. 3755–3760.

[10] J. A. Cretel, G. Lightbody, G. P. Thomas, and A. W. Lewis, "Maximisation of energy capture by a wave-energy point absorber using model predictive control," in *Proceedings of the 18th IFAC World Congress, Milano, Italy, Aug*, 2011, pp. 3714–3721.

[11] J. Hals, J. Falnes, and T. Moan, "Constrained Optimal Control of a Heaving Buoy Wave-Energy Converter," *Journal of Offshore Mechanics and Arctic Engineering*, vol. 133, no. February, p. 011401, 2011.

[12] R. H. Hansen, M. M. Kramer, and E. Vidal, "Discrete displacement hydraulic power take-off system for the wavestar wave energy converter," *Energies*, vol. 6, no. 8, pp. 4001–4044, 2013.

[13] M. M. Kramer, L. Marquis, and P. Frigaard, "Performance Evaluation of the Wavestar Prototype." EWTEC European Wave and Tidal Energy Conference, 2011.

[14] M. Simulink and M. Natick, "The Mathworks," *Inc., Natick, MA*, 1999.

[15] R. H. Hansen and M. M. Kramer, "Modelling and Control of the Wavestar Prototype." EWTEC European Wave and Tidal Energy Conference, 2011.

[16] C.-H. Lee, *WAMIT theory manual*. Massachusetts Institute of Technology, Department of Ocean Engineering, 1995.

[17] P. Frigaard and T. L. Andersen, "Technical Background Material for the Wave Generation Software AwaSys 5," Aalborg University Department of Civil Engineering, Tech. Rep. 64, jan 2010.

[18] T. L. Andersen and P. Frigaard, "Wave Generation in Physical Models: Technical documentation for AwaSys 6," Department of Civil Engineering, Aalborg University, Tech. Rep., 2014.

[19] R. H. Hansen, T. O. Andersen, and H. C. Pedersen, "Model based design of efficient power take-off systems for wave energy converters," in *The 12th Scandinavian International Conference on Fluid Power, May 18-20, Tampere, Finland*, 2011.

Paper D

Experimental Study of Forces on Point Absorber

Morten M. Jakobsen, Gregorio Iglesias, Morten M. Kramer and Enrique Vidal

The conference proceedings has been published in the
5th International Conference on The Application of Physical Modelling to Port and Coastal Protection, Coastlab Vol. 2, pp. 15–24, 2014.

The layout has been revised.

EXPERIMENTAL STUDY OF FORCES ON POINT ABSORBER

MORTEN M. JAKOBSEN [(1)], GREGORIO IGLESIAS[(2)], MORTEN KRAMER [(3)], ENRIQUE VIDAL [(4)]

[(1)] Ph.D. Student, Aalborg University, Sohngaardsholmsvej 57, Aalborg, DK-9000, Denmark. mmj@civil.aau.dk

[(2)] Professor of Coastal Engineering, School of Marine Science and Engineering, Plymouth, Devon, PL4 8AA, United Kingdom. gregorio.iglesias@plymouth.ac.uk

[(3)] Associate Professor, Aalborg University, Sohngaardsholmsvej 57, Aalborg, DK-9000, Denmark. mmk@civil.aau.dk

[(4)] Senior Researcher, Wavestar, Park Allé 350A, Brøndby, 2605, Denmark. evs@wavestarenergy.com

Abstract

Wave-Structure interactions of offshore Wave Energy Converters (WECs) are still in an early stage of research. Understanding both current and wave induced loading on these devices is of fundamental importance in terms of both performance and durability. In an effort to advance the knowledge within this field, a large scale point absorber has been tested in the COaST Ocean Wave Basin at Plymouth University. This investigation is concerned with the experimental setup, data acquisition techniques and wave-WEC interactions using different control strategies for the tested device.

Keywords: WEC; Forces; Pressure distribution; Hydraulic PTO;

1. Introduction

The Wavestar wave energy converter is a point-absorber, which harvests energy by absorbing the oscillatory motion of buoyant hemispheres using hydraulic power take-off. Small scale laboratory experiments have been carried out extensively throughout the lifetime of Wavestar, which at present spans a decade. Throughout the experiments the focus has progressively changed from looking at major design decisions towards more specialized device behaviour to the latest look into multi-float interactions. The development of the model continued alongside the experiments, including, which includes an efficient linear magnetic actuator (e.g. Hansen *et al.*, 2011; and Kramer *et al.*, 2012). For singular device development and the research into advanced Wave-WEC interactions with power take-off (PTO) the research has reached a point for small scale experiments where the effects of the Reynolds versus Froude scaling issues has to be overcome by using larger scale devices.

In the past, medium to large-scale experiments with Wavestar were carried out in the form of real sea testing. Two devices were tested in real sea so far, the smaller scale 1:10 with one-meter floats in the sheltered environments of Nissum Bredning and the large scale 1:2 device installed in the North Sea outside Hanstholm harbor in Denmark, Kramer *et al.*, 2011. Real-sea testing of the large-scale device has had a tremendous value in performance assessment, optimization of the PTO system and the fatigue assessments of the components. However to

assess the survivability of the device in extreme conditions it is preferable to test the device in a controlled environment.

The material presented in this paper outlines the laboratory experiments at the large Ocean Wave Basin of the COaST laboratory (Plymouth University). The actual testing in the basin took place during four weeks of September 2013 through the MARINET access program. The basin measures 35x15 m and has a water depth of 3 m, with adjustable floor and a hyperbolic impermeable beach. In the experiments, the maximum regular wave height successfully produced (well formed) was 70 cm in the wave period range 2.0-2.6 s. In terms of wave periods, the lower range of regular waves produced was T = 1.4 s as the wave heights below this threshold were insignificant. The upper limit was T = 4.0 s due to constraints of the wave makers maximum stroke length. The outcome of the experiments carried out in Plymouth includes various wave and wave-current scenarios including non-deterministic predefined irregular waves specifically tailored to contain severe conditions while maintaining the JONSWAP spectral shape. Freak waves, based on the New Wave Theory by Tromans *et al.* 1991, are tested both uni-directional and with a directional focus. In this paper the focus has been limited to the regular waves to keep in line with the page limit.

The device used in the experiments in Plymouth is from the old testing site in Nissum Bredning. The exception being the float itself, which was a spare, never used in real sea. The setup used in the experiments is illustrated in Figure 1 below. The station-keeping of the device is established by mounting the float onto the gantry in the basin using a custom-fitted frame and arm structure. The frame is created with hinges, which gives the option to turn the device at 0, 45 and 90-degree angles and thereby examine load cases with waves of different directionalities relative to the device. Ball bearings are fitted between the arm and the frame on the gantry to ensure that only the pitch-motion of the device is possible. To control the pitching motion and resemble the PTO system a hydraulic based piston is attached to the support frame and roughly halfway down the arm. This allows testing the device with three different behaviour: non-moving in a fixed position, moving free floating with no PTO control, and in operation with the PTO active using various control strategies.

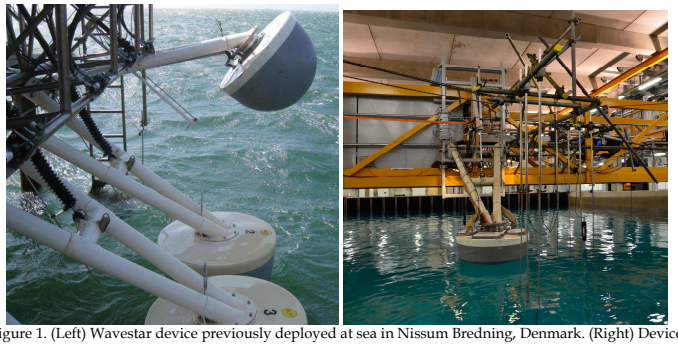

Figure 1. (Left) Wavestar device previously deployed at sea in Nissum Bredning, Denmark. (Right) Device setup in the Ocean Wave Basin at COaST with Plymouth University, UK.

2. Sensor Overview

The forces on the WEC are measured at several locations throughout the structure as seen in Figure 2. The six forces and torques components are measured on the float in the joint between the float and the arm. These six force and torque components measures the total force exerted on the float. To measure the forces transferred to the main structure force sensors are located by the ball bearings and at the actuator.

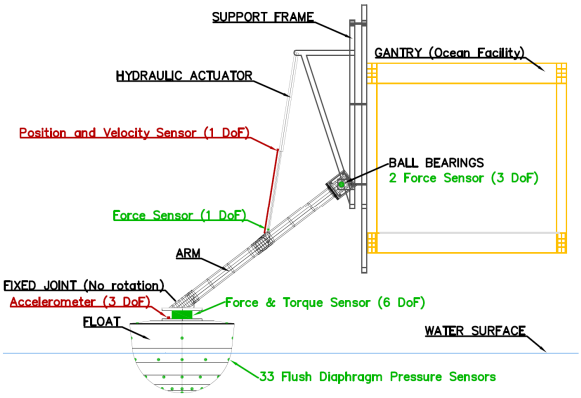

Figure 2. Sensors used to monitor the WEC. Motion sensors in red and load sensors in green.

The pressure exerted on the surface of the float is measured by flush diaphragm pressure sensors, which are distributed in eight discrete direction at five heights including additional four sensors on top of the float. This brings the total number of pressure sensors to 33, which has been determined to be sufficient to obtain a reasonable mapping of the pressure distributions.

Resistive wave gauges are used in the basin to measure the surface elevation (see Figure 3). These include a six gauge pentagon array in front of the device to measure the directional wave spectrum. Series of three gauges measures wave radiation from the device and wave reflections from the walls. Two sets of gauges are placed around the float in the default 90 deg. Position (purple outline on Figure 3). One set is placed towards the closest wall when the device is turned 0 deg.

To measure the particle velocity around the float two acoustic velocity profilers are used. One is placed in front of the device together with the pentagon array to measure the incident waves and/or current. The second is placed in the same location as the float; offset perpendicular to the flow direction to obtain approximate particle velocities at the float location. Both acoustic Doppler velocity profilers are placed to measure current velocities in a range from 32 – 35cm below still water level.

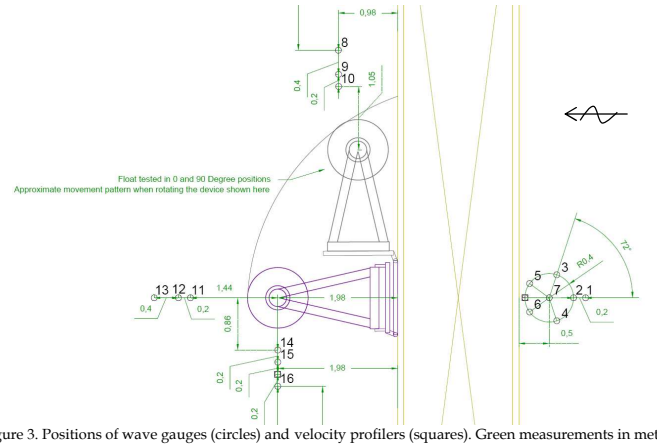

Figure 3. Positions of wave gauges (circles) and velocity profilers (squares). Green measurements in meter.

3. Wave-WEC Forces

The experiments in this section is the regular wave experiments carried out for the 90 degree setup (purple outline in Figure 3), a complete listing of these are found in Table 2. The forces on the cylinder are defined by the governing force equation $F_{cyl} = Bv + Kx$, where control parameters are damping and stiffness. The cylinder force can be obtained directly from measurement using a force sensor placed in the far end of the actuator rod, F_{cyl}, and verified by deriving it from the pressure sensors measuring the hydraulic pressure on either side of the piston, denoted F_{hyd},. The forces obtained are chosen as the average of the maximum forces from the first 15 fully developed waves. The difference in magnitude between F_{cyl} and F_{hyd} being the friction in both the cylinder of the actuator and the ball bearings. In Figure 4, the correlation between cylinder forces is shown with variation in the damping coefficient used on the hydraulic actuator. The experiments are carried out so that the wave height is kept constant (H = 0.10 m) and the wave period is varied and vice versa (T = 1.4 s). It should be noted that damping D = 0 is not to be mistaken as true free floating as the flow of the hydraulic oil is limited by the inlets and outlets of the actuator. A subset of the experiments with variations in damping is shown in Figure 4, where at good correlation is shown with wave height when the wave period is kept constant. The increase in cylinder forces for zero damping for shorter wave periods suggest that the device was in resonance with the waves.

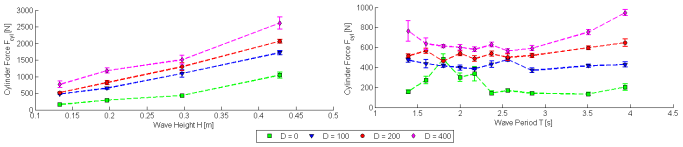

Figure 4: Cylinder force plotted against wave height and period in regular wave experiments with varying damping coefficients of the PTO.

To show variation in both wave height and period and thereby give a more wholesome indication of the effects of the WEC under damped PTO conditions the cylinder forces normalized with the linear theory are compared to the wave steepness, *S*, and the H²T relation. The cylinder forces from the complete set of regular wave experiments are shown in Figure 5. As the purpose of the damping experiments was to determine the device during both high and low degrees of damping it was necessary to limit the wave height to maximum of 38cm, which means that the maximum forces measured, are insignificant compared to the survivability conditions. Not surprisingly, there is a clear indication that larger damping leads to higher forces on the cylinder, but there is also an indication that there is an increase in the non-linear contribution, to the forces in the wave steepness range examined.

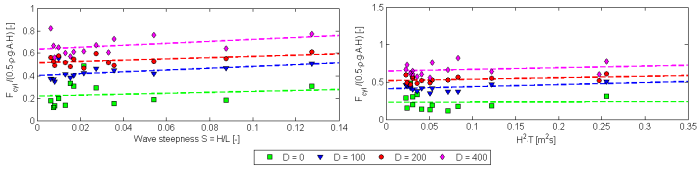

Figure 5. Overview of cylinder force during 54 regular waves.

The six degrees of freedom (DOF) are measured at the joint between the float and arm using a F/T sensor with load range $F_{x,y}$, F_z, $M_{x,y,z}$: 3600 N, 9000 N, 700 Nm and accuracy $F_{x,y}$, F_z, $M_{x,y,z}$: 4.25%, 2.25%, 3.25%. Only the significant DOFs are listed in Figure 6, and the hydrostatic forces are removed to show only the maxima of the dynamic components.

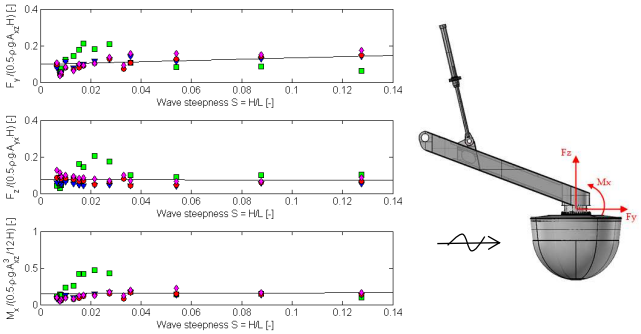

Figure 6. Governing float forces and moments for the regular wave series.

A more thorough experimentation with various float controls was tested under three distinct regular waves, the results are listed in Table 1. In free float conditions, it was necessary to limit the experiments carried out due to safety concerns regarding the stroke length of the actuator. It should be noticed that two types of free float conditions are listed below. One method using control but with no damping and stiffness, and one where the hydraulic system is open-ended and oil is drained thereby reducing the damping further.

Table 1. Float force and moment using various control strategies. RA02: H=0.15m, T=1.4s. RC02: H=0.25m, T=2.8s. Rext: H=0.68m, T=2.0s.

Float Force F_y /M_x [N/Nm]	RA02	RC02	REXT
FREE FLOAT (NO HYD. CIRC.)	158.5/71.0	308.2/131.8	-
FREE FLOAT D=0	131.4/43.8	-	-
DAMPED D=50	153.1/45.5	-	-
DAMPED D=100	177.4/43.2	-	-
CONTROL D=100 K=50	161.0/48.3	184.4/43.2	895.1/119.0
DAMPED D=200	197.0/47.8	-	-
DAMPED D=200	236.2/59.8	158.2/34.3	856.0/117.5
DAMPED D=400	245.6/72.1	-	-
LOCKED	219.0/61.3	182.8/72.3	906.2/207.1

From Table 1 it is evident that the two free float scenario leads to different load scenarios, with a significantly higher moment in the float-arm joint, which could seem to suggest that the hydraulic PTO has a significant passive damping. The experiments with both damping and stiffness control is not tuned to the individual regular wave series. In spite of this there are still a clear indication that the forces increases significantly for the larger waves with long wave periods. The curious difference between the two experiments with D = 200 is unknown, but is observed in velocity measurements as well and might be due to wrongfully setup damping in the second attempt as that is the outlier when using best straight line between the damping experiments.

4. Wave-WEC Surface Pressures

The pressure sensors used in the experiments are positioned to have the sensor membrane completely flush with the surface of the hemisphere to avoid air pockets. The gauge pressure sensors operates in the range ±5 m water column with an accuracy: ±0.04%. A complete overview of the pressure sensors and the numbering are shown in Figure 7, where the main axis corresponds to the axis shown in Figure 6. To present the pressure sensors in a meaningful way, only a select few sensors are examined in this section. Starting out with the before mentioned regular waves and the sampling rate fs = 100 Hz.

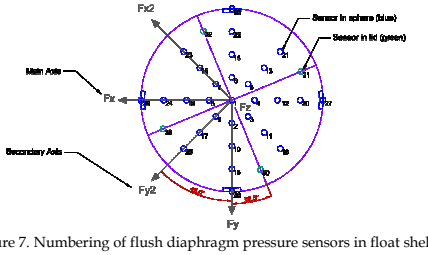

Figure 7. Numbering of flush diaphragm pressure sensors in float shell.

The general characteristics of the pressures on the float under regular waves are shown in Figure 8, where the sensors in the middle of the float are selected on the side of the incident wave. For the pressure sensors, the hydrostatic pressures are included. Evidently, the pressures closer to the water surface are progressively better correlated with the wave steepness.

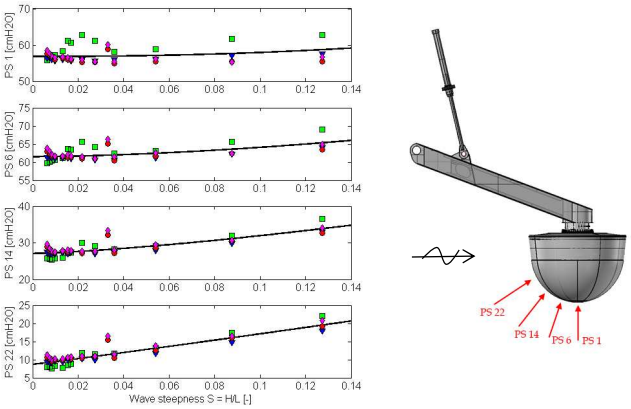

Figure 8. Pressure on the float shell on the side of the incident wave.

5. Conclusions

The experience was overwhelmingly positive in working with both the new setup and using the Ocean Wave Basin at the COaST facility. Within one week of setting up the device and hydraulic PTO the device was up and running and all sensors were measuring according to specifications.

The device performance was satisfactory, both in terms of mechanical response of the system and the quality of the acquired data. The most essential tests were carried out during the testing phase, however some had to be dropped either due to physical limitation of the wave maker, PTO or simply due to time constraints.

The first results collected from the regular wave experiments are presented here. They provide a general insight into the loads on the device during normal operation conditions using various control strategies and special scenarios. For the experiments with varying damping coefficients there seems to be a reasonable constant relation between the measured forces normalized with the linear analytical theory and the steepness of the waves. The forces from the complete list of control strategies appears to be coherent with a reasonably linear fit between the incremental damping coefficients.

Only the surface of the results has been examined so far, and it is the intention of the authors to start to compare the results with numerical and analytical solutions in the near future. A numerical Morison model is under development and should be ready for the regular wave series later this the year, and more advanced models based on OpenFOAM are being developed at partner universities. The results and measured data from these experiments are available upon request, for more information and details about the project see the webpage http://homes.civil.aau.dk/mmj/AAUWS.

Acknowledgments
The authors acknowledges the support.

MARINET, a European Community - Research Infrastructure Action under the FP7 “Capacities” Specific Programme.

FLOAT2, “New Flexural UHPC Application for Wave Converters 2” and "Digital Hydraulic Power Take Off for Wave Energy" which are funded through the Danish ForskEL-programme by Energinet.dk.

SDWED, Structural Design of Wave Energy Devices, an international research alliance supported by the Danish Council for Strategic Research.

COaST staff and research group at Plymouth University.

References

[1] Hansen, R. H. and Kramer, M. M., 'Modelling and Control of the Wavestar Prototype', Ewtec, 2011.
[2] Kramer, M. M., Zurkinden, A., Vidal, E., Hansen, R., 'Comparison between linear numerical models and experimental results on a Wavestar point absorber'. Proc. ICOE2012, Dublin, Ireland, 2012.
[3] Kramer, M. M., Marquis, L., Frigaard, P., 'Performance Evaluation of the Wavestar Prototype', Ewtec, 2011.
[4] Tromans, P.S., Anaturk, A.R., Hagemeijer, P., 1991. 'A new model for the kinematics of large ocean waves—applications as a design wave'. Proceedings of the 1st International Offshore and Polar Engineering Conference, Edinburgh, vol. 3, pp. 64–71.

Appendices

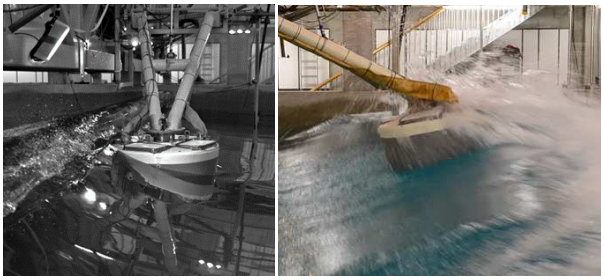

Figure 9. Freak waves caught with high-speed camera.

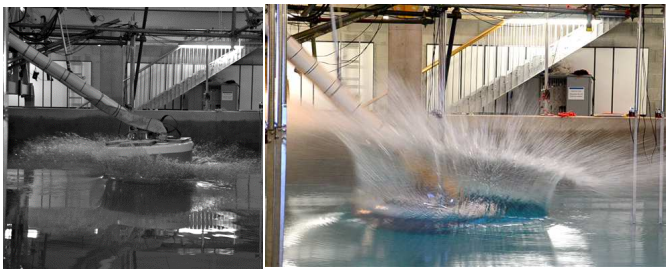

Figure 10. Drop test where the hydraulic system is bypassed to allow a free decay drop.

Table 2. List of successful regular wave tests

Regular Waves	H (m)	T (s)	NoFloat	Locked	Damped						Free*	Free**
Name					0	50	100	200	400	500		
RA01	0.1	1.4	x	x	x	x	x	x	x	x	x	
RA02	0.15	1.4	x	x	x	x	x	x	x		x	x
RA03	0.25	1.4	x	x	x	x	x	x	x		x	
RA04	0.38	1.4	x	x	x	x	x	x	x		x	
RB01	0.1	2	x	x	x	x	x	x	x		x	
RB02	0.25	2	x	x							x	
RB03	0.4	2	x	x								
RB04	0.55	2	x	x								
RB05	0.65	2	x									
RExt01	0.68	2	x	x				x				x
RC01	0.1	2.8	x	x	x	x	x	x	x		x	
RC02	0.25	2.8	x	x				x			x	x
RC03	0.4	2.8	x	x							x	
RC04	0.6	2.8	x									
RD01	0.1	3.5	x	x	x	x	x	x	x		x	
RD02	0.25	3.5	x	x							x	
RD03	0.5	3.5	x								x	
RE01	0.1	4	x	x							x	
RE02	0.15	4	x	x							x	
RE03	0.21	4	x								x	
RF01	0.1	1.6	x	x	x	x	x	x	x		x	
RF02	0.25	1.6	x	x							x	
RF03	0.4	1.6	x								x	
RF04	0.48	1.6	x									
RG01	0.1	2.4	x	x	x	x	x	x	x		x	
RG02	0.25	2.4	x	x				x	x		x	
RG03	0.4	2.4	x	x							x	
RG04	0.6	2.4	x									
RG05	0.7	2.4	x									
RH01	0.1	1.8	x	x	x	x	x	x	x		x	
RH02	0.25	1.8	x	x							x	
RH03	0.4	1.8	x	x							x	
RH04	0.5	1.8	x									
RH05	0.6	1.8	x									
RI01	0.1	2.2	x	x	x	x	x	x	x		x	
RI02	0.25	2.2	x	x							x	
RI03	0.4	2.2	x	x							x	
RI04	0.55	2.2	x								x	
RI05	0.7	2.2	x									
RJ01	0.1	2.6	x	x	x	x	x	x	x		x	
RJ02	0.25	2.6	x	x							x	
RJ03	0.4	2.6	x	x							x	
RJ04	0.55	2.6	x								x	
RJ05	0.7	2.6	x									

* Electrical system disabled but hydraulic oil still circulates.

** Disconnected hydraulics.

Paper E

Layout of Wave Gauge Array for Estimation of 3D Waves

Morten M. Jakobsen and Peter Frigaard

The conference proceedings has been published in the
4th International Conference on The Application of Physical Modelling to Port and Coastal Protection, Coastlab Vol. 1, pp. 400–407, 2012.

The layout has been revised.

LAYOUT OF WAVE GAUGE ARRAY FOR ESTIMATION OF 3D WAVES

MORTEN M. JAKOBSEN [1] & PETER FRIGAARD [2]

[1] *Ph.D. Student, Department of Civil Engineering, Aalborg University, Sohngaardsholmsvej 57, Aalborg, 9000, Denmark. mmj@civil.aau.dk*

[2] *Head of Department, Department of Civil Engineering, Aalborg University, Sohngaardsholmsvej 57, Aalborg, 9000, Denmark. pf@civil.aau.dk*

Abstract

Wave gauge array are commonly used to estimate significant wave properties of multi-directional waves. The objective of this study is to gain insight into which parameters influence the accuracy of an array. The approach chosen is to determine the accuracy of an array by comparing generated waves with estimates obtained through analysis in the frequency domain. In this study the waves are generated using a random phase method not including noise; which are then analysed using an implementation of the Bayesian Directional Method. Then using this method various wave gauge array are tested using synthetic data.
The long term goal of this research is to incorporate the findings into existing wave analysis methods by updating their weighting function and improve the accuracy. It would also be possible to create software able to help determine which wave gauge array is advisable based on the laboratory facility.
Keywords: Lag-array, Bayesian Directional Method, Frequency domain analysis, Wave gauge array evaluation.

1. Introduction

Wave analysis is one of the most fundamental aspects of ocean engineering. The aspects of obtaining the height, period and direction of waves is by no means new. In fact one of the most commonly used wave gauge array today dates back to the publication of the Cerc array, created by Borgman L. E. (Panicker and Borgman, 1970). The Cerc wave gauge array is shown in Figure 1.

Since then several new measuring techniques and devices has been developed, but using wave gauge array is still among the preferred methods today. This is due to the high accuracy and the low cost involved when using this device.

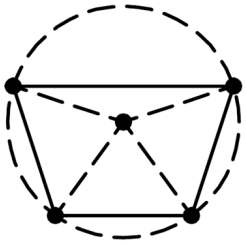

Figure 1. Cerc wave gauge array by Borgman, L. E.

The main purpose of this study is to determine which parameters are affecting the accuracy of a wave gauge array for multi-directional waves. Preceding this study (Haubrich, 1968; Davis and Regier, 1977) worked with a method here named a lag-array. This method is essentially a mapping of the time or distance between wave gauges. Some general properties of the lag-array were outlined which will be part of the basis of this study. In an intermediate study by (Goda and Suzuki, 1976) a proposal was made for advisable limits of the distance between wave gauges relative to the wavelength. This

study where aimed at laboratory experiments of unidirectional waves. It is here examined if these limits also apply for determining directional spreading of waves.

It is then sought to find a procedure which can be used to evaluate the accuracy of a wave gauge array. In this context the accuracy of the array is determined by the parameters commonly sought for using these arrays. The approach chosen is that of frequency domain analysis. This means that the criteria which affect the accuracy of a wave gauge array will be the directional wave spectrum (DWS). To obtain the DWS an implementation of the so-called Bayesian Directional Method (BDM) will be used, which is a high accuracy and fairly robust probability domain method created by (Hashimoto and Kobune, 1988). This method requires a smooth DWS and for this reason it is chosen to use a realistic sea state with directional spreading. This complicates the interpretation of the results but it is chosen because the probabilistic BDM method smoothens and weighs the information obtained from the wave gauges. This smoothing and weighting would otherwise not be considered. To limit the number of uncertainties involved in the evaluation of the spectral estimates some simplifications are made to the initial procedure. The most important one is that only synthetic data obtained from computer generated data will be considered at this point. This approach is chosen as it rules out uncertainties involved in laboratory testing.

The performance of various existing wave gauge array are compared using this evaluation technique. The simulated data are varied on peak frequency and mean direction relative to the array. Based on the obtained results it is sought to determine how the placement of wave gauges affect the results.

2. Methods

In order to evaluate and compare wave gauge array it is necessary to decide which criteria has the highest priorities. The most apparent is the accuracy of the array which will be further examined shortly. Another parameter that will be taken into account is the number of wave gauges used, which may be a limiting factor for the laboratory facilities. Practical parameters may also be of importance such as the extent of an array and the difficulty in the placement of the gauges. The practical requirements of the array is outside the scope of this study, only the number of wave gauges and the accuracy will be taken into account.

The parameters which are attributing to the accuracy of an array are here defined as the wave height, peak period, the mean wave direction and the directional spreading. These parameters can be obtained from the DWS in the frequency domain. One way of determining the accuracy of the wave gauge array is to compare each of these criteria as seen in (Hawkes, P. et al., 1997). As the target DWS used for the wave simulation is known it is more convenient to compare this to the estimate obtained from the BDM. The comparison is made for each discrete frequency and direction in the spectra. By doing this only the deviation between the target and estimated spectrum needs to be compared for each test.

The way the BDM works is by making some a priori assumptions about local smoothness of the DWS. This necessitates the use of a smooth spectrum for both frequency and direction which has led to the use of the Jonswap spectrum with a cosine directional distribution. This spectrum is chosen as it is traditionally used when modelling a sea state from the North Sea. The generation of these waves is done using deterministic Random PHase Inverse Fast Fourier Transformation, (here referred to as RPH-IFFT). It is expected that the generated spectrum will be well approximated by the target DWS by choosing the sample duration based on the sample length of the IFFT block size over the sampling frequency.

The parameters which might affect the accuracy of a wave gauge array are determined using a mapping of the latencies between gauges called the lag-array or co-array depending on the literature see (Haubrich, 1968; Davis and Regier, 1977; Goda, 2010). In this array only unique lags are considered to contribute to the limitation of the side-lobes of the resolving window and thereby the accuracy of the cross spectral density functions and the DWS estimate. The criteria which are considered to be affecting the DWS estimate are the number of elements in the lag-array, the uniformity of the distribution of elements and the minimum and maximum extent of the array (Davis and Regier, 1977). These conditions are explained by example using the 2D array with four wave gauges in Figure 2.

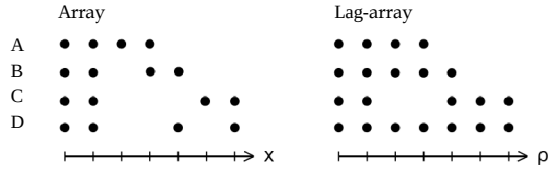

Figure 2. Line array using four gauges and corresponding lag-array.

Array A is a simple line-array with equal distance between gauges, without sacrificing the uniformity of the lag-array the array in B increases the number of elements in the lag-array. C increases the extent further but sacrifices the uniformity of the array. The array of (Barber, 1963), shown in D achieves the theoretical maximum.

Additional specifications are made to the extents of the lag-array using the non-dimensional gauge separation distance λ / L in which λ is the gauge separation distance, and L is the wave length. For laboratory experiments on 2D waves (Goda and Suzuki, 1976) suggested to use the limits specified in Equation 1.

$$0.05 < \lambda / L < 0.45 \qquad [1]$$

These limits are used as a guideline for these simulated wave series as well. For values surpassing the lower limit it is understood that the gauge separation is too small to accurately determine the directionality of the waves; but in general the accuracy is expected to decline with a decreasing distance between the gauges. The upper limit is in place to avoid aliasing which will occur at $\lambda / L = 0.50$ and any multiple thereof.

In this project the implementation of the lag-array will be three dimensional, to include the directionality of the waves. The way this is done is by calculating the projections of each wave gauge pair onto each discrete direction as seen in Figure 3. For illustration purposes the array used consists of only three of the five gauges in the Cerc array. This array is not useful in practice but is well suited to describe the concept.

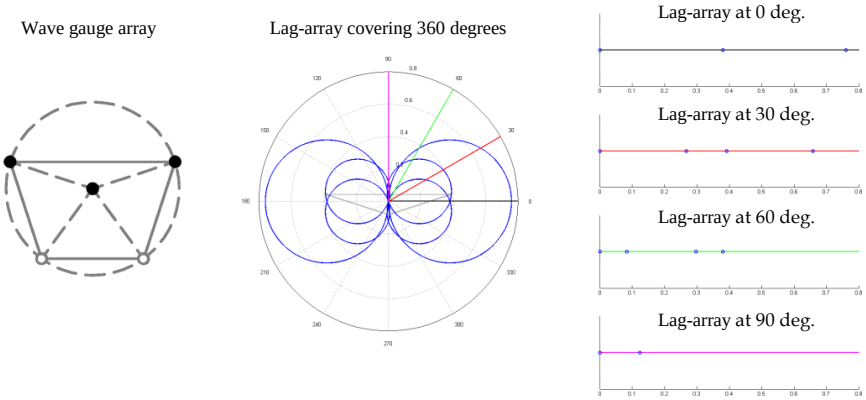

Figure 3. From left to right: Geometry of the reduced Cerc array, the corresponding 360 deg. lag-array, and an outtake of lag array for individual directions.

Applying the upper and lower limits to the lag-array an indication of the directional accuracy is starting to form. This is visualized in Figure 4, where the frequency band is determined by the frequency range in which significant energy is present. Waves are then generated using the RPH-IFFT and analysed using the BDM. The target DWS is then compared to the estimate obtained from the BDM for each discrete frequency and direction and an overall deviation is calculated. A comparison of the spreading function at the peak wave frequency ω_p is used to visualize the deviation of the obtained DWS from the target, see Figure 5.

The primary obstacle is then to show a correlation between Figure 4 and Figure 5. Depending on the strength of the correlation between the two it is possible to determine the accuracy of a wave gauge array using the lag-array.

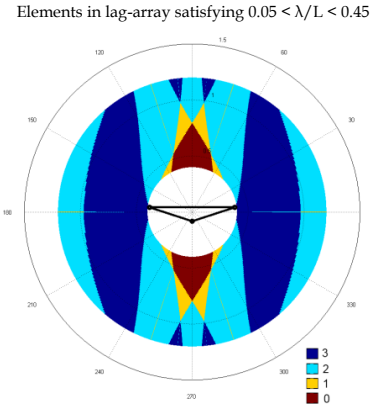

Figure 4. Elements in lag-array satisfying the limits by (Goda and Suzuki, 1976).

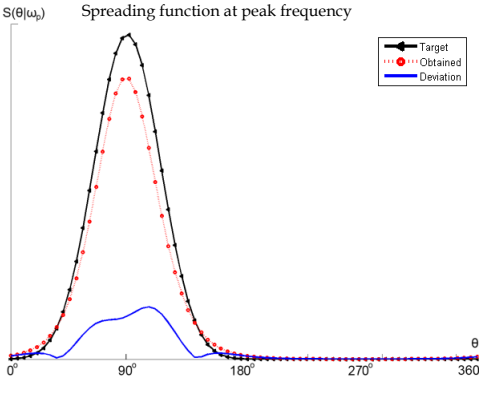

Figure 5. Target and obtained spreading function at the peak frequency for the 3-gauge array.

3. Results and discussion

Using the method described several existing wave gauge array are tested and compared to help determine how the uniformity of the array and the upper and lower limits affects the accuracy. These arrays are a star array, the so-called Cerc array, the pentagon and the Haubrich array shown in Figure 6. It should be noted that the dashed and full lines are only there to help interpret the geometry of the array. The Star, Cerc and pentagon array are chosen as have shown to perform well for their respective sizes. The Haubrich array is chosen as it is an example of an array with a uniform distribution of the elements in the lag-array, see Figure 7.

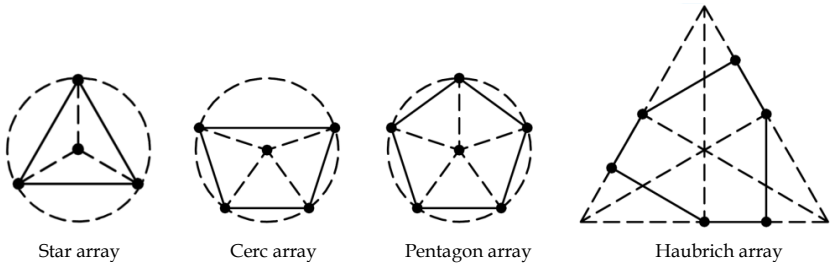

Figure 6. From left to right: 4-gauge Star array, 5-gauge Cerc array, 6-gauge Pentagon array and 6-gauge Haubrich array.

The size of the array is here chosen as the distance from the center of the array to the node closest. For these four arrays it means that the Haubrich array has three nodes at a greater distance than the nominated size of the array.

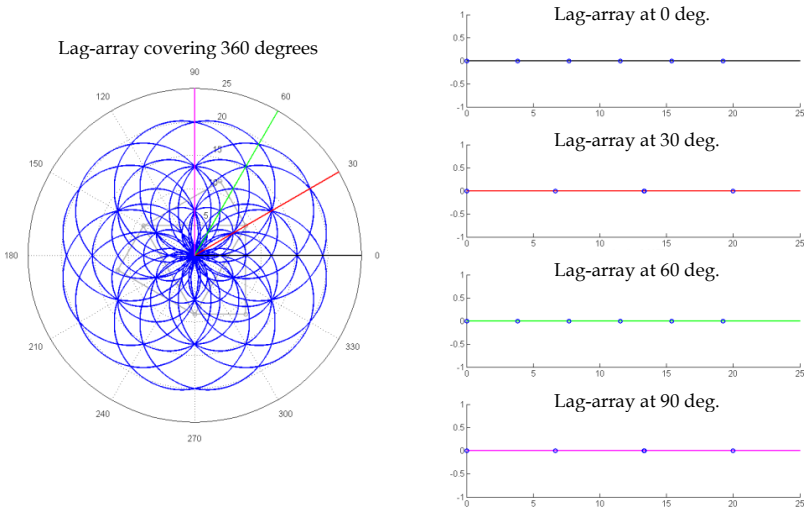

Figure 7. Lag-array for the Haubrich wave gauge array in which the lag-array has a highly uniform distribution.

To ensure that each array is subjected to the same wave conditions the four arrays are tested on the same wave series. The characteristics of this wave series are a water depth of 3m, wave peak period of 3s and significant wave height of 0.8m which results in a significant wave length of 12.7m for 1st order theory. The tests performed are focusing on the array to wave length ratio and the direction of the waves. To limit the effect of the discretized spectrum the changing of the mean wave direction is managed by rotating the arrays. The array to wave length ratio is obtained by adjusting the distances between the wave gauges.

The tests performed are listed in Table 1. They are chosen to examine the effect when moving near the upper and lower limits. It is important to notice here that λ^* / L^* is a scale ratio and will only be used for relative comparison between the three sets of tests. This is because the before mentioned size of the array is used to scale the array as the actual elements in the lag array span over a large variety lengths and the wave lengths are varying in the irregular wave series.

Table 1. Tests performed to evaluate the performance of the wave gauge array.

Test no.	Array/Wave length scale ratio λ^* / L^*	Direction θ [deg.]
1.1	0.1	0
1.2	0.1	45
1.3	0.1	90
2.1	0.4	0
2.2	0.4	45
2.3	0.4	90
3.1	0.7	0
3.2	0.7	45
3.3	0.7	90

The resulting deviation between the target spectrum and the spectrum estimated using the BDM analysis is listed in Table 2.

Table 2. Resulting deviation between the target directional spectrum and the estimate of the BDM method on the four selected wave gauge array.

Test no.	Star dev. [%]	Cerc dev. [%]	Pentagon dev. [%]	Haubrich dev. [%]
1.1	14.8	15.4	11.3	20.4
1.2	12.3	10.8	14.1	12.5
1.3	14.4	14.5	11.6	14.1
2.1	11.0	10.4	10.0	10.1
2.2	10.1	12.4	9.6	10.7
2.3	11.5	9.9	11.8	10.3
3.1	16.4	12.5	11.6	10.9
3.2	16.0	13.0	12.3	13.1
3.3	14.9	12.0	12.0	14.3

The average value for all wave gauge array in $\lambda^* / L^* = 0.1$ is 13.9, for $\lambda^* / L^* = 0.4$ it is 10.7 and $\lambda^* / L^* = 0.7$ is 13.3. This indicates that there is a likely correlation between the overall accuracy of an array and the Array/Wave length ratio and might suggest that there is a decrease in the

accuracy when an increasing amount of the elements in the lag-array are outside the limits $0.05 < \lambda / L < 0.45$.

Comparing the Pentagon array with the Haubrich array there is no indication that the uniformity of the lag-array and the accuracy of the array. This has both been the case in the recent tests shown in Table 2 and through comparison of the directional spreading which were performed prior to the revised comparison procedure. In Figure 8 only the Haubrich and Cerc array are compared using a fixed array size of 0.5m with varying wave peak frequencies from 0.2Hz to 5Hz. The relative spreading used to define the deviation in the figure is determined by the estimated spreading over the target spreading.

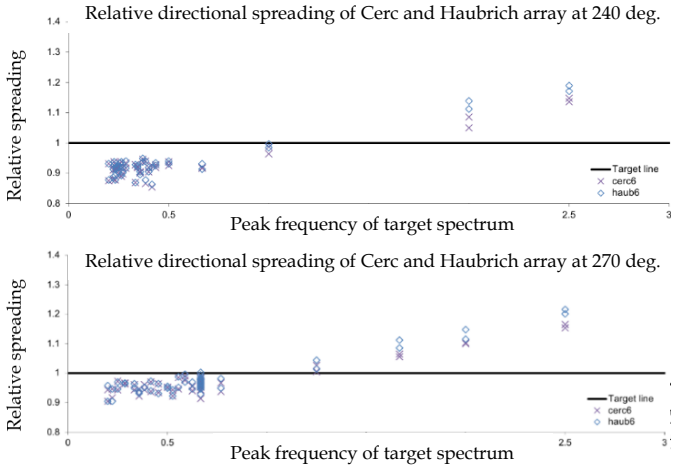

Figure 8. Directional spreading of the Cerc and Haubrich array. The relative spreading is defined as the spreading estimate over the target estimate.

4. Conclusions

Part of the purpose of this study was to make a connection directly between the accuracy of the estimates obtained from the wave analysis software. But this presented uncertainties particularly in regards to the irregular short-crested waves. However; the results did indicate that there is possibly a connection between the λ / L ratio and the accuracy of the array. It is still uncertain exactly how the λ / L ratio affects the accuracy. But all tests seem to indicate that when the elements in the lag-array are within the limits $0.05 < \lambda / L < 0.45$ they produce reasonable accuracy whereas when they are getting too close or too far the accuracy is reducing.

The effect of aliasing ($\lambda / L = 0.5n$, for $n = 1,2,...,N$) was smaller than expected. But this is likely due to the irregular wave series.

The uniformity of the lag-array has not shown to be important for the accuracy of the array. At least not when considering the Haubrich array as it has not shown better accuracy when compared to the Pentagon array.

Future work should focus on trying to create a stronger connection between the λ / L ratio and the accuracy of the array. It should then be incorporate into existing wave analysis

methods by updating their weighting function whereby an increased accuracy should be obtained.

The next step is to include artificial noise in the measurements to resemble what is seen in laboratory environments and determine how this affects the results. By this point it should be possible to predict which waves gauge array would be most suitable for a specific wave basin.

References

Barber, N. F., 1961. 'The directional resolving power of an array of an array of wave detectors', Ocean Wave Spectra, Prentice-Hall, Englewood Cliffs, N. J., p. 137-150.

Borgman, L. E., Panicker, N. N., 1970. 'Directional spectra from wave-gage arrays', *Proceedings of the Twelfth Coastal Engineering Conference*, 12, pp. 117-136.

Davis, R. E., Regier, L. A., 1977. 'Methods for estimating directional wave spectra from multi-element arrays', *Journal of marine research*, 35 (3), pp. 453-477.

Goda, Y., Suzuki, Y., 1976. 'Estimation of incident and reflected waves in random wave experiments'. *Proceedings of the 15th Coastal Engineering Conference*. Vol. 1. New York, pp. 828-845.

Goda, Y., 2010. 'Random seas and design of maritime structures', 3rd Edition. Vol. 33 of Advanced Series on Ocean Engineering, World Scientific Publishing Co. Pte. Ltd., 5 Tok Tuck Link, Singapore. ISBN: 981-4282-40-5.

Hashimoto, N., Kobune, K., 1988. 'Directional spectrum estimation from a Bayesian aproach', *Proc. 21st ICCE*, 21(1), pp. 62-76.

Haubrich, R. A., Jun. 1968. 'Array design', *Bulletin of the Seismological Society of America*, 58 (3), pp. 977-991.

Hawkes, P., Ewing, J., Harford, C., Klopman, G., Stansberg, C., Benoit, M., Briggs, M., Frigaard, P., Hiraishi, T., Miles, M., Santas, J., Schäffer, H., 1997. 'Comparative Analyses of Multidirectional Wave Basin Data', *Proc. IAHR*, 27, pp. 25-43.

Isobe, M., Kondo, K., Horikawa, K., Jun. 1984. 'Extension of MLM for estimating directional wave spectrum', *Symp. Description and Modelling of Directional Seas*, Vol. A6. DHI & MMI, pp. 1-15.

Part I

Appendices

Appendix F

Water-Structure Interactions on a Point Absorber

Morten M. Jakobsen

The DCE Technical Report has been published in the
Videnbasen for Aalborg Universitet, VBN, Department of Civil Engineering DCE
Technical Reports Series, no. 183, p. 23, 2015.

The layout has been revised.

Water-Structure Interactions on a Point Absorber

Morten Møller Jakobsen

ISSN 1901-726X
DCE Technical Report No. 183

DEPARTMENT OF CIVIL ENGINEERING
AALBORG UNIVERSITY

Aalborg University
Department of Civil Engineering
Wave Energy Research Group

DCE Technical Report No. 183

Water-Structure Interactions on a Point Absorber

by

Morten Møller Jakobsen

February 2015

Scientific Publications at the Department of Civil Engineering

Technical Reports are published for timely dissemination of research results and scientific work carried out at the Department of Civil Engineering (DCE) at Aalborg University. This medium allows publication of more detailed explanations and results than typically allowed in scientific journals.

Technical Memoranda are produced to enable the preliminary dissemination of scientific work by the personnel of the DCE where such release is deemed to be appropriate. Documents of this kind may be incomplete or temporary versions of papers—or part of continuing work. This should be kept in mind when references are given to publications of this kind.

Contract Reports are produced to report scientific work carried out under contract. Publications of this kind contain confidential matter and are reserved for the sponsors and the DCE. Therefore, Contract Reports are generally not available for public circulation.

Lecture Notes contain material produced by the lecturers at the DCE for educational purposes. This may be scientific notes, lecture books, example problems or manuals for laboratory work, or computer programs developed at the DCE.

Theses are monograms or collections of papers published to report the scientific work carried out at the DCE to obtain a degree as either PhD or Doctor of Technology. The thesis is publicly available after the defence of the degree.

Latest News is published to enable rapid communication of information about scientific work carried out at the DCE. This includes the status of research projects, developments in the laboratories, information about collaborative work and recent research results.

Published 2015 by
Aalborg University
Department of Civil Engineering
Sofiendalsvej 11,
DK-9200 Aalborg SV, Denmark

Printed in Aalborg at Aalborg University

ISSN 1901-726X
DCE Technical Report No. 183

Recent publications in the DCE Technical Report Series

ISSN 1901-726X
DCE Technical Report No. 183

Contents

Preface **ix**

Introduction **1**

1 Current Flumne **3**
1.1 Method . . . 3
1.2 Results . . . 3
1.3 Discussion . . . 5

2 Wave Basin **7**
2.1 Introduction . . . 7
2.1.1 Setup . . . 8
2.1.2 Wave Conditions . . . 9
2.2 Methods . . . 10
2.3 Results . . . 11
2.4 Discussion . . . 16

Conclusion **17**

Bibliography **19**

A Instrumentation and Data Acquisition in Wave Basin **21**
A.1 The Float and embedded sensors . . . 21
A.2 Force and Torque transducer . . . 22
A.3 Simulink and XPC data acquisition . . . 22
A.4 Surface Elevation and Velocimetry . . . 23
A.5 The Basin and Wave Series . . . 25

Preface

All experiments in this report is from sessions in the current flume and wave basin at Aalborg University. The experiments span two years, 2012-2013, with experiments repeated in both the flume and basin. Only the most recent experiments are presented.
The experiments were carried out with Morten Mejlhede Kramer and technicians Nikolaj Holk and Niels Drustrup throughout the experiments. Other researchers involved in the experiments includes, Francesco Ferri, Scott Beatty, Morten Thøtt Andersen, Thomas Viuff and Oana Coman.

Morten Møller Jakobsen
mmj@civil.aau.dk
http://homes.civil.aau.dk/mmj/
Sofiendalsvej 11, Room: 11.218
9000 Aalborg

Introduction

This technical report presents experiments carried out in the current flume and wave basin at Aalborg University in 2012 and 2013. The results of the experiments were never published under pee-review. The experience from the experiments (good and bad) has been the primary catalyst to more successful work later and may be helpful to others working with physical models and experiments.

The purpose of the experiments is to examine the wave and current induced loads on a floating point absorber (wave energy converter). Wave energy converters are used in ocean- or costal regions where significant wave loads occur. This means that wave loads will be the governing force to account for, which will typically mean that forces are inertia dominated with some drag contribution. The results presented will determine the magnitude of these load components using Morison's equation.

First chapter determines the drag component using a variety of current velocities in the stream canal. Second chapter primarily determines the inertia component from regular wave experiments in the wave basin. The contribution from drag is estimated in the latter and compared with those found in the former.

Chapter 1

Current Flumne

The primary purpose of the experiments in the current flume was to determine the drag coefficient of the hemisphere. This was strongly motivated by the anticipation difficulty in separating drag from the inertia-dominated waves in the basin.

1.1 Method

The setup in the current flume is seen in Fig. 1.1a, with the dimensions of the float in Fig. 1.1c. It consisted of a 25 cm Styrofoam hemisphere with a painted surface with a 6-axis load-cell on top. During the experiments, the float was kept in place using an overlaying crossbeam. The level of submersion was closely monitored to ensure that the wetted surface area remained constant. The velocity was measured 5 cm below the water surface using both a propeller and from ultrasonic measurements cf. Fig. 1.1b.
In pure current the drag coefficient is calculated using Eq. 1.1 and the Reynolds Number from Eq. 1.2.

$$C_D = \frac{F_y}{0.5 \cdot \rho \cdot u^2 A} \tag{1.1}$$

$$Re = \frac{u \cdot D}{\mu} \tag{1.2}$$

1.2 Results

Undisturbed velocity profiles were made with low- and mid-range velocities cf. Fig. 1.2.

Using Eq. 1.1 the drag coefficients were plotted with Reynolds numbers in Fig. 1.3. Additional results were included from experiments carried out with a similar setup in 2008.

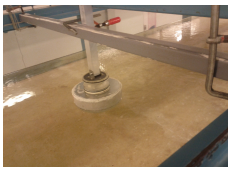

(a) Float and mount.

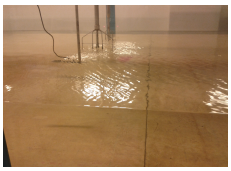

(b) Velocimeters.

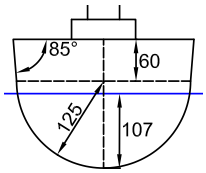

(c) Float proportions.

Figure 1.1: Experimental setup in flume in Aalborg. Measurements in mm.

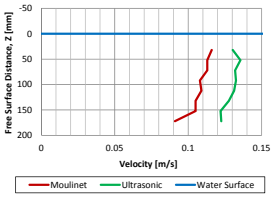

(a) $u \approx 0.125$ m/s.

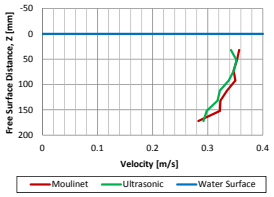

(b) $u \approx 0.345$ m/s.

Figure 1.2: Velocity profile in low- and mid-range currents.

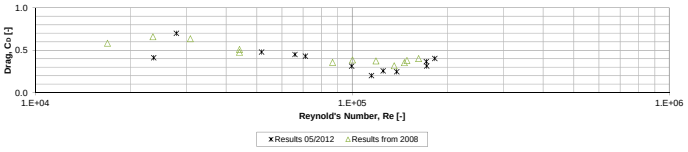

Figure 1.3: Drag coefficient from stream canal experiments.

1.3 Discussion

The water level in the flume was kept rather high compared to normal operation to limit the effect of the boundary layer. This had the adverse effect that the pump would reach maximum capacity. This led to some unfortunate time-dependent fluctuations in the velocity, and from observations, a rapidly increasing turbulence. Data series with significant fluctuations were discarded and used to determine the upper limit on the velocity range.
As seen in Fig. 1.2a, the lower velocities caused the propeller to deviate quite severely from the ultrasonic measurements. This was attributed to friction in the propeller. For velocities lower than 0.2m/s the propeller measurements were discarded. With velocities greater than 0.2 m/s the deviation between the two was less than 5%. With these limitations the velocity range still covered 0.08 to 0.72 m/s equivalent to a Reynolds range of $2.36 \cdot 10^4$ to $1.82 \cdot 10^5$ seen in Fig. 1.3.

Chapter 2

Wave Basin

Experiments are performed in both current flume and wave basin to determine current and wave interactions with a hemispherical point absorber. Firstly an investigation is performed on the device to determine the influence of drag and inertia forces in various wave conditions for the specific device. Secondly it is shown how the causal control of the floats motions will affect the fluid-structure interactions.

2.1 Introduction

Established developers of renewable energy devices have long been struggling for these devices to become economically feasible alternatives to fossil fuels. This is a steep challenge for emerging industries such as wave energy, which is still attempting to bring their models to a commercial stage. The typically used measurement is the cost of energy, which includes, structural costs, operation and maintenance. To reduce structural cost, cheaper production materials and production methods are often considered.
The glass fiber and steel structure solutions that have been used so far is an expensive solution. For the Wavestar device an alternative is considered using reinforced concrete for the arm and fiber-reinforced concrete for the shell. A significant drawback of concrete when used in this context is the weight. The own weight affects the system when the floats needs to be pulled out of the water during storm protection (where the device jacks further up for protection against the waves). For the half-scale prototype, the solution is to increase the size of the cylinder lifting. The larger cylinder size increases the initial cost, operation and reduces the efficiency. This is, however, offset by the decrease in the float and arm expenses. Reducing the expenses further can be done by increasing the knowledge of the loads on the float. This report seeks to study these forces both with the float in a stationary (locked) position, but some initial evaluation of the effects of causal control strategies (i.e. Hansen and Kramer (2011)) are considered too.
This paper will present the results of experiments with a small-scale device (1:40 of full-scale). Both drag and inertia contributions are examined in heave and surge

(wave propagation direction) in regular wave series. These coefficients are determined by locking the device in its natural buoyancy position to limit uncertainties. To determine the wave excitations on an active WEC the device is released from the locked position to allow it to oscillate freely within the confines of the arm and ball bearings. This is done is by not applying any force to the actuator. In this so-called free float state the regular wave series are repeated.
The third state tested is done using a causal controlled Power Take-Off (PTO) system. The PTO is not optimized for the waves in these experiments.

2.1.1 Setup

The device used is a new hemispherical float made in glass fiber shown in Fig. 2.1. The float has a diameter of 250mm which is a scale 1:20 of the Wavestar device installed at Hanstholm harbor in Denmark, eg. Kramer et al. (2011). The scale of the device has been chosen to correspond to the constraints given by the wave basin. The basin dimensions are 15.7m x 8.5m x 1m which allows for 0.65m water depth and wave heights of about 0.30m. For additional information on the instrumentation see Appendix A.

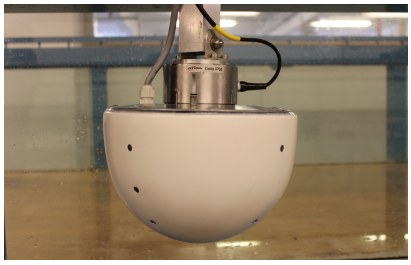

Figure 2.1: Hemisphere with 6-axis F/T-transducer and pressure sensors installed.

In the wave basin the device is connected to a frame on the platform above the basin, see Fig. 2.2. It consists of an arm extending at a fixed angle from the device to a bearing at the vertical support. The PTO control is implemented using a linear magnetic actuator.

To measure the environmental conditions to which the device is subjected to both resistive wave gauges and an Acoustic Doppler Velocimeter (ADV) are used. The measuring equipment used to monitor the excitation and the response of the device is a six Degree of Freedom (DoF) F/T sensor positioned between arm and float. The measurements of the pressure gauges will be omitted in this paper as they showed to be unreliable. The PTO force is determined using a force sensor placed between arm and the cylinder of the actuator. A laser displacement sensor

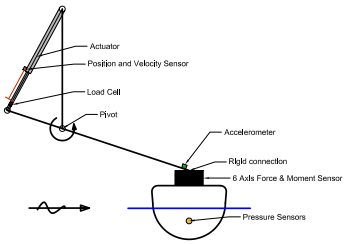

(a) Experimental concept.

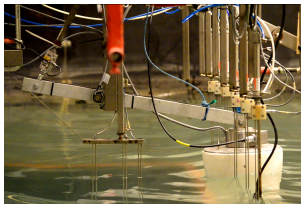

(b) Experimental setup.

Figure 2.2: Setup used during experiments in the wave basin.

is used to measure the position of the cylinder, which is used to determine angular velocity and acceleration of the arm by kinematic relations. This is cross-checked using an accelerometer located in the same location as the F/T sensor. Due to the extra measuring equipment the float is too heavy to float correctly in the water by buoyancy alone. To compensate for the extra weight it was necessary to apply a proportional uplifting moment in the ball bearings, which is achieved by applying a dynamic force offset to the actuator's control system.

2.1.2 Wave Conditions

For regular/monochromatic waves a total of 46 unique waves of varying wave heights and periods are used. The wave series reaches the upper and lower bounds of what is possible to make in the basin. At the selected water depth the bounds supplied to the wave generation software are wave heights between $H = 0.02 - 0.31$ m and periods from $T = 0.7 - 2.0$ s which leads to wave with steepness factors in the range of $s = 0.01 - 0.10$. This leads to a distribution of regular waves as shown in Fig. 2.3.

The wave makers are set to run each regular wave series for 60 seconds and rest for 45 seconds between each test. This is decided to be sufficient to determine the interactions with regular waves as reflections from the beach will affect the results. Each test is run for each of the three cases with the float in place and once with no float to use as an undisturbed reference. For irregular/panchromatic waves it is sought to provide a comparable scenario for all the wave series. This is done by using a common reference wave series, which is made with unit properties $H_{m0} = 1$ m and $T_p = 1$ s. By using a white noise filtering method it is ensured that the wave series is non-deterministic. The frequency spectrum is a parameterised Pierson-Moskowitz spectrum. The sample length is chosen to be $l_s = 1200 \cdot T_p$ with a sampling frequency $f_s = 109.23$ Hz which is convenient when generating the signal in the wave making software which uses the inverse FFT and the original phases to approximate the requested signal. By choosing this sampling frequency the block size is a power of

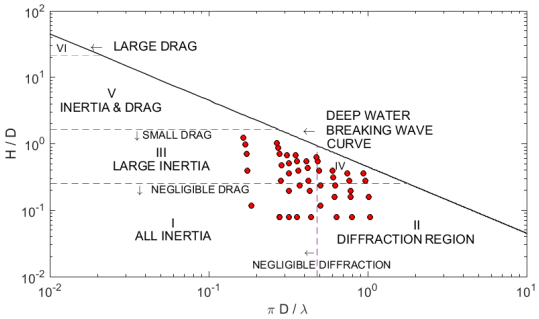

Figure 2.3: Wave regime Chakrabarti (1987).

two $N = l_s \cdot f_s = 2^{17}$.
The values of the reference wave series is then scaled in magnitudes based on the wave heights needed and the peak wave period is adjusted by changing the sampling frequency used by the wave generation software.

2.2 Methods

The regular wave series are reduced to 10 succeeding waves to reduce the influence of reflection from the beach. The waves are chosen as the first wave surpassing 3/4th of the largest wave in each wave series. This has shown to be enough waves to accurately determine the wave properties.
Some wave series were improperly produced in the basin, resulting in misshaped profiles in the far field in the testing area. This happened with wave periods $T > 1.4$ s and for series with very high or low wave heights. As high order wave theory is used to determine the velocities, these series have been removed in the results presented.
To obtain continuous measurements of fluid particle velocity from the waves, the ADV was placed 20 cm below the water surface so it would not protrude through the surface during wave troughs. However, the fluid particle velocity of interest for the Float is 10 cm below the water surface at the centroid of the submerged volume. Thus, the stream function wave kinematic theory by Dean (1965) (with modifications by Chaplin (1980) and Brorsen (2007)) was validated using of the ADV measurements at 20 cm water depth, then used to calculate the velocity at the WEC (10 cm depth). For some of the steeper waves it was not possible to reach convergence, regardless of the number of stream functions used. When no convergence was possible Stoke's 5th order theory by Fenton (1985) was used instead.
Both of the high order wave models are dependent of determining the characteristic

wave heights and periods. These characteristics were determined using a time domain model on the wave series. The velocities were first calculated for 20 cm water depth to ensure that the theoretical approximations used to calculate the velocity corresponeded with the ADV. The standard deviations for all samples are $\sigma^2 < 0.01$.

It is sought to determine the contributions from drag, C_D, and inertia, C_M, in both vertical and horizontal wave propagation direction. This is done by locking the float, measuring the excitation forces using Morison's equation in Eq. 2.1 and then estimating the coefficients.

$$F_p = \frac{1}{2} C_D \rho A u|u| + C_M \rho V \frac{Du}{Dt} \tag{2.1}$$

Two methods are used to obtain the coefficients. The first method determines the coefficients by methodically running through ranges of realistic drag and inertia coefficients in the Morison's equation (Brute force). The best solution is determined by calculating the minimum variance (MV) between measured force F_m and "predicted" F_p. This effectively leads to one solution for each regular wave. The second method proposed by Dean and Dalrymple (1984) seeks to obtain the two coefficients by an least squares optimum fit approach (LS). This is done using the minimum squared error between the predicted force F_p and the measured force F_m shown in Eq. 2.2. The analytical gradients of the objective function with respect to the unknowns C_D and C_M are shown in Eq. 2.3.

$$\epsilon^2 = \frac{1}{I} \sum_{i=1}^{I} (F_{m,i} - F_{p,i})^2 \tag{2.2}$$

$$\begin{aligned} \frac{\partial \epsilon^2}{\partial C_D} &= \frac{2}{I} \sum_{i=1}^{I} (F_{m,i} - F_{p,i}) \frac{\partial F_{p,i}}{\partial C_D} = 0 \\ \frac{\partial \epsilon^2}{\partial C_M} &= \frac{2}{I} \sum_{i=1}^{I} (F_{m,i} - F_{p,i}) \frac{\partial F_{p,i}}{\partial C_M} = 0 \end{aligned} \tag{2.3}$$

To obtain the particle velocity used in Eq. 2.1 the previously mentioned wave theory is used to determine the velocity at the center of the float. Eq. 2.4 shows the simple PI control scheme used. The values are not optimized for the individual regular wave series, but kept constant ($k = -50$ and $c = 10$).

$$f_c(t) = c \cdot \dot{\theta}(t) + k \cdot \theta(t) \tag{2.4}$$

2.3 Results

Fig. 2.4 shows the results of the two methods used to estimate the drag and inertia coefficients in surge. By minimizing the variance between the MV method produces coefficients for each wave series. With the LS fit each regular series is divided into bins based on Reynolds Number.

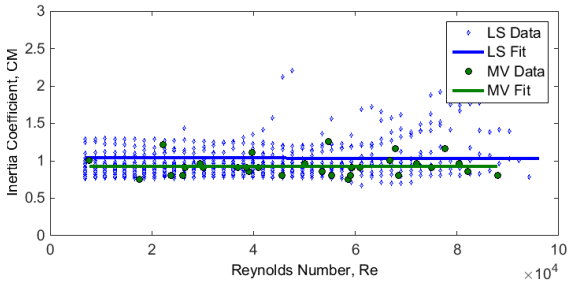

(a) Inertia.

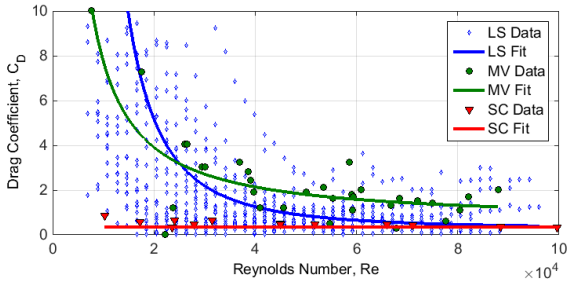

(b) Drag.

Figure 2.4: Drag and inertia coefficients obtained from the regular wave series in the wave propagation direction. Data points are shown with best fitting tendency lines. LS is the results of the least squares method, MV is the minimum variance method, and SC is the results obtain from the stream canal

Fig. 2.5 shows the results obtained from calculation of the coefficients in heave.

The measured forces are plotted against the corresponding wave heights in Fig. 2.6 and periods in Fig. 2.7. The hydrostatic force has been removed from the results. In Fig. 2.8 the forces are normalized using Froude-Krylov.

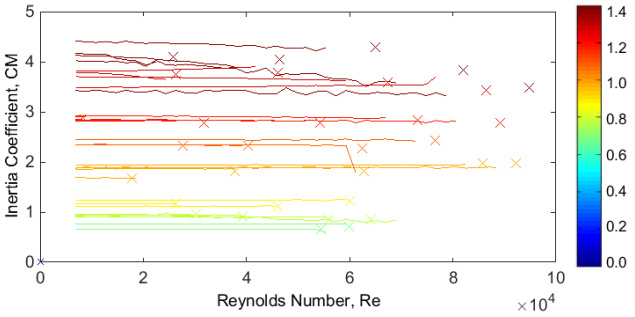

(a) Inertia. The wave periods of the waves are indicated by the color gradient. The solid lines represent one wave series analyzed using the LS fitting method and the crosses are the calculated values from the MV method.

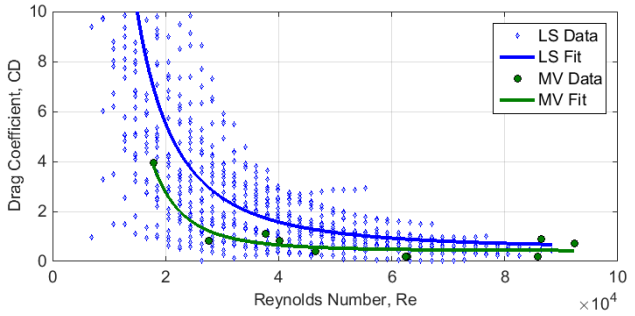

(b) Drag coefficients with data points are shown with best fitting tendency lines.

Figure 2.5: Drag and inertia coefficients obtained from the regular wave series in vertical direction.

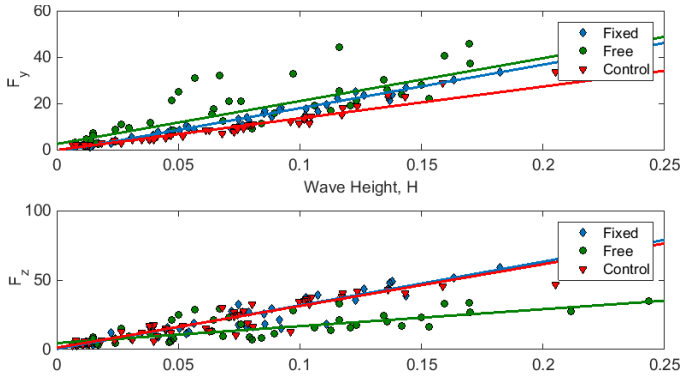

Figure 2.6: Measured forces on float for the regular wave series.

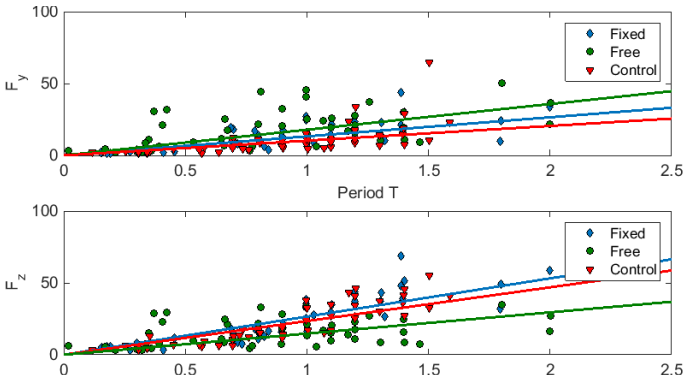

Figure 2.7: Measured forces on float for the regular wave series.

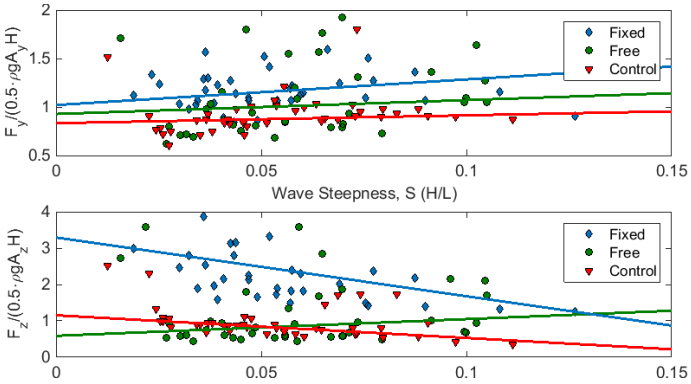

Figure 2.8: Normalized forces on float for the regular wave series.

2.4 Discussion

Fig. 2.3 showed the regular waves regimes carried out in the experiments. For some of the regular waves with shorter periods this could result in scattering and diffraction of the waves on the device. Using the fundamental Morison's equation in these cases may lead to inaccurate estimate of the load contributions. The effect of diffraction is not examined in this report.
With increasing wave heights, the effects of drag increases. Unfortunately the contribution from drag is limited in these experiments. To properly measure the drag in waves the wave length would need to exceed 10 m and the height be more than 1 m for the device used to ensure that the experiments were in the combined drag and inertia regime.

The effect of the inertia dominated regime is evident in Figs. 2.4b and 2.5b. With increasing Reynold's numbers both the LS and MV methods converges. The estimates are still rough compared to the results from the stream canal (cf. Fig. 2.4b). Due to the inherent scale of drag dominated waves it is unlikely to be a critical factor. With this in mind the found coefficients are considered to be sufficiently accurate.
The scatter with high Reynold's numbers in Fig. 2.4b is curious; it may be partly attributed to uncertainties caused by increasing drag.
The spreading of the C_M values in Fig. 2.5b are evidently related to the wave period. This will be examined further in later projects.
The remaining culprits could be the estimation of the particle velocity near the surface of the device, scaling effects, or need for additional parameters in the Morison Equation for the low particle velocity regime.

Figs. 2.6 and 2.7 suggest that the control scheme used will not increase the horizontal forces, compared to the fixed and free floating conditions. There is no apparent pattern in the fluctuations that could be anticipated from resonance around the eigenfrequency of the device. The maximum vertical forces are, however, as great as the case with the float locked in place. By normalizing the results with the Froude-Krylov estimate in Fig. 2.8 and plotting against the wave steepness the only significant outlier is the vertical forces of the fixed float. This is likely explained by the forced submergence of the float leading to increased forces (no changes are made to the wetted surface in the Froude-Krylov forces).

Conclusion

Experiments were carried out in current flume and wave basin. The device used, a 1:40 scale point absorber, was subjected to various current velocities and then a wide range of regular waves. From the experiments, the inertia and drag coefficients were estimated using two distinct methods on the float locked in place. The results were compared with result from the canal. Then the float was released from the locked position and put in two states: floating freely and controlled using a PTO. The resulting forces were shown in both vertical and in the wave propagation direction, with respect to wave period and height. Then the results were normalized using Froud-Krylov.

Getting accurate values for both drag and inertia coefficients proved difficult in the wave basin. The obtained inertia coefficients generally stay within a reasonable degree of scattering, but particularly in heave the values still vary more than anticipated. The contributions from drag is very small compared to inertia and generally results in poorer estimates. For increasing Reynolds numbers the contribution increases relatively and the results improve noticeably. Near the highest Reynolds values, the drag coefficient in surge that corresponds to the value obtained in the stream canal. This should be sufficient to put some confidence in the found values.

Unfortunately, several issues make it difficult to make any concluding remark on the free and controlled cases. Firstly, the control parameters were never optimized for the wave conditions and, secondly, the results found had significant scattering.

Several experiments were dropped due to complications. The small pressure sensors did not produce satisfying results, which were often contradictory and inconsistent. Trying to acquire new and more accurate sensors has been unsuccessful to date. Several sensors have been tested from manufacturers claiming to have appropriate sensors. However, the trade-off between sensitivity and frequency response has been a prevailing issue. Another issue is the thermal response from the sensors during submersion and temporal fluctuations. In the end this was dropped entirely for this small-scale device, but it was picked up with success at larger scale experiments later on. These later experiments also led to the explanation of the vertical inertia-dependency on wave periods.

Bibliography

Brorsen, M. (2007). Non-linear Waves. Technical Report 9, Aalborg University Department of Civil Engineering.

Chakrabarti, S. (1987). *Hydrodynamics of Offshore Structures*. WIT press.

Chaplin, J. R. (1980). Development of stream function wave theory. *Journal of Coastal Engineering*, (2):179–205.

Dean, R. (1965). Stream function representation of nonlinear ocean waves. *J. Geophys. Res.*, 70:4561–4572.

Dean, R. G. and Dalrymple, R. A. (1984). *Water wave mechanics for engineers and scientists*. Prentice-Hall, inc.

Fenton, J. D. (1985). A Fifth-Order Stokes Theory for Steady Waves. *J. Waterway Port Coastal and Ocean Engng*, 111(2):216–234.

Frigaard, P. and Andersen, T. L. (2010). Technical Background Material for the Wave Generation Software AwaSys 5. Technical Report 64, Aalborg University Department of Civil Engineering.

Hansen, R. H. and Kramer, M. M. (2011). Modelling and Control of the Wavestar Prototype. EWTEC European Wave and Tidal Energy Conference.

Kramer, M. M., Marquis, L., and Frigaard, P. (2011). Performance Evaluation of the Wavestar Prototype. EWTEC European Wave and Tidal Energy Conference.

Appendix A

Instrumentation and Data Acquisition in Wave Basin

A.1 The Float and embedded sensors

The components used for the float is shown in Fig. A.1. The pressure sensors used are connected in a junction box inside the float and send through a multi-conductor cable. This solution was chosen to improve the water-sealing of the device. This also meant that the individual cables could be shortened significantly (to ca. 30 cm). This served to reduce the blockage of the air pipe used by the differential pressure sensors. In the past the long cables would twist and constrict airflow through the pipe resulting in slower response. The 13 pressure sensors embedded in the shell are

Figure A.1: Disassembled float showing pressure sensors, with the junction box, glass fiber shell and lid.

vented gauges from Kullite. The rated pressure is 1 bar, with a sensitivity of 73 mV/bar. The technical specifications are shown in Fig. A.2. The placement of the pressure sensors are shown on the Fig. A.3. The symmetry lines were chosen to have

redundancy in the measurements.

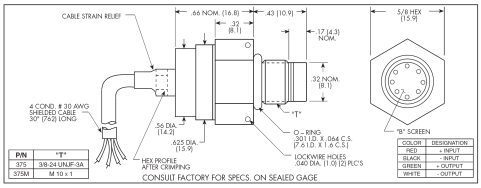

Figure A.2: Pressure sensor specifications. The membrane is 8.1 mm in diameter and ventilated through the attached cable.

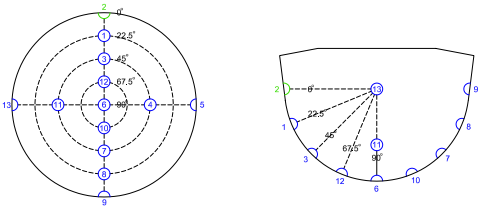

Figure A.3: Pressure sensor placement. Blue and green circles indicates the locations of the sensors. The green marked sensor faces the wave maker.

A.2 Force and Torque transducer

To measure the force and torque on the float a 6-axis sensor is used. This sensor shown in Fig. A.4 is a Delta SI-330-30 from ATI Industrial Automation. The sensor is able to measure forces up to 330 N and torque up to 30 Nm. The accuracy of the sensor is $F_{x,y,z} = 1.5\%$, $M_{x,y} = 1.5\%$ and $M_z = 2.0\%$. A calibration matrix is supplied by the manufacturer. The offset is removed in-situ by applying known loads in all axial directions.

A.3 Simulink and XPC data acquisition

The wave generation software used in the basin is handled using the in-house software AwaSys cf. Frigaard and Andersen (2010).
Data acquisition is handled by a National Instrument Data Acquisition unit (DAQ) which is connected to a dedicated PC running Matlab's Simulink connected to a

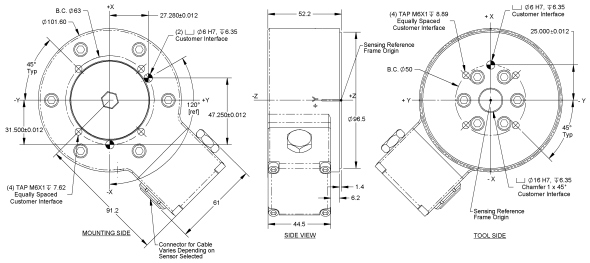

Figure A.4: Six degree of freedom force transducer. Coordinate system and force/moment definition.

remote (target) xPC running a custom operating system. This solution is chosen due to the flexibility and real-time data processing on the xPC. The channel configuration is shown in Table A.1.

Table A.1: DAQ Channel configuration for experiments in wave basin.

Channel	Type	Sym.	Description
00	Force	F_{cyl}	Cylindrical force transducer
01	Force	F_{acc}	Reference force from accelerometer
02	Distance	x_{cyl}	Cylinder position
03	Distance	K	Cylinder arm to pivot
04	Angle	θ_{cyl}	Angular position of cylinder
05	Velocity	$\dot{\theta}_{cyl}$	Angular velocity from angle of rotation
06	Acceleration	$\ddot{\theta}_{cyl}$	Angular acceleration from angular velocity
07	Acceleration	$\ddot{\theta}_{acc}$	Raw angular acc. from accelerometer
08	Acceleration	$\ddot{\theta}_{acc,filt}$	Filtered ang. acc. from accelerometer
09	Power	P	Power produced
10	Trigger		Awasys wave generation trigger
11-26	Elevation	η	Resistive wave gauges
27-39	Pressure	p	Pressure sensors in float shell
40-43	Velocity	u	Acoustic Doppler Velocimeter (ADV)
44-49	Force & moment	FT	6-Axis F/T-transducer

A.4 Surface Elevation and Velocimetry

The placement of the wave gauges and the ADV is shown in Fig. A.5. Wave gauges 8 to 13 and the ADV are placed in line with the float to get the particle velocity and

wave elevation that affects the float. To determine the wave spectrum and separate incident waves from reflected waves from the beach additional wave gauges are placed parallel with the wave propagation direction. To measure the current velocity an

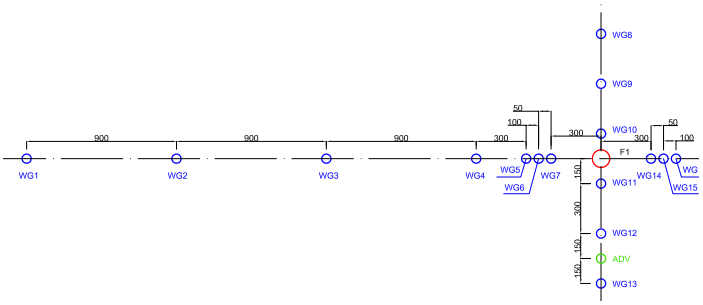

Figure A.5: Layout of wave gauges and floating devices in experiment. The red circle is the float location. The green circle is the ADV used for velocimetry, the blue circles are wave gauges for measurement of wave elevation.

Acoustic Doppler Velocimeter (ADV) from Nortek is used, see Fig. A.6. This device measures particles in the water to determine the velocity and can provide an analogue output to the DAQ. The measuring range used is ±1 m/s with a measurement accuracy of ±0.5%. The ADV is able to measure both the X,Y and two values in the Z direction. To ensure that the ADV does not breach the water surface during the wave troughs the ADV is placed deeper than the largest through. For these experiments this location was determined to be 0.21 m below the mean water level.

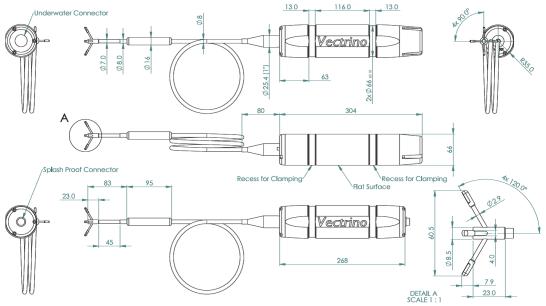

Figure A.6: Dimensions of velocimeter from Nortek.

A.5 The Basin and Wave Series

The wave basin dimensions and location of the float are shown in Fig. A.7. The

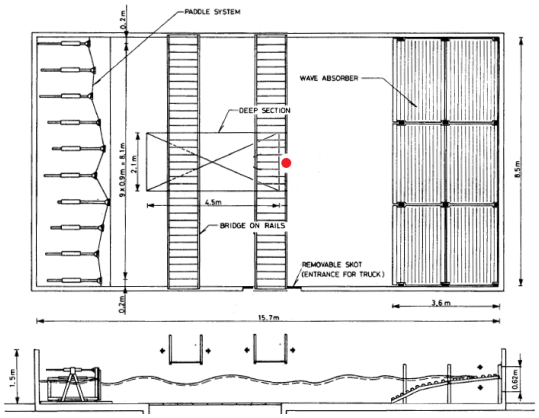

Figure A.7: Sketch of 3D wave basin with floater (red marker) in position.

regular test series which has been used in these tests are given in Table A.2. Each sub-series consist of a single wave period and increasing wave height. The wave makers are set to run each regular wave series for 60 seconds and rest for 45 seconds between each test. This is deemed to be sufficient to calm the basin between each series of regular waves.

Table A.2: Summary of regular waves.

ID	Height, H	Period, T	Length, L	Steepness, S (H/L)
RA01	0.02 m	0.7 s	0.771 m	0.026
RA02	0.04 m	0.7 s	0.785 m	0.051
RA03	0.07 m	0.7 s	0.821 m	0.085
RA04	0.09 m	0.7 s	0.851 m	0.106
RB01	0.03 m	1.0 s	1.552 m	0.019
RB02	0.06 m	1.0 s	1.568 m	0.038
RB03	0.10 m	1.0 s	1.605 m	0.062
RB04	0.14 m	1.0 s	1.654 m	0.085
RB05	0.16 m	1.0 s	1.682 m	0.095
RC01	0.02 m	1.4 s	2.762 m	0.007
RC02	0.07 m	1.4 s	2.777 m	0.025
RC03	0.12 m	1.4 s	2.810 m	0.043
RC04	0.18 m	1.4 s	2.870 m	0.063
RC05	0.22 m	1.4 s	2.920 m	0.075
RC06	0.26 m	1.4 s	2.977 m	0.087
RD01	0.03 m	2.0 s	4.503 m	0.007
RD02	0.10 m	2.0 s	4.539 m	0.022
RD03	0.18 m	2.0 s	4.625 m	0.039
RD04	0.25 m	2.0 s	4.734 m	0.053
RD05	0.31 m	2.0 s	4.845 m	0.064
RE01	0.02 m	0.8 s	1.003 m	0.020
RE02	0.04 m	0.8 s	1.015 m	0.039
RE03	0.05 m	0.8 s	1.023 m	0.049
RE04	0.07 m	0.8 s	1.044 m	0.067
RE05	0.09 m	0.8 s	1.070 m	0.084
RF01	0.02 m	1.2 s	2.153 m	0.009
RF02	0.06 m	1.2 s	2.166 m	0.028
RF03	0.10 m	1.2 s	2.193 m	0.046
RF04	0.14 m	1.2 s	2.232 m	0.063
RF05	0.17 m	1.2 s	2.267 m	0.075
RG01	0.02 m	0.9 s	1.265 m	0.016
RG02	0.04 m	0.9 s	1.274 m	0.031
RG03	0.06 m	0.9 s	1.288 m	0.047
RG04	0.08 m	0.9 s	1.308 m	0.061
RG05	0.10 m	0.9 s	1.332 m	0.075
RH01	0.02 m	1.1 s	1.848 m	0.011
RH02	0.05 m	1.1 s	1.858 m	0.027
RH03	0.07 m	1.1 s	1.870 m	0.037
RH04	0.11 m	1.1 s	1.904 m	0.058
RH05	0.14 m	1.1 s	1.938 m	0.072
RI01	0.02 m	1.3 s	2.458 m	0.008
RI02	0.05 m	1.3 s	2.466 m	0.020
RI03	0.09 m	1.3 s	2.487 m	0.036
RI04	0.13 m	1.3 s	2.520 m	0.052
RI05	0.17 m	1.3 s	2.562 m	0.066
RJ01	0.02 m	1.5 s	3.061 m	0.007

Appendix G

MARINET Infrastructure Access Report

Morten M. Jakobsen

The Infrastructure Access Report has been published on the *Marine Renewables Infrastructure Network, MARINET* Homepage accessible at, http://www.fp7-marinet.eu/access_user_projects_AAUWS.html, last visited June 15th 2015.

The layout has been revised.

MARINET

Marine Renewables Infrastructure Network

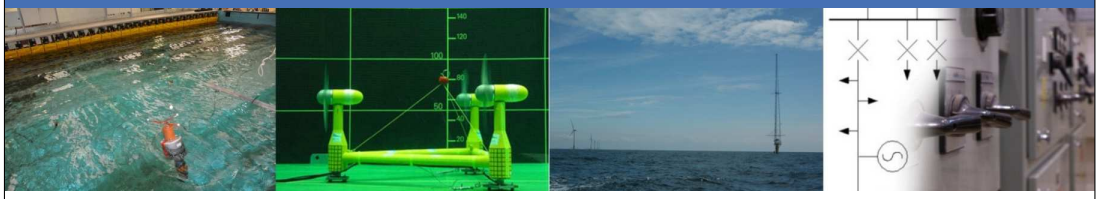

Infrastructure Access Report

Infrastructure: PU COaST - Coastal Ocean and Sediment Transport Laboratories

***User-Project*: AAUWS**

Wave-Structure interactions on point absorber

Morten M. Jakobsen*, Morten Kramer*, Nikolaj Holk*, Mikael Pedersen^, Enrique Vidal^.
*) Aalborg University, ^) Wavestar

Status: Final
Version: 02
Date: 06-Feb-2014

EC FP7 "Capacities" Specific Programme
Research Infrastructure Action

ABOUT MARINET

MARINET (Marine Renewables Infrastructure Network for emerging Energy Technologies) is an EC-funded network of research centres and organisations that are working together to accelerate the development of marine renewable energy - wave, tidal & offshore-wind. The initiative is funded through the EC's Seventh Framework Programme (FP7) and runs for four years until 2015. The network of 29 partners with 42 specialist marine research facilities is spread across 11 EU countries and 1 International Cooperation Partner Country (Brazil).

MARINET offers periods of free-of-charge access to test facilities at a range of world-class research centres. Companies and research groups can avail of this Transnational Access (TA) to test devices at any scale in areas such as wave energy, tidal energy, offshore-wind energy and environmental data or to conduct tests on cross-cutting areas such as power take-off systems, grid integration, materials or moorings. In total, over 700 weeks of access is available to an estimated 300 projects and 800 external users, with at least four calls for access applications over the 4-year initiative.

MARINET partners are also working to implement common standards for testing in order to streamline the development process, conducting research to improve testing capabilities across the network, providing training at various facilities in the network in order to enhance personnel expertise and organising industry networking events in order to facilitate partnerships and knowledge exchange.

The aim of the initiative is to streamline the capabilities of test infrastructures in order to enhance their impact and accelerate the commercialisation of marine renewable energy. See www.fp7-marinet.eu for more details.

Partners

Ireland
University College Cork, HMRC (UCC_HMRC) *Coordinator*
Sustainable Energy Authority of Ireland (SEAI_OEDU)

Denmark
Aalborg Universitet (AAU)
Danmarks Tekniske Universitet (RISOE)

France
Ecole Centrale de Nantes (ECN)
Institut Français de Recherche Pour l'Exploitation de la Mer (IFREMER)

United Kingdom
National Renewable Energy Centre Ltd. (NAREC)
The University of Exeter (UNEXE)
European Marine Energy Centre Ltd. (EMEC)
University of Strathclyde (UNI_STRATH)
The University of Edinburgh (UEDIN)
Queen's University Belfast (QUB)
Plymouth University(PU)

Spain
Ente Vasco de la Energía (EVE)
Tecnalia Research & Innovation Foundation (TECNALIA)

Belgium
1-Tech (1_TECH)

Netherlands
Stichting Tidal Testing Centre (TTC)
Stichting Energieonderzoek Centrum Nederland (ECNeth)

Germany
Fraunhofer-Gesellschaft Zur Foerderung Der Angewandten Forschung E.V (Fh_IWES)
Gottfried Wilhelm Leibniz Universität Hannover (LUH)
Universitaet Stuttgart (USTUTT)

Portugal
Wave Energy Centre – Centro de Energia das Ondas (WavEC)

Italy
Università degli Studi di Firenze (UNIFI-CRIACIV)
Università degli Studi di Firenze (UNIFI-PIN)
Università degli Studi della Tuscia (UNI_TUS)
Consiglio Nazionale delle Ricerche (CNR-INSEAN)

Brazil
Instituto de Pesquisas Tecnológicas do Estado de São Paulo S.A. (IPT)

Norway
Sintef Energi AS (SINTEF)
Norges Teknisk-Naturvitenskapelige Universitet (NTNU)

DOCUMENT INFORMATION

Title	Wave-Structure interactions on point absorber
Distribution	**Public**
Document Reference	MARINET-TA1-AAUWS
User-Group Leader, Lead Author	Morten M. Jakobsen Aalborg University, Denmark Morten M. Jakobsen (MMJ)
User-Group Members, Contributing Authors	Morten Kramer (MMK) Aalborg University, Denmark Nikolaj Holk (NH) Aalborg University, Denmark Mikael Pedersen (MP) Wavestar A/S, Denmark Enrique Vidal (EV) Wavestar A/S, Denmark Josh Davidson (JD) National University of Ireland, Maynooth
Infrastructure Accessed:	PU COaST - Coastal Ocean and Sediment Transport Laboratories
Infrastructure Manager (or Main Contact)	Stuart Stripling

REVISION HISTORY

Rev.	Date yyyymmdd	Description	Prepared by (Name)	Approved By Infrastructure Manager	Status (Draft/Final)
01	20131204	First Draft	MMJ		Draft
02	20140206	Final revision	MMJ	Stuart Stripling	Final

About This Report

One of the requirements of the EC in enabling a user group to benefit from free-of-charge access to an infrastructure is that the user group must be entitled to disseminate the foreground (information and results) that they have generated under the project in order to progress the state-of-the-art of the sector. Notwithstanding this, the EC also state that dissemination activities shall be compatible with the protection of intellectual property rights, confidentiality obligations and the legitimate interests of the owner(s) of the foreground.

The aim of this report is therefore to meet the first requirement of publicly disseminating the knowledge generated through this MARINET infrastructure access project in an accessible format in order to:

- progress the state-of-the-art
- publicise resulting progress made for the technology/industry
- provide evidence of progress made along the Structured Development Plan
- provide due diligence material for potential future investment and financing
- share lessons learned
- avoid potential future replication by others
- provide opportunities for future collaboration
- etc.

In some cases, the user group may wish to protect some of this information which they deem commercially sensitive, and so may choose to present results in a normalised (non-dimensional) format or withhold certain design data – this is acceptable and allowed for in the second requirement outlined above.

Acknowledgement

The work described in this publication has received support from MARINET, a European Community - Research Infrastructure Action under the FP7 “Capacities” Specific Programme.

Legal Disclaimer

EXECUTIVE SUMMARY

The purpose of this project is to investigate wave-body interaction on a floating hemisphere. The set-up used in the project is part of the Wavestar wave energy converter, which is a modified version of a one meter in diameter float (scale 1:10) which has previously been deployed for real sea testing at the small-scale test site in Nissum Bredning, Denmark. The experiments have taken place in the Ocean Wave Basin at COaST with Plymouth University.
The rationale for testing the float in the new wave basin at Plymouth University is to get reliable high quality wave measurements together with the measurements from the device. In comparison with previous measurements in Nissum Bredning, the new float will be instrumented with state-of-the-art flush diaphragm pressure sensors in the float shell and force sensors at arm bearings and at the cylinder rod end.
The main measurements to be recorded are the wave forces acting on the float and the pressure distribution on the float surface. The long-term goal is to use the results to improve the design of the point absorber structure, and at the same time, ensure a low probability of structural damage when point absorbers are in operation during extreme wave conditions.

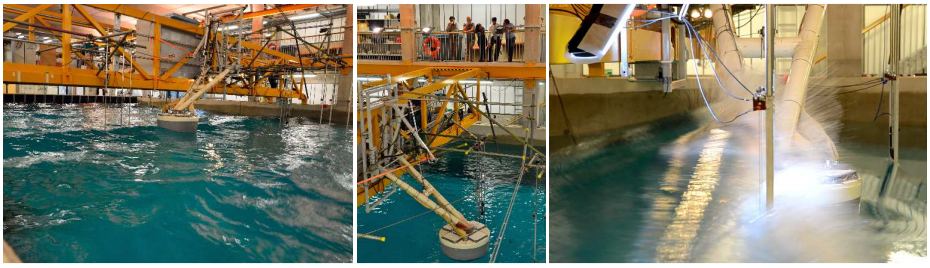

From left to right: Wavestar device in realistic sea state rotated 90 degrees. Presentation of device during AAUWS seminar in Plymouth. Device exposed to plunging wave based on modified new wave theory.

CONTENTS

1 INTRODUCTION & BACKGROUND 7

1.1 INTRODUCTION 7
1.2 DEVELOPMENT SO FAR 7
1.2.1 Stage Gate Progress 7
1.2.2 Plan For This Access 8

2 OUTLINE OF WORK CARRIED OUT 9

2.1 SETUP 9
2.2 TESTS 10
2.2.1 Test Plan 10
2.3 RESULTS 12
2.4 CONCLUSIONS 13

3 MAIN LEARNING OUTCOMES 14

3.1 PROGRESS MADE 14
3.1.1 Progress Made: For This User-Group or Technology 14
3.1.2 Progress Made: For Marine Renewable Energy Industry 14
3.2 KEY LESSONS LEARNED 14

4 FURTHER INFORMATION 14

4.1 SCIENTIFIC PUBLICATIONS 14
4.2 WEBSITE & SOCIAL MEDIA 15

5 APPENDICES 15

5.1 STAGE DEVELOPMENT SUMMARY TABLE 15
5.2 MINI-SEMINAR IN PLYMOUTH 17

1 INTRODUCTION & BACKGROUND

1.1 INTRODUCTION

The academic purpose of this project is to investigate wave-body interaction on a floating hemisphere. The set-up used in the project is part of a wave energy converter from Wavestar. The device is a point absorber moored to a fixed structure using a rigid arm-float joint. For this experiment, the one meter in diameter float from Nissum Bredning will be used including the arm, the hydraulic pump and the hydraulic and electrical control box.
The predominant measurements to be made are the wave excitation forces acting through the construction and the pressure distribution on the surface of the float. The device will be tested both with and without a control strategy in place to control the motion. This is done because the optimization of the control strategy is expected to increase the amplitudes of the oscillating point absorber.
The long-term goal is to use the results to improve the design of the floating structure and, at the same time, ensure a low probability of structural damage when the device is in operation during extreme wave conditions.
The results of this set-up are a continuation of small-scale experiments performed in the deep water wave basin at Aalborg University.

1.2 DEVELOPMENT SO FAR

1.2.1 Stage Gate Progress

Previously completed: ✓
Planned for this project: ➲

STAGE GATE CRITERIA	Status
Stage 1 – Concept Validation	
• Linear monochromatic waves to validate or calibrate numerical models of the system (25 – 100 waves)	✓
• Finite monochromatic waves to include higher order effects (25 –100 waves)	✓
• Hull(s) sea worthiness in real seas (scaled duration at 3 hours)	✓
• Restricted degrees of freedom (DofF) if required by the early mathematical models	✓
• Provide the empirical hydrodynamic co-efficient associated with the device (for mathematical modelling tuning)	✓
• Investigate physical process governing device response. May not be well defined theoretically or numerically solvable	✓
• Real seaway productivity (scaled duration at 20-30 minutes)	✓
• Initially 2-D (flume) test programme	✓
• Short crested seas need only be run at this early stage if the devices anticipated performance would be significantly affected by them	✓
• Evidence of the device seaworthiness	✓
• Initial indication of the full system load regimes	✓
Stage 2 – Design Validation	
• Accurately simulated PTO characteristics	➲
• Performance in real seaways (long and short crested)	✓
• Survival loading and extreme motion behaviour.	➲
• Active damping control (may be deferred to Stage 3)	➲
• Device design changes and modifications	✓
• Mooring arrangements and effects on motion	➲
• Data for proposed PTO design and bench testing (Stage 3)	✓
• Engineering Design (Prototype), feasibility and costing	➲

STAGE GATE CRITERIA	Status
• Site Review for Stage 3 and Stage 4 deployments	✓
• Over topping rates	➲
Stage 3 – Sub-Systems Validation	
• To investigate physical properties not well scaled & validate performance figures	➲
• To employ a realistic/actual PTO and generating system & develop control strategies	✓
• To qualify environmental factors (i.e. the device on the environment and vice versa) e.g. marine growth, corrosion, windage and current drag	✓
• To validate electrical supply quality and power electronic requirements.	✓
• To quantify survival conditions, mooring behaviour and hull seaworthiness	➲
• Manufacturing, deployment, recovery and O&M (component reliability)	✓
• Project planning and management, including licensing, certification, insurance etc.	✓
Stage 4 – Solo Device Validation	
• Hull seaworthiness and survival strategies	✓
• Mooring and cable connection issues, including failure modes	✓
• PTO performance and reliability	✓
• Component and assembly longevity	✓
• Electricity supply quality (absorbed/pneumatic power-converted/electrical power)	
• Application in local wave climate conditions	
• Project management, manufacturing, deployment, recovery, etc	
• Service, maintenance and operational experience [O&M]	
• Accepted EIA	
Stage 5 – Multi-Device Demonstration	
• Economic Feasibility/Profitability	
• Multiple units performance	
• Device array interactions	
• Power supply interaction & quality	
• Environmental impact issues	
• Full technical and economic due diligence	
• Compliance of all operations with existing legal requirements	

1.2.2 Plan For This Access

The purpose of this project is to investigate wave-body interaction on a floating hemisphere. The set-up used in the project is part of the Wavestar wave energy converter. The experiments at Plymouth University will utilize a modified version of a one meter in diameter float complete with a hydraulic actuator to simulate a PTO system. To control the actuator a hydraulic and electric power station is used, with HMI and Ethernet connection for remote control. The float is instrumented with 33 flush diaphragm pressure sensors in the shell and a six degree of freedom force/torque sensor connecting the float and arm as well as numerous other force and pressure sensors throughout the system to monitor device behaviour and loads. The device will be connected to the gantry above the Ocean Wave Basin using a mounting frame that allows the device to be rotated 90 degrees. COaST with Plymouth University will supply computers and software to control the wave maker, wave elevation gauges and velocity profilers and do the calibration of the wave gauges once pr. day. Additionally COaST supplies underwater cameras and high-speed cameras for documentation purposes. The main measurements to be recorded are the wave forces acting on the float and the pressure distribution on the outer float shell surface.

2 OUTLINE OF WORK CARRIED OUT

Initial concept Building Assembly & Installation

2.1 SETUP

Measuring equipment

The WEC is equipped with a large number of sensors which are able to continuously monitor the performance of the device. These sensors are classified in four groups:

- Hydraulic sensors:
  - Operation of the hydraulic pump station and the pressure of the piston.
- Environmental sensors:
  - Wave elevation gauges supplied by Plymouth University.
  - Velocity profilers supplied by Plymouth University.
- Mechanical sensors:
  - Displacement and velocity equipment on float and cylinder.
  - Force/Torque transducers for monitoring of the float, arm and cylinder.
  - Pressure sensors attached to shell surface.
- Pressure sensors (33 Flush-Diaphragm imbedded in shell surface)

For documentation purposes both video and photography equipment is installed at the basin.

Setup schedule:

Date	Description
Aug.-Sep. 2013	Production of mounting frame to fit the bridge of the wave basin created and hydraulic and electrical station prepared. The hydraulic and electrical equipment is tested in Hanstholm. Pressure sensors, accelerometer and force sensors are fitted in the float. DAQ and measuring devices prepared.
15 Sep. 2013	Morten Jakobsen Travel to Plymouth University for a 3-month stay with the COaST research group to facilitate the preparation and set-up first hand at the testing location.
1-3 Nov. 2013	Morten Kramer and Nikolaj Holk transport device from Hanstholm in Denmark to COaST Ocean Wave basin at Plymouth University in UK.
4-8 Nov. 2013	Set-up in laboratory by AAUWS and local staff: 1) Mounting Frame & Arm 2) Deploying Hydraulic & Electrical station on gantry 3) Preparing sensors in float 4) Connecting Float to Arm 5) Positioning Wave gauges, ADCPs, Cameras, etc. 6) Preparing DAQ and Hydraulic pipes 7) Testing the Hydraulic & Electrical station and HMI 8) Testing DAQ 9) Lowering floor in basin, calibrating monitoring equipment

Table 2.1 Setup schedule

2.2 TESTS

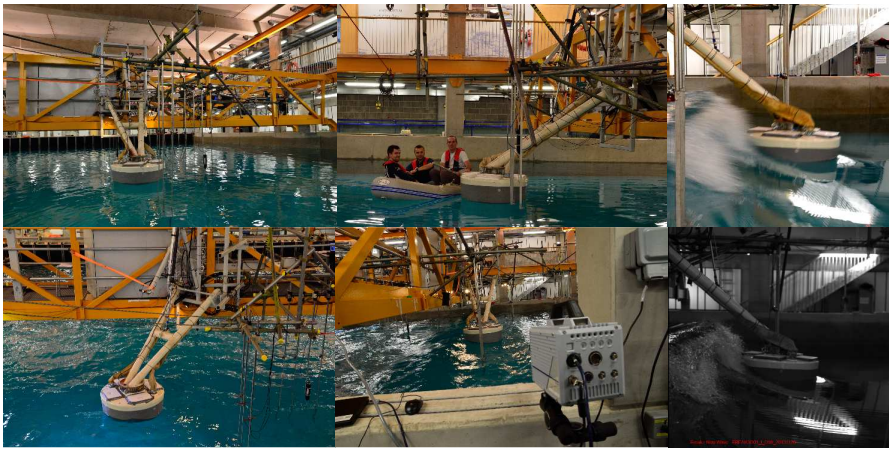

Testing Schedule:

Date	Description
11-15 Nov.	Initial tests by Morten Jakobsen(MMJ) and Josh Davidson
18-22 Nov.	Continuation on tests by MMJ
25 Nov.	AAUWS Seminar at Plymouth University (See Appendix 6.2) hosted by Morten Kramer (MMK), Nikolaj Holk (NH) and MMJ. Adjustment (rotation) of device (planed) by Mikael Pedersen.
26-28 Nov.	Final tests by MMJ, MMK, NH

2.2.1 Test Plan

Device operation and orientation

The device was tested in what we refer to as a 90-degree angle (with the float nearest the beach parallel to the wave propagation direction) throughout most of the testing period. During the last week of testing, the device was rotated to 45 and 0 degrees and through a reduced set of tests it is the intent to determine the wave loading from other directions. The device was tested in three states:

- Locked, predominantly located in the natural buoyancy position, but also tested with the device above and below this position. To lock the device, we closed the in- and outlet valves on the actuator (hydraulic cylinder).
- Controlled by the PTO (reactive control), first stepping up the damping coefficient to determine the optimum and then attempting to optimize the PTO using both stiffness and optimized damping coefficients.
- Free floating, where the pipes connecting the actuator was disconnected from the hydraulic station. As the unconstrained motion of the device quickly reached near the endstops of the cylinder, we had to limit the experiments done in this scenario.
- No Float, where the float is raised and latched in storm protection mode to get the undisturbed wave and current conditions.

Wave & current experiments

During weeks 2 and 3, a total of 46 different regular waves were used to test the device with controlled motion with five different damping coefficients (including zero damping). Then a few long, non-deterministic irregular wave series (1200 waves) were used in similar conditions to have statistically sound irregular sea states.

Later, the number of experiments were reduced to three regular tests and seven short irregular wave series (100 waves). The short irregular wave series has two rough events; one in the beginning and one near the end. The Irregular wave series are grouped in two sets determined by the wave steepness. These series are also optimized to reach the limit of the wavemaker.

Identifier	sP (Hm0/LP)	Hm0 [m]	LP [m]	TP [s]	T0,2 [s]
IRA1	0.025	0.15	6.0	1.96	1.49
IRA2	0.025	0.28	11.2	2.78	2.11
IRA3	0.025	0.36	14.4	3.28	2.49
IRB1	0.050	0.15	3.0	1.39	1.05
IRB2	0.050	0.30	6.0	1.96	1.49
IRB3	0.050	0.40	8.0	2.29	1.74
IRB4	0.050	0.50	10.0	2.59	1.97

A number of current and current+wave experiments were carried out as well where it was sought to obtain the highest current velocities that could maintain a reasonably laminar flow. This was decided to be 70 % of the maximum power as one of the pumps stopped responding with a percentage higher than this (and larger eddies and fluctuations started to occur).

Finally, we used two freak waves based on new wave theory; one long-crested (plunging/breaking) and one focus wave (non-breaking, created using a flat sweep). These waves were also recorded using the high-speed camera.

Determining the device behaviour

A series of drop tests were carried out which appear to have a reasonable decay (some of these drops are recorded on 500 fps high-speed cam as well). During these tests, we disconnected the hydraulic pipes from the cylinder so minimal resistance of the cylinder was obtained.

Besides those tests, “step tests” were made where the device behaviour is changed into force control (we supplied a resulting force that the cylinder should maintain). In these step tests, a significant change in force was requested of the hydraulic station which the cylinder should adjust to immediately. What is obtained from these tests are the delay in response plus the resulting motions from the abrupt changes in position.

DAQ logging of the set-up was made after the float and arm was disconnected to determine the weight of those (from the force sensors in the ball bearings). Unfortunately, the device had taken in a good deal of water (about 10 cm) so the behaviour might have changed during the last week of testing.

Overview of experiments carried out in COaST Ocean Wave Basin

1) Testing of slow motion in air (gravity)
2) Testing of slow motion in calm water (hydrostatics)
3) Fast sinusoidal motion in air (mass inertia moment)
4) Fast sinusoidal motion in calm water (wave radiation forces)
5) Fixed float in current, no waves (drag forces)
6) Fixed float in waves (wave excitation forces)
7) Fixed float in combined wave and current
8) Freely moving float in waves. Cylinder is disconnected, i.e. no PTO force
9) Float moving in waves with control. Resistive and reactive control strategy
10) Bottom-slamming in still water. Float is released from high position and hits the water with a high velocity, and the impact pressures on the shell is measured (slamming coefficient)
11) Wave slamming. Focusing of waves in wave generation software.

2.3 RESULTS

Results from evaluation of the performance of the facility and the validation of the set-up is provided in the following. This includes the assessment and comparison between the provided input to the wave and current maker and the measured waves at the device location through measurement of the wave elevation and current velocity.
There are mechanical and electrical concerns, which have been monitored throughout the various experiments, including the general performance of the hydraulic system, the physical constrains of the actuator, the vulnerability of vibration propagation through the device and gantry, the magnitude of noise and drift in the data acquisition systems, etc.

Performance assessment of wave maker
A comparison is given of the supplied/target irregular wave (black dots), the corresponding numerical approximation (black dashes) at target location by wave generation software and the measured wave gauge elevation readings at the target location (Blue/Green/Red). The target destination was adjusted in wave generation software (+/- 10 cm) to determine if the measured location was correct.

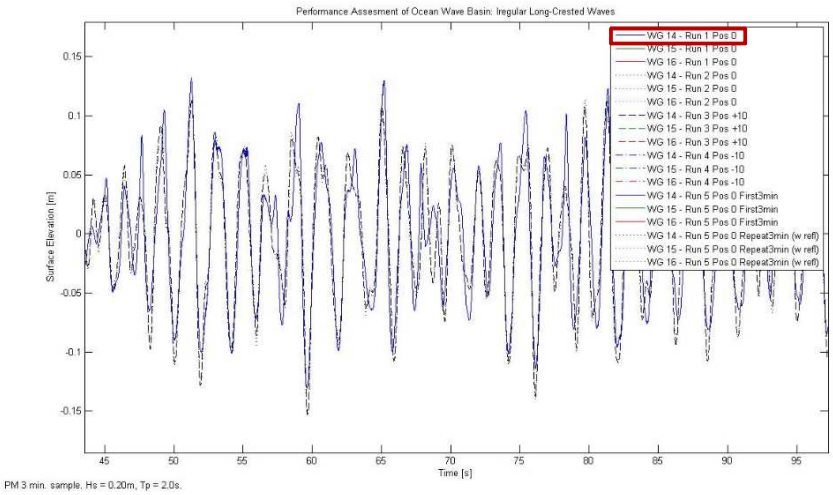

Figure 2.1. Wave maker assessment. Example showing wave gauge 14 (blue) compared to the requested wave (black dashed).

Example Regular wave
Identifier: RC02_D200_K0_D45
Wave characteristics:
- ID: RC02
- Wave height: H=0.25m
- Wave period: T=2.8s

Device characteristics:
- Rotation 45 degrees (45 degrees to the wave propagation direction)
- PTO settings
  - Damping: D=200N
  - Stiffness: K=0

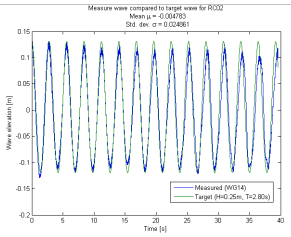

Wave elevation measurement using Wave Gauge 14 compared to anticipated wave (Target).

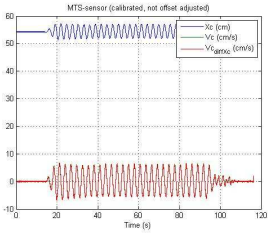

Position and velocity MTS-sensor on the hydraulic actuator.

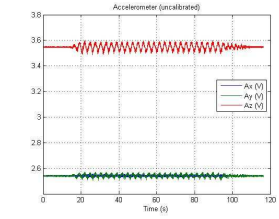

Axial components of the accelerometer on the float, to be compared to MTS-sensor.

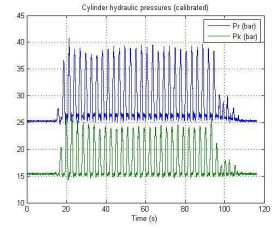

Hydraulic pressure readings from sensors on hydraulic actuator.

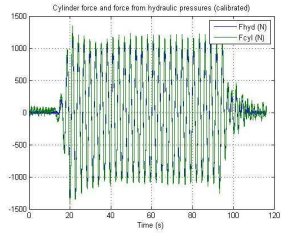

Comparison between calculated force from hydraulic pressure readings and force sensor on cylinder piston.

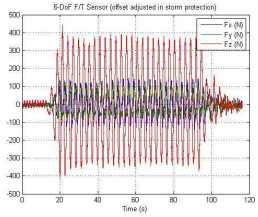

Force component readings from 6-axis Force and Torque sensor.

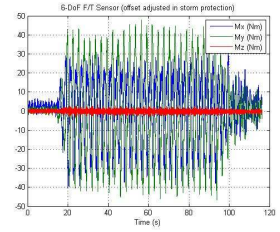

Torque(Moment) component readings from 6-axis Force and Torque sensor.

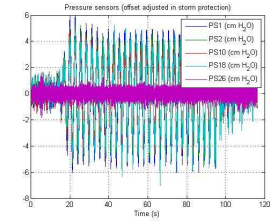

Pressure readings from five flush-diaphragm pressure sensors on leeward from the wave propagation direction

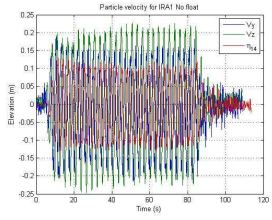

Comparing phases of ADCP and wave gauge located in same cross-section of basin (20 cm separation perpendicular to wave propagation direction).

Figure 2.2. Outtake of validation process undertaken during experiments. Example Regular wave, with identifier: RC02_D200_K0_D45.

2.4 CONCLUSIONS

The overall experience within the COaST facility and the associated staff has been outstanding. The wave and current generation was satisfactory and accommodated the requests of AAUWS, including combined wave-current scenarios, generating custom supplied time series and focus/new waves.
The device performance was satisfactory, both in terms of mechanical response of the system and the quality of the acquired data. All essential goals were reached during the testing phase along with most “good to have” tests, though some of these had to be dropped due to time constraints.

3 MAIN LEARNING OUTCOMES

3.1 PROGRESS MADE

3.1.1 Progress Made: For This User-Group or Technology

By creating a condition where both great control of the environmental conditions and highly accurate model behaviour it is possible to obtain results of the experiments that should help Wavestar and partners in further developing the WEC, by providing state-of-the-art insight into Wave-WEC interactions.
Specifically this will help in the development of the internal float structure, by providing greater information about the pressure distribution in extreme operation conditions. By knowing more precisely what the device is subjected to during extreme events it will be possible to reinforce critical areas and reduce material in non-critical areas.
With the force and pressure sensors throughout the structure it is possible to look into force distributions and propagation through the shell into the arm and through the cylinder to the main structure. Which ultimately could help in tailoring the components throughout the structure.

3.1.2 Progress Made: For Marine Renewable Energy Industry

Monday the 25th of September 2013 AAUWS hosted an open seminar in a conference room at Plymouth University (See appendix 6.2). Wavestar is generally forthcoming with sharing the results and data from the AAUWS experiments. At this time collaboration is ongoing with the COaST group at Plymouth University and Josh Davidson (JD), National University of Ireland, Maynooth.
The results of the experiments will be available to the public through future conferences/journals and through the webpage (c.f. 4.2).

3.2 KEY LESSONS LEARNED

List of key lessons learned:

- Doing laboratory experiments takes longer than you expect.
- Create a plan for storing your data and map and describe the unique identifiers for each experiment.
- Survey the laboratory facility before testing your device.
- Communicate and familiarize yourself with the local staff and their areas of expertise, preferably before or in the beginning of the testing period.
- Learn how to operate the software and the facility.
- Photo and Video documentation is vital when re-viewing and sharing data. No matter how trivial a detail is in the situation, you will appreciate the photo/video later.
- Regularly do check-up on the equipment and acquired data.
- Use a trigger system to ensure everything can be synchronized during data processing (including video!).

4 FURTHER INFORMATION

4.1 SCIENTIFIC PUBLICATIONS

List of any scientific publications planned as a result of this work:

- Experiment overview and initial results.
- Various approaches to estimating drag and inertia coefficients (continued work from previous set-up).
- Comparison of forces, pressure distributions etc. with linear (e.g. Wamit) and non-linear (OpenFOAM*) numerical models.
- Analysis of device response (including actuator response, free decay response, etc.).
- Pressure distribution on the shell during various device behaviours**.
- Device behaviours** influences on loads

*) The works of non-linear models are headed by JD and Ph.D. Student Edward Ransley from the local COaST group.
**) Free floating condition, PTO control (herein variation in damping) and complete fixation of the device in natural buoyancy position, and above and below this location (by mechanically locking the cylinder).

4.2 WEBSITE & SOCIAL MEDIA

Website: http://homes.civil.aau.dk/mmj/AAUWS
YouTube Link(s): Yes, see website.
LinkedIn/Twitter/Facebook Links: www.linkedin.com/in/mmjakobsen
Online Photographs Link: Yes, see website

5 APPENDICES

5.1 STAGE DEVELOPMENT SUMMARY TABLE

The table following offers an overview of the test programmes recommended by IEA-OES for each Technology Readiness Level. This is only offered as a guide and is in no way extensive of the full test programme that should be committed to at each TRL.

DEVELOPMENT PROTOCOL	STAGE 1 CONCEPT VALIDATION			STAGE 2 DESIGN VALIDATION	STAGE 3 SYSTEMS VALIDATION		STAGE 4 DEVICE VALIDATION		STAGE 5 ECONOMICS VALIDATION
	TRL 1: Confirmation of Operation	**TRL 2: Performance Convergence**	**TRL 3: Device Optimisation**	**TRL 4: Sub-Systems Assessment**	**TRL5: Sub-Assembly Bench Tests**	**TRL 6: Full System Sea Trials**	**TRL 7: Solo, Sheltered, Grid Emulator**	**TRL 8: Solo, Exposed, Grid Connected**	**TRL 9: Multi-device Array (3-5)**
Objectives/ Investigations	Op. Verification Design Variables Physical Process Validate/Calibrate Maths Model Damping Effect Signal Phase	Real Generic Seas Design variables Damping PTO Natural Periods Power Absorption Wave to Devise Response Phase	Hull Geometry Components Configurations Power Take-Off Characteristics Design Eng. (Naval Architects)	Final Design Accurate PTO [Active Control] Mooring system Survival Options Power Production Added mass	PTO Method Options & Control Inst. Power Absorption Electricity Production & Quality	Scale effects of Overall Performance Characteristics Mooring & Anchorage Security Environmental Influences & Factors	Oper & Mains Procedures Electrical Output Quality Grid Supply, Stability & Security PTO Performance at all phases Control Strategy Seaworthiness, Survival & Lifecycle Analysis Device Array Interaction (Stages 1 & 2)		Grid Connection Array Interaction Maintenance Service Schedules Component Life Economics
Output/ Measurement	Vessel Motion Response Amplitude Operators & Stability Pressure / Force, Velocity RAOs with Phase Diagrams Power Conversion Characteristic Time Histories Hull Seaworthiness; Excessive Rotations or Submergence Water Surface Elevation Abeam of Devices			Motion RAOs Phase Diagrams Power v Time Wave Climates @ *head, beam, follow*	PTO Forces & Power Conversion Control Strategies	Incident Wave Field 6 D of F Body Motion & Phase Seaworthiness of Hull & Mooring [Survival Strategies]	Full On-Board Monitoring Kit for Extended Physical Parameters Power Matrix Supply forecasting	Array Interaction Annual Power Prod. Elec. Power Perfrm. Failure Rates Grid EIA reviews	Service, Maintenance & Production Monitor. Telemetry for Periodic checks & Evaluation
Primary Scale (λ)	$\lambda = 1 : 25 - 100$ (:. $\lambda_e = 1 : 5 - 10$)			$\lambda = 1 : 10 - 25$	$\lambda = 1 : 2 - 10$		$\lambda = 1 : 1 - 2$		$\lambda = 1:1$, Full size
Facility	2D Flume or 3D Basin			3D Basin	Power Electronics Lab	Benign Site	Sheltered Full Scale Site	Exposed Full Scale Site	Open Location
Duration –*inc Analysis*	1-3months	1-3months	1 3 months	6 – 12 months	6 – 18 months		12 – 36 months		1 – 5 years
Typical No. Tests	250 - 750	250 - 500	100 - 250	100 - 250	50 - 250		Continuous		Statistical Sample
Budget (€,000)	1 – 5	25-75	25-50	50 - 250	1,000 – 2,500		10,000 – 20,000		2,500 – 7,500
Device	Idealised with Quick Change Options Simulated PTO (0–∞ Damping Range) Std Mooring & Mass Distribution		Distributed Mass Minimal Drag Design Dynamics	Final design (internal view) Mooring Layout	Advanced PTO Simulation Special Materials	Full Fabrication True PTO & Elec Generator	Grid Control Electronics or Emulator Emergency Response Strategies Pre-Production	Pre-Commercial	Operational Multi-Device
Excitation / Waves	Monochromatic Linear (10-25Δf) (25-100 waves)	Panchromatic Waves (20min scale) +ve 15 Classical Seaways Spectra Long crested Head Seas		Deployment -Pilot Site Sea Spectra Long, Short Crested Classical Seas Select Mean wave Approach Angle		Extended Test Period to Ensure all Seaways inc.	Full Scatter Diagram for initial Evaluation Continuous Thereafter Time & Frequency Domain Analysis		
Specials	Doff (heave only) 2-Dimentional Solo & Multi Hull	Short Crest Seas Angled Waves As Required	Storm Seas (3hr) Finite Regular As required	Power Take-Off Bench Test PTO & Generator	Device Output Repeatability Survival Forces	Salt Corrosion Marine Growth Permissions	Grid Emulator Quick Release Cable Service Ops	Stakeholder Consult. Health & Safety Issues	Small Array (Up-grade to Generating Station)?
Maths Methods (Computer)	Hydrodynamic, Numerical Frequency Domain to Solve the Model Undamped Linear Equations of Motion		Finite Waves Applied Damping Multi Freq Inputs	Time Domain Response Model & Control Strategy Naval Architects Design Codes for Hull, Mooring & Anchorage System. Economic & Business Plan			Economic Model Electrical Stab. Array Interaction	Grid Simulation Wave forecasting	Array Interaction Market Projection for Devise Sales
	EVALUATION [Stage Gates]								
Absorbed Power Converted [kW]									
Weight, [tonnes]									
Manufacturing Cost [€]									
Capture [kW/tonne] or [kW/m^3]	[200-50 m^3]								
Production [c/kW]	< 25 €c / kW			≤ 15 €c / kW			≤ 10 €c / kW		≤ 5 €c / kW

5.2 MINI-SEMINAR IN PLYMOUTH

When: Monday 25 November 2013
Location: 24 James St, Plymouth PL4 6EQ, UK

09.00: Welcome and coffee (MMJ)

09.30-10:00: Wave energy activities at COaST/University of Plymouth (Gregorio Iglesias)

10.00-11:00: COaST Laboratory tour (Gregorio Iglesias & Peter Arber)

11:00–11:30: Break

11.30-11:50: Wave energy activities at Aalborg University (Morten Kramer)

11.50-12:10: Status, visions and plans for Wavestar development (Laurent Marquis)

12.10-13:10: Lunch

13.10-13:30: Results from initial experiments with Wavestar float (MMJ)

13.30-17:00: Ocean wave basin tests with Wavestar, hands-on and discussions in laboratory (MMJ)

19:00-22:00: Dinner

Participants:

	Name:	Company/Department:	E-mail:
1	Morten Kramer	AAU, dept 6	mmk@civil.aau.dk
2	Morten M. Jakobsen	AAU, dept 6	mmj@civil.aau.dk
3	Nikolaj Holk	AAU, dept 6	nh@civil.aau.dk
4	Morten T. Andersen	AAU, dept 6	mta@civil.aau.dk
5	Amélie Tetu	AAU, dept 6	at@civil.aau.dk
6	Arthur Pecher	AAU, dept 6	afsp@civil.aau.dk
7	Mikael Pedersen	Wave Star	mpe@wavestarenergy.com
8	Laurent Marquis	Wave Star	lma@wavestarenergy.com
9	Bendt Aarup	Hi-Con	BKA@hi-con.dk
10	Florian Saupe	IFP Energies nouvelles	florian.saupe@ifp.fr
11	Anup Nambiar	Edinburgh University	A.Nambiar@ed.ac.uk
12	Gregorio Iglesias	Plymouth University	gregorio.iglesias@plymouth.ac.uk
13	Deborah Greaves	Plymouth University	deborah.greaves@plymouth.ac.uk
14	Thomas Vyzikas	Plymouth University	thomas.vyzikas@plymouth.ac.uk
15	Javier A. Tercero	Plymouth University	javier.abanadestercero@plymouth.ac.uk
16	Martyn Hann	Plymouth University	martyn.hann@plymouth.ac.uk
17	Carlos Perez	Plymouth University	carlos.perezcollazo@plymouth.ac.uk
18	Peter Arber	Plymouth University	peter.arber@plymouth.ac.uk
19	Alastair Reynolds	Plymouth University	alastair.m.reynolds@plymouth.ac.uk
20	Edward Ransley	Plymouth University	edward.ransley@plymouth.ac.uk
21	Adi Kurniawan	Plymouth University	adi.kurniawan@plymouth.ac.uk
22	Kieran Monk	Plymouth University	kieran.monk@plymouth.ac.uk

Large scale tests on a Wavestar point absorber

Morten Jakobsen[2], Morten M Kramer[1,2], Nikolaj Holk[2], Mikael Pedersen[1], Enrique S Vidal[1], Rico Hansen[1,2], Gregorio Iglesias[3], Carlos Perez[3], Peter Arber[3], Alastair Reynolds[3]

1) Wave Star A/S, 2) Aalborg University, 3) Plymouth University

Introduction

Laboratory experiments are carried out in the wave tank at Plymouth University with small scale pivoting Wavestar absorbers designed for wave energy extraction. The main objective is to investigate the wave-body interaction on the floating hemisphere. The experiments utilize a modified version of a one meter in diameter float which has previously been deployed for real sea testing at the small scale test-site in Denmark, Nissum Bredning. The rationale for testing the float in the wave basin at Plymouth University is to get reliable high quality wave measurements together with measurements from the device. In comparison with previous measurements in Nissum Bredning the new float is instrumented with state of the art flush diaphragm pressure sensors in the float shell and force sensors at arm bearings and at the cylinder rod end. The main measurements to be recorded are the wave forces acting on the float and the pressure distribution on the outer float shell surface. The long term goal is to use the results to improve the design of point absorber structures and at the same time ensure a low probability of structural damage when point absorbers are in operation during extreme wave conditions.

Background

When designing and building wave energy converters, the complex interaction between waves, structure and control strategy is still not known in sufficient detail to avoid failures and problems. The results from the new experiments and the further development on non-linear numerical models are expected to enable better predictions of the pressure and force distributions on point absorbers operating in high seas. Hereby a more optimized structural design can be found, thereby lowering the cost of energy and increasing the reliability of wave energy devices.

The absorber has a float diameter of 1.0 m, corresponding to scale 1:5 of the Wavestar Prototype at Hanstholm in Denmark. For further description see the Wavestar Website: www.wavestarenergy.com.

Laboratory set-up

The pivoting absorber is equipped with a hydraulic power take off which controls the force and thereby power extraction in real time. The hydraulic actuator can apply any force or motion (within some wide ranges) utilizing any user specified control strategy.
Measurements of motions are performed by a position sensor, a velocity sensor, and a 3 axis accelerometer. Forces are measured by 13 strain gauge force transducers, and the pressures on the float shell is measured by 33 flush type pressure sensors. 15 wave gauges and 3 velocity profilers describes the wave conditions, and several video cameras (2 sub sea, 1 high speed, 3 normal) and a 3D laser scanner takes care of providing visual images.

Plans for testing

The testing covers:

1. Testing of slow motion in air (gravity)
2. Testing of slow motion in calm water (hydrostatics)
3. Fast acceleration in air (mass inertia moment)
4. Fast sinusoidal motion in calm water (wave radiation forces)
5. Fixed float in current, no waves (drag forces)
6. Fixed float in waves (wave excitation forces)
7. Fixed float in combined wave and current
8. Freely moving float in waves, i.e. no PTO force
9. Float moving in waves with control. Resistive and reactive control strategy
10. Bottom-slamming in still water. Float is released from high position and hits the water with a high velocity, and the impact pressures on the shell is measured (slamming coefficient)
11. Wave slamming. Focusing of waves in wave generation software.

Regular and irregular waves with different wave incidence angles will be tested. Current in combination with waves is also tested.

Acknowledgements

The authors wish to thank the financial support from the EU MARINET project no 190, the Danish DSF project SDWED 09-067257 and ForskEL FLOAT2 10754.

Contact

Morten Møller Jakobsen, E-mail: mmj@civil.aau.dk
Aalborg University, Department of Civil Engineering
Sohngaardsholmsvej 57, DK-9000 Aalborg, Denmark.

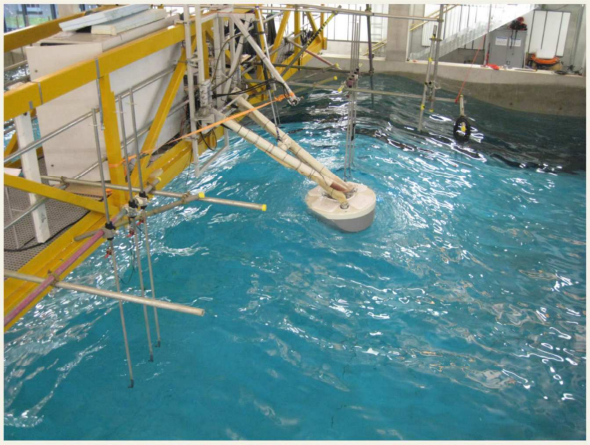

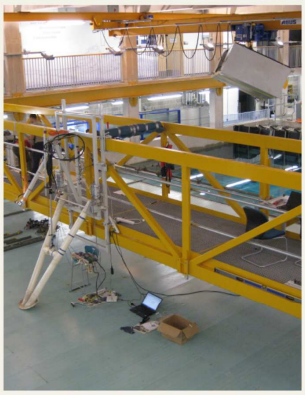

Appendix H

Manual for open wave generation and analysis software

Morten M. Jakobsen

The DCE Technical Report has been published on the
Videnbasen for Aalborg Universitet, VBN, Department of Civil Engineering DCE
Technical Reports Series, no. 191, p. 20, 2015.

The layout has been revised.

DEPARTMENT OF CIVIL ENGINEERING
AALBORG UNIVERSITY

Manual for wave generation and analysis software in Matlab

Morten M. Jakobsen

ISSN 1901-726X
DCE Technical Report No. 191

Aalborg University
Department of Civil Engineering
Group Name

DCE Technical Report No. 191

Manual for wave generation and analysis software in Matlab

by

Morten M. Jakobsen

July 2015

Scientific Publications at the Department of Civil Engineering

Technical Reports are published for timely dissemination of research results and scientific work carried out at the Department of Civil Engineering (DCE) at Aalborg University. This medium allows publication of more detailed explanations and results than typically allowed in scientific journals.

Technical Memoranda are produced to enable the preliminary dissemination of scientific work by the personnel of the DCE where such release is deemed to be appropriate. Documents of this kind may be incomplete or temporary versions of papers—or part of continuing work. This should be kept in mind when references are given to publications of this kind.

Contract Reports are produced to report scientific work carried out under contract. Publications of this kind contain confidential matter and are reserved for the sponsors and the DCE. Therefore, Contract Reports are generally not available for public circulation.

Lecture Notes contain material produced by the lecturers at the DCE for educational purposes. This may be scientific notes, lecture books, example problems or manuals for laboratory work, or computer programs developed at the DCE.

Theses are monograms or collections of papers published to report the scientific work carried out at the DCE to obtain a degree as either PhD or Doctor of Technology. The thesis is publicly available after the defence of the degree.

Latest News is published to enable rapid communication of information about scientific work carried out at the DCE. This includes the status of research projects, developments in the laboratories, information about collaborative work and recent research results.

Published 2015 by
Aalborg University
Department of Civil Engineering
Sofiendalsvej 9-11
DK-9200 Aalborg SV, Denmark

Printed in Aalborg at Aalborg University

ISSN 1901-726X
DCE Technical Report No. 191

Recent publications in the DCE Technical Report Series

ISSN 1901-726X
DCE Technical Report No. 191

Contents

Preface **ix**

1 Manual for wave generation and analysis software in Matlab **1**
1.1 Wave generation 1
1.2 Wave analysis 2

2 Implementation of 3D wave analysis **5**
2.1 Maximum Likelihood Method 6
2.2 Bayesian Directional Method 7

Bibliography **9**

Preface

This Manual is for the included wave generation and analysis software and graphical user interface. The package is made for Matlab and is meant for educational purposes. The code is free to use under the GNU Public License (GPL). It is still in development and should be considered as such.
If you have questions, suggestions, or additions to the code you can contact the author.

Morten Møller Jakobsen
mmj@civil.aau.dk
http://homes.civil.aau.dk/mmj/
Sofiendalsvej 11, Room: 11.218
9000 Aalborg

Chapter 1

Manual for wave generation and analysis software in Matlab

The wave generation and analysis software presented here is an open source software package for Matlab. While the code is inspired by the Wavelab by Andersen (2010) and DIWASP by MetOcean Solutions LTD (2002) software it is written independently. The software by this author is for educational purposes only and should not be used commercially. The software has a Graphical User Interface (GUI) facade. The interface calls separate generation and analysis scripts that can run without the GUI.

To start the program browse to the *GUI* folder and open the GenerationGUI.m or AnalysisGUI.m in Matlab, then click *Run* or press *F5*.

1.1 Wave generation

To generate unimodal waves[1] a Random Phase Method (RPM) is used. The method uses inverse Fourier transformation to calculate the coefficients in the discrete spectrum based on Frigaard and Andersen (2010). For the bimodal spectrum the much slower superposition of regular waves is used.

Running the wave generation software the *GenerationGUI* opens as seen in Fig. 1.1. The output formats implemented is a generic type based on Hawkes et al. (1997) *"Comparative Analyses of Multidirectional Wave Basin Data"* and another format readable by Wavelab.
Clicking the *Load Array* button opens the *WGArray* window. After selecting the nodes to be used for the array and the wave parameters the target spectra can be examined using the *Plot* option as seen in Fig. 1.2. The text based outputs from the software is put into structures for a clean workspace. The two structures *geninput*

[1] single peak spectrum, i.e. only swell waves or wind waves

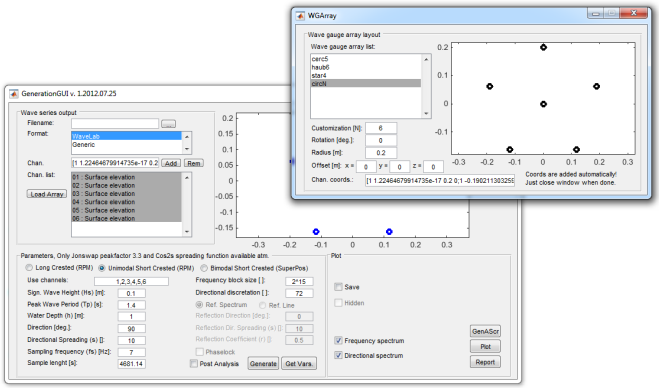

Figure 1.1: Wave Generation GUI.

and *generation* contain the inputs to the generation scripts and the output respectively. To run the wave analysis on the generated wave series the *Post Analysis* checkbox can be ticked. Alternately the saved file can be analyzed manually later.

1.2 Wave analysis

The 3D wave analysis methods referred to as Bayesian Directional Method (BDM) and Maximum Likelihood Method (MLM) has been implemented as seen in Fig. 1.3. The methods and implementations are explained in Section 2.
To do the analysis the water depth and the sampling frequency used in the samples are needed. The selection of incident and reflected wave directions are only used to process reflection coefficients and the calculation of separate incident and reflected significant wave heights.
The output from the analysis software can be plotted similar to the wave generation in Fig. 1.2. The two structures *anainput* and *analysis* contain the inputs to the model and the output respectively.

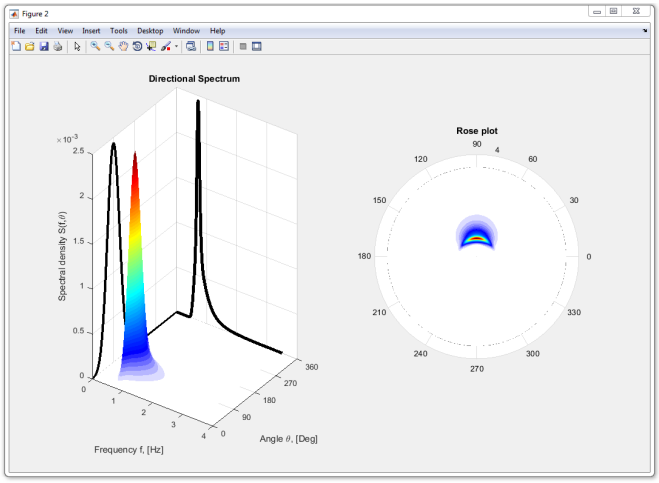

Figure 1.2: Plots of two common representations of the directional spectrum.

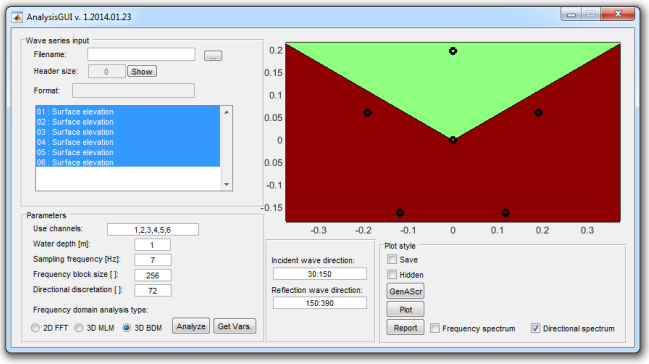

Figure 1.3: Wave analysis user interface.

Chapter 2

Implementation of 3D wave analysis

It is recommended to read the literature which outlines and explains the most commonly used methods to estimate the directional spectrum i.e. Hashimoto et al. (1987); Isobe et al. (1984); Davis and Regier (1977); Sand (1979); Benoit et al. (1997); Hawkes et al. (1997). This section will be an abridged version of the underlying theory and an explanation of how these methods are derived from the probabilistic methods.

Relation between the directional spectrum $S(f,\theta)$, the frequency spectrum $S(f)$ and the spreading function $D(\theta|f)$ is shown in Eq. 2.1.

$$S(f,\theta) = S(f) \cdot D(\theta|f) \tag{2.1}$$

The spreading function is subject to the constraint in Eq. 2.2.

$$\int_{-\pi}^{\pi} D(\theta|f)d\theta = 1 \tag{2.2}$$

To do the 3D analysis it is necessary to estimate the directional wave spectrum $S(f,\theta)$. A relation between the directional wave number-spectrum $S(k,\sigma)$ and the spectral matrix $\Phi(f)$ is outline through Fourier Transformation in Eq. 2.3 Isobe et al. (1984).

$$\Phi_{mn}(\sigma) = \int_k H_m(k,\sigma)H_n^*(k,\sigma)e^{-ik(\mathbf{x}_{nm})}S(k,\sigma)dk \tag{2.3}$$

Where k is the wave number can be determined from the dispersion equation using either Chebyshev(used here) or Newton-Raphson convergence theorem. H is a transfer function which depends of the type of sensor data used, $H = 1$ is used if the time series are from surface elevation measurement by Hashimoto et al. (1987); Benoit et al. (1997). $\mathbf{x}_{nm}$ represents the distance between each gauge pair, which can be described by Cartesian or Polar coordinates in Eq. 2.4 and 2.5 respectively.

Eq. 2.1 is used to isolate the spreading function rather than the directional wave spectrum, cf. Sand (1979).

$$\frac{\Phi_{mn}(f)}{S(f)} = \int_{-\pi}^{\pi} H_m(f,\theta) H_n^*(f,\theta) e^{-ik((x_m-x_n)\cdot cos(\theta)+(y_m-y_n)\cdot sin(\theta))} D(\theta|f) d\theta \quad (2.4)$$

or

$$\frac{\Phi_{mn}(f)}{S(f)} = \int_{-\pi}^{\pi} H_m(f,\theta) H_n^*(f,\theta) e^{-i\,k\,r_{mn}\,cos(\theta-\beta_{mn})} D(\theta|f) d\theta \quad (2.5)$$

The solution to Eqs. 2.3, 2.4 and 2.5 is the subject to a wide range of analyzing procedures. Those used in the software are explained in the following.

2.1 Maximum Likelihood Method

The first implementation of the Maximum Likelihood Method was introduced in the field of seismic research but is useful within marine research using wave gauge arrays as well, cf. Capon et al. (1967); Capon (1969).

$$\hat{P}(\gamma,k) = \left[\sum_{m,n} \Phi_{mn}(\gamma)^{-1} e^{ik\mathbf{x}_{mn}}\right]^{-1} \quad (2.6)$$

where $\hat{P}$ is the estimate of the power output subject to the Maximum Likelihood filter. γ is the normalized frequency $\gamma = \omega T$.
$\hat{P}$ is proportional to the directional wave spectrum, so under the constraint of Eq. 2.2 the expression can be rewritten to Eq. 2.7.

$$\hat{S}(k,\sigma) = \alpha \cdot \left[\sum_{m,n} \Phi_{mn}(\sigma)^{-1} e^{ik\mathbf{x}_{mn}}\right]^{-1} \quad (2.7)$$

$\Phi_{mn}(\sigma)^{-1}$ being the inverse spectral density matrix and α being a proportionality constant. To include other types of sensory data an extension was made to the MLM, which included the transfer function H as suggested by Isobe et al. (1984).

$$\hat{S}(k,\sigma) = \alpha \cdot \left[\sum_{m,n} \Phi_{mn}(\sigma)^{-1} H_m^*(k,\sigma) H_n(k,\sigma) e^{ik\mathbf{x}_{mn}}\right]^{-1} \quad (2.8)$$

The implementation in the analysis code uses the spreading function as suggested earlier together with the constraint in Eq. 2.2 to determine α. Then knowing the spreading of the waves the directional wave spectrum is determined by Eq. 2.1.
One of the issues with the method is the inverted matrix that makes the method vulnerable to truncation errors in the spectrum where there is little energy.

2.2 Bayesian Directional Method

The Bayesian Directional Method is the method suggested by default as it has shown to be more accurate and reliable by Hashimoto et al. (1987); Hashimoto and Kobune (1988). This method only makes assumption about local smoothness of the spectrum. By introducing the sample data functions x and y and implicitly assuming that the expression is subject to a priori information Bayes' Theorem is expressed in Eq. 2.9.

$$p(y|x) = \frac{p(y)p(x|y)}{p(x)} \tag{2.9}$$

Considering x as the measured data function the model distributions $p(x|y)$ is interpreted as the likelihood function $L(x, \sigma^2)$. $p(y)$ is the prior information redefined as $p(x|u^2, \sigma^2)$ and $p(y|x)$ is the posterior distribution, $p_{post}(x|u^2, \sigma^2)$. This leads to the proportionality in 2.10.

$$p_{post}(x|u^2, \sigma^2) \propto L(x, \sigma^2)p(x|u^2, \sigma^2) \tag{2.10}$$

Where the prior distribution is given by 2.11 and the likelihood function by 2.12.

$$p(x|u^2, \sigma^2) = \left(\frac{u}{\sqrt{2\pi}\sigma}\right)^K exp\left(-\frac{u^2}{2\sigma^2}\sum_{k=1}^{K}(x_k - 2x_{k-1} + x_{k-2})^2\right) \tag{2.11}$$

$$L(x, \sigma^2) = \frac{1}{(2\pi\sigma^2)^N} exp\left(-\frac{1}{2\sigma^2}\sum_{i=1}^{2N}\left(\phi_i - \sum_{k=1}^{K}\alpha_{i,k}exp(x_k)\right)^2\right) \tag{2.12}$$

where

$$M = N(N+1)/2 \tag{2.13}$$

$$\phi_i(f) = \Re\left(\frac{\Phi_{mn}(f)}{S(f)W_{mn}(f)}\right),\ i = 1, ..., M \tag{2.14}$$

$$\phi_i(f) = \Im\left(\frac{\Phi_{mn}(f)}{S(f)W_{mn}(f)}\right),\ i = M+1, ..., 2M \tag{2.15}$$

$$\alpha_{i,k}(f) = \Re\left(\frac{\Delta\theta H_m(f, \theta_k)H_n^*(f, \theta_k)e^{ik\mathbf{x}_{nm}}}{W_{mn}(f)}\right),\ i = 1, ..., M \tag{2.16}$$

$$\alpha_{i,k}(f) = \Im\left(\frac{\Delta\theta H_m(f, \theta_k)H_n^*(f, \theta_k)e^{ik\mathbf{x}_{nm}}}{W_{mn}(f)}\right),\ i = M+1, ..., 2M \tag{2.17}$$

Where N is the number of wave guages, W is a weighting function, u is a hyper-parameter and σ is the standard deviation. These are chosen through Akaike (1980)'s Bayesian Information Criterion (ABIC), by minimizing Eq. 2.18.

$$ABIC = -2ln\int L(x, \sigma^2)p(x|u^2, \sigma^2)da \tag{2.18}$$

Which should be maximized to obtain the estimate of x. In the implementation x is discrete, which is distinguished by x_k, where $k = 1, .., K$. The directional spreading function is then obtained from Eq. 2.19.

$$\hat{D}(\theta|f) = \sum_{k=1}^{K} e^{x_k(f)} I_k(\theta) \tag{2.19}$$

$$I_k(\theta) = \begin{cases} 1 & : (k-1)\Delta\theta \leq \theta < k\Delta\theta \\ 0 & : otherwise \end{cases} \tag{2.20}$$

It is significant to note that the method to calculate W of the spectral density functions was greatly improved by Hashimoto (1997). The newer method is implemented here which is defined in Eq. 2.21.

$$W_{mn}(f) = \sqrt{(\Phi_{mm}(f) \cdot \Phi_{nn}(f) \pm C_{mn}(f)^2 \pm Q_{mn}(f)^2)/2N_a} \tag{2.21}$$

Where N_a is the number of ensemble averages. When calculating the weighting function Eq. 2.16 uses positive coincident spectral density and negative quadrature while 2.17 uses negative coincident spectral density and positive quadrature. It should be noticed that this new method can result in $W_{mn}(f) = 0$, and in this rare case it is revert back to the old method in the implementation.

In an attempt to get even better results a *relaxation* of the new estimates are performed when no new solution was found. For stability and to avoid long computational time, the number of iterations are limited which dramatically reduces the computational time at the cost of some accuracy. The expressions in Eq. 2.22 and 2.23 are used to reduce the computational time need for convergence further suggested by Hashimoto (1997).

$$u = ab^m \qquad , a = 1.0, b = 0.5, m = 1, 2, ... \tag{2.22}$$

$$x_0(i) = ln(1/2\pi) \quad , i = 1, ..., K \tag{2.23}$$

Bibliography

Akaike, H. (1980). Likelihood and the Bayes procedure. *Bayesian statistics, Valencia: University Press*, 31(1):143–166.

Andersen, T. L. (2010). *WaveLab*. Version 3.0 and 3.34. Download: 03-05-2010.

Benoit, M., Frigaard, P., and Schäffer, H. (1997). Analysing multidirectional wave spectra: A tentative classification of available methods. In *IAHR Seminar Multi-directional Waves and their Interaction with Structures*, 27th IAHR Congress. The International Association for Hydro-Environment Engineering and Research, The National Research Council of Canada.

Capon, J. (1969). High-Resolution Frequency-Wavenumber Spectrum Analysis. *Proceedings of the IEEE*, 57(8):1408–1418.

Capon, J., Greenfield, R. J., and Kolker, R. J. (1967). Multidimensional Maximum-Likelihood Processing of a Large Aperture Seismic Array. In *Proceedings of the IEEE*, volume 55, pages 192–211. IEEE.

Davis, R. E. and Regier, L. A. (1977). Methods for estimating directional wave spectra from multi-element arrays. *Journal of marine research*, 35(3):453–477.

Frigaard, P. and Andersen, T. L. (2010). Technical Background Material for the Wave Generation Software AwaSys 5. Technical Report 64.

Hashimoto, N. (1997). *Analysis of the directional wave spectrum from field data*, volume 3 of *Advances in coastal and ocean engineering*, pages 103–143. World Scientific Publishing Co. Pte. Ltd.

Hashimoto, N. and Kobune, K. (1988). Directional Spectrum Estimation from a Bayesian Approach. *Coastal Engineering*, 1:62–77.

Hashimoto, N., Kobune, K., and Kameyama, Y. (1987). Estimation of Directional Spectrum using the Bayesian Approach, and its Application to Field Data Analysis. 26(5):57–100.

Hawkes, P., Ewing, J., Harford, C., Klopman, G., Stansberg, C., Benoit, M., Briggs, M., Frigaard, P., Hiraishi, T., Miles, M., Santas, J., and Schäffer, H. (1997).

Comparative Analyses of Multidirectional Wave Basin Data. In *IAHR Seminar Multidirectional Waves and their Interaction with Structures*, 27th IAHR Congress. The International Association for Hydro-Environment Engineering and Research, The National Research Council of Canada.

Isobe, M., Kondo, K., and Horikawa, K. (1984). Extension of MLM for estimating directional wave spectrum. In *Symposium on Description and Modelling of Directional Seas,*, volume A6, pages 1–15. DHI & MMI.

MetOcean Solutions LTD (2002). *DIWASP, a directional wave spectra toolbox for MATLAB*. Centre for Water Research, University of Western Australia, Perth.

Sand, S. E. (1979). *Three-Dimensional Deterministic Structure of Ocean Waves*. PhD thesis, Technical University of Denmark, Lyngby, Denmark.

ISSN (online): 2246-1248
ISBN (online): 978-87-7112-331-9

AALBORG UNIVERSITY PRESS